Universität für Bodenkultur Wien
University of Natural Resources and Applied Life Sciences, Vienna
Department of Chemistry, Division: Analytical Chemistry

DIPLOMARBEIT

# Determination of $^{90}Sr$ in soil samples using inductively coupled plasma mass spectrometry equipped with dynamic reaction cell (ICP-DRC-MS)

von
Juliet Feuerstein
H0140258

Betreuer:
Ao. Prof. Dr. Thomas Prohaska
Dr. Sergei Boulyga

# Acknowledgement

In order of appearance:

Elisabeth

Manfred

Renate

Ludwig

Maria

Alois

Tahereh

Franziska

Silvia

Hans

Janine

Tom

Prof. Thomas Prohaska

Marion

Christiane

Dr. Sergei Boulyga

Patrick

Sigi

Alex

Karin

Monika

Vienna - December 2007

# Table of Content

# Abstract

Environmental monitoring of radioactive contaminants is an important issue. Rapid analytical methods are required for obtaining information about possible contamination with hazardous radionuclides within short time particularly in cases of emergency.
The non-natural isotope $^{90}Sr$ is formed in nuclear reactors and during the explosion of nuclear weapons. This isotope is highly radiotoxic and can be accumulated in skeleton and bone tissue creating irradiation doses on bone marrow and resulting in e.g. leukaemia. Common radioanalytical techniques require analysis time of several days up to three weeks for determination of $^{90}Sr$ in environmental samples.

The aim of this work was to develop a rapid method for the determination of $^{90}Sr$ in environmental samples using inductively coupled plasma mass spectrometry (ICP-MS). Sample preparation and measurement procedure were focused mainly on overcoming the isobaric interference of the isotope $^{90}Zr$, which is present in soils at concentrations higher by more than six orders of magnitude compared to $^{90}Sr$. The interfering $^{90}Zr$ was reduced by a factor of more than $10^7$ in two steps: (i) off-line by ion exchange using a strontium specific resin and (ii) directly in the dynamic reaction cell of an ICP-MS by using oxygen as reaction gas.
Soil samples from the vicinity of the Chernobyl Nuclear Power plant were used for validation of the developed method.

The abundance sensitivity of the inductively coupled plasma mass spectrometer, mainly influenced by the peak tailing of $^{88}Sr$ on mass 90 u, was studied systematically and found to be about $3 \times 10^{-9}$. A detection limit of 4 fg $g^{-1}$ (0.02 Bq $g^{-1}$) was achieved in strontium solutions containing no zirconium. A detection limit of 0.2 pg $g^{-1}$ soil (1 Bq $g^{-1}$ soil) was determined in digested uncontaminated soil samples after matrix separation and in a solution of 5 µg $g^{-1}$ strontium and 50 ng $g^{-1}$ zirconium.
$^{90}Sr$ concentrations in three soil samples collected in the vicinity of the Chernobyl Nuclear Power Plant were determined with the developed method to be 4.66 ± 0.27, 13.48 ± 0.68 and 12.9 ± 1.5 pg $g^{-1}$ corresponding to specific activities of 23.7 ± 1.3, 68.6 ± 3.5 and 65.6 ± 7.8 Bq $g^{-1}$, respectively. These results were close to the activities measured earlier by radiometry. ICP-DRC-MS represents a time- and cost-effective alternative technique for fast monitoring although the performance is inferior to commonly used radiometric methods or to accelerator mass spectrometry with respect to the achievable minimum detectable activity.

# Zusammenfassung

Umweltmonitoring infolge radioaktiver Kontamination ist ein wichtiges Thema. Besonders in Notfällen sind schnelle Analysenmethoden nötig, um Information über mögliche Kontamination mit gefährlichen Radionukliden in angemessener Zeit zu erhalten.
Das künstliche Isotop $^{90}Sr$ entsteht in Kernreaktoren und infolge der Explosion von Atomwaffen. Dieses Isotop ist äußerst radiotoxisch und kann im Skelett und im Knochengewebe akkumulieren, das Knochenmark verstrahlen und letztendlich z.B. zu Leukämie führen. Herkömmliche Methoden benötigen relativ lange Analysenzeiten von mehreren Tagen bis zu drei Wochen zur Bestimmung von $^{90}Sr$ in Umweltproben.

Ziel dieser Arbeit war es, eine schnelle Methode zur Bestimmung von $^{90}Sr$ in Umweltproben unter Verwendung der induktiv gekoppeltem Plasma Massenspektrometrie (ICP-MS) zu entwickeln. Die Probenvorbereitung und die Messprozedur waren auf das Beseitigen der isobaren Interferenz des Isotopes $^{90}Zr$ ausgerichtet, welches im Boden in einer mehr als sechsfach höheren Konzentration als $^{90}Sr$ vorhanden ist. Zirkonium wurde von Strontium in zwei Schritten um einen Faktor von mehr als $10^7$ abgetrennt: (i) Im ersten Schritt durch Ionenaustausch mit Hilfe eines Strontium spezifischen Harzes und (ii) im zweiten Schritt direkt im ICP-MS durch Reaktion mit Sauerstoff als Reaktionsgas in einer dynamischen Reaktionszelle (DRC).
Kontaminierte Bodenproben aus der Nähe des Kernkraftwerkes Chernobyl wurden für die Validierung der entwickelten Methode verwendet.

Die Empfindlichkeit auf der Masse 90 wird weitgehend vom Peak-Tailing von $^{88}Sr$ beeinflusst. Die systematische Analyse ergibt ein Empfindlichkeitsverhältnis von $3 \times 10^{-9}$. Eine Nachweisgrenze von 4 fg $g^{-1}$ (0.02 Bq $g^{-1}$) wurde beim Messen von Zirkonium-freien Strontiumlösungen erreicht. In einer Lösung aus 5 µg $g^{-1}$ Strontium and 50 ng $g^{-1}$ Zirconium und in aufgeschlossenen unkontaminierten Bodenproben wurde nach Matrixabtrennung eine Nachweisgrenze von 0.2 pg $g^{-1}$ Boden (1 Bq $g^{-1}$ Boden) erreicht.
Die $^{90}Sr$ Konzentration in den drei Bodenproben aus der Nähe des Kernkraftwerkes Chernobyl wurden mit der entwickelten Methode als 4.66 ± 0.27, 13.5 ± 0.7 und 12.9 ± 1.5 pg $g^{-1}$ bestimmt, was spezifischen Aktivitäten von 23.7 ± 1.3, 68.6 ± 3.5 and 65.6 ± 7.8 Bq $g^{-1}$ entspricht. Diese Ergebnisse liegen nahe der zuvor radiometrisch bestimmten Aktivitäten. Obwohl die ICP-DRC-MS herkömmlichen radiometrischen Methoden in Bezug auf erreichbarer minimal messbarer Aktivität unterlegen ist, repräsentiert sie eine zeit- und kosteneffektive Alternative für schnelles Monitoring.

# 1 Introduction

## *1.1 $^{90}Sr$*

### 1.1.1 Origin and health risks

Strontium has four stable, naturally occurring isotopes, $^{84}Sr$, $^{86}Sr$, $^{87}Sr$, and $^{88}Sr$ with the isotopic abundance of 0.56%, 9.86%, 7.00% and 82.58% (KAERI 2000), respectively. Since Sr is a chemical proxy for Ca in the human body, it is incorporated in bones and teeth (Acar and Acar 2004), which results in a long biological half-life of 49.3 years (Goutelard et al. 2000, Acar and Acar 2004). While in adults, the Sr attaches to the surface of bones, in children, whose bones are still growing, it may be used by the body to create the hard bone mineral itself. This results in a long storage of the Sr in the bone, until it is eliminated from the body through urine, faeces, and sweat. This 'bone-seeking' behaviour is the cause of concern regarding oral or inhalation exposures of radioactive strontium isotopes. Such radionuclides incorporate into bone and irradiate the bone cells, the hemopoietic bone marrow, and potentially, the soft tissues surrounding bone, especially in the skull. Radioactive strontium isotopes may cause cancer as a result of damage to the genetic material (DNA) in cells, especially thyroid cancer and leukaemia (U.S. Department of health and human services 2004).

Thus, the anthropogenic isotope $^{90}Sr$ is one of the mostly hazardous radionuclides. It is formed in nuclear reactors and during the explosion of nuclear weapons. $^{90}Sr$ has a physical half-life ($T_{1/2}$) of 28.9 years (Schrader 2004) and is a pure beta emitter (KAERI 2000). Beta emissions have limited ability to penetrate through tissue, but if $^{90}Sr$ is internalised or in close contact with tissue, it introduces local irradiation. $^{90}Sr$ has been released by nuclear weapon tests in the 1950s and 1960s and by nuclear power plant accidents. Radiostrontium occurs in radioactive fallout, as well as $^{137}Cs$ ($T_{1/2}$ = 30 years), $^{131}I$ ($T_{1/2}$ = 8 days), $^{134}Cs$ ($T_{1/2}$ = 2 years), and was widespread especially in the northern hemisphere. The global release of $^{90}Sr$ of atmospheric nuclear testing was 622 PBq (UNSCEAR 2000a). In Chernobyl, the radionuclide inventory in Unit 4 reactor core at the time of the accident on 26 April 1986 was about 200 PBq of $^{90}Sr$, of which 8 - 10 PBq have been released (UNSCEAR 2000b). Whereas $^{134}Cs$ and $^{131}I$ have a rather short half-life, $^{137}Cs$ and $^{90}Sr$ show a longer half-life, which makes them suitable for environmental monitoring even after several decades after the accident. While $^{90}Sr$ is a pure beta emitter, $^{137}Cs$ is as well beta as gamma emitter and can therefore be easily and rapidly determined by gamma-spectrometry.

Rapid $^{90}Sr$ determination after its release is especially important since it is taken up from soil by plants like rice and wheat (Choi et al. 2007, Gastberger et al. 2000, Yamaguchi et al. 2007)

and consequently enters the food chain and is for example transferred to milk (Gastberger et al. 2001).

The Annual Limit on Intake (ALI) of $^{90}Sr$ for ingestion is $7 \times 10^5 - 7 \times 10^6$ Bq (US. Department of health and human services, 2004). The becquerel (Bq) is the SI unit of activity and is defined as the activity of a quantity of radioactive material in which one nucleus decays per second.

$^{90}Sr$ has no beneficial aspect for human kind, but it could be useful for forensic science for determination of time since death (Neis et al. 1999).

## 1.1.2 $^{90}Sr$ determination

Common analytical techniques for determination of $^{90}Sr$ are liquid scintillation counting and Cherenkov counting. Mass spectrometric methods play an increasingly important role for determination of radionuclides. Accelerator mass spectrometry (AMS), resonance ionisation spectrometry (RIMS) and inductively coupled plasma mass spectrometry (ICP-MS) methods are available for determination of $^{90}Sr$. Especially ICP-MS is widely applied for determination of radionuclides (Becker 2005, Lariviere et al. 2006). Unlike radioanalytical methods, mass spectrometric methods do not determine radionuclides by their radiation, but by counting the ions formed in the analytical process.

### 1.1.2.1 Beta-spectrometry

Liquid scintillation counting (LSC) is a standard method measuring radiation from beta-emitting nuclides. A beta particle is essentially any electron that has been discharged from the nucleus of an unstable nuclide. Electron discharge occurs under certain conditions in which nuclides with excess neutrons reach stability by the conversion of a neutron to a proton.

In LSC, the energy from beta particles is converted into visible light, which is then detected by a liquid scintillation counter. Production of light is facilitated by placing the radioactive samples in a solution known as a cocktail. Cocktails generally contain a solvent and a chemical compound known as fluor. Toluene, xylene, pseudocumenes and monoalkylated benzenes are some of the more commonly used cocktail solvents. Fluors produce a flash of light when they interact with a beta particle. Many cocktails also contain solubilisers (e.g., surfactants) which are necessary to get some samples into solution.

Fluor molecules (e.g. PPO/bis-MSB) are directly or indirectly excited by ionising radiation from the sample, resulting in the emission of photons. These photons react with the photocathode of a photomultiplier tube to yield photoelectrons from the photocathode surface. The amount of photoelectrons being emitted, which is directly proportional to the amount of ionising radiation,

is translated to CPM's (count per minute) at the data output controls of the liquid scintillation counter (MP Biomedicals 2007).

The counting efficiencies under ideal conditions range from about 30% for Tritium, a low-energy beta emitter, to nearly 100% for Phosphorus-32, a high-energy beta emitter. Some chemical compounds and highly coloured samples can interfere with the counting process. This interference, known as 'quenching', can be overcome through data correction or through careful sample preparation. High-energy beta emitters such as $^{32}P$ can also be counted in a scintillation counter without the cocktail. This technique is known as Cherenkov counting and relies on the Cherenkov radiation being detected directly by the photomultiplier tubes (N.N. 2007).

$^{90}Sr$ is pure beta emitter and it decays into $^{90}Y$ ($T_{1/2}$ = 2.67 days), which is also a beta emitter, and finally decays into non-radioactive $^{90}Zr$. While $^{90}Sr$ irradiates beta particles with energies of up to 0.546 MeV, its daughter nuclide $^{90}Y$ emits highly energetic electrons ($E_{max}$ = 2.2 MeV) which makes $^{90}Y$ more suited for radiochemical detection techniques after it achieves equilibrium with its parent nuclide $^{90}Sr$. Beta counting allows minimum detectable activity in urine samples of about 0.07 Bq $L^{-1}$ to 0.1 Bq $L^{-1}$ corresponding to 0.02 pg $L^{-1}$ of $^{90}Sr$ (Alvarez et Navarro, 1996; Shiraishi et al. 2006).

### 1.1.2.2 Accelerator mass spectrometry

The difference of accelerator mass spectrometry (AMS) to other mass spectrometric methods is that it accelerates ions to extraordinarily high kinetic energies before mass analysis. The sample is put into the sputter ion source and is ionised by bombarding it with Cs ions. Due to an acceleration potential and electrostatic ion optics, a well-focused beam of fast negative ions is produced. The ions are separated for their energies in the 90°-electrostatic sector field. The first magnet is used in the same way as the magnet in an ordinary mass spectrometer. In order to measure different isotopes quasi-simultaneously, a pulsed high voltage is applied to the isolated vacuum chamber of the magnet. Because of the very short change in the energy of the ions, each isotope can pass the magnet. The negative ions enter the accelerator. There they are accelerated because of the positive voltage of 5 MV in the terminal. In the terminal of the tandem accelerator, the ions collide with a very thin carbon foil and all molecular ions are broken up into charge states of more than 2+. After passing the stripping foil, the ions are accelerated down the second half of the tandem accelerator reaching energies of about 25 MeV. The ions are selected for their charge in a 15°-electrostatic deflector. Broken up molecular particles are removed there as well. The 120°-magnet, which is used for heavier ions like Sr, separates the remaining particles by their mass. The ions are focused into in a gas-filled ionisation detector. There they deposit kinetic energy by ionising the counter gas

(isobutene). The analyte ions can be distinguished from accidental background particles by measuring the total energy deposited and the so-called differential energy deposit dE (N.N. 2007a).

Separation of $^{90}Zr$ has to be done prior to measurement for $^{90}Sr$ determination with AMS. Arslan et al. (1994) measured Zr free samples because the high-quality chemical pre-treatment they wanted to apply was not developed by then. Paul et al. (1997) identified $^{90}Sr$ ions and discriminated them from $^{90}Zr$ by measuring time of flight, total energy and energy-loss signals in an ionisation chamber. This is not an easy task for such heavy nuclides, since the differential energy losses of the two elements differ by only 3 – 4 %. Moreover, the rare $^{90}Sr$ has the lower atomic number, a disadvantage because of the overlap of $^{90}Sr$ signals with tails of $^{90}Zr$ in differential energy loss measurements.

Arslan et al. (1994) used an EN tandem accelerator for determination of $^{90}Sr$. They achieved a detection limit of 39 Bq when 10 mg of $SrF_2$ was used. Paul et al. (1997) determined the detection limit in environmental samples to be 19-37 mBq $L^{-1}$ with a Rehovot 14 UD Pelletron accelerator. In this case Sr was injected as hydride.

### 1.1.2.3 Resonance-ionisation mass spectrometry

Resonance-ionisation mass spectrometry (RIMS) is an element and even isotopic selective method. It is based on resonant laser ionisation. Nearly complete isobaric suppression, better than $10^8$, is obtained by the uniqueness of optical transitions, especially in multi-step excitations. High isotopic selectivity is achieved by combination of both isotopic specific properties of the method: isotope abundance sensitivity and optical isotope selectivity in the laser excitation process. The optical selectivity can be increased by reducing Doppler-broadening, either in multi-step processes or by utilisation of the Doppler-shift in collinear excitation on fast atomic beams. One particularly successful field for analytical application of RIMS is the ultratrace determination of long-lived radioisotopes (Wendt et al. 2000).

After chemical preparation, involving solvent extractions with crown ethers, in order to perform a Sr/matrix separation, the sample (Sr) is transferred into the graphite tube furnace of the ion source (Zimmer et al. 1994). There it is evaporated to form a source of neutral target atoms in the gas phase. Single- or multi-step excitation is carried out on these atoms by irradiation with lasers operating at the atomic resonance frequencies. Ionisation of the excited atoms may them be accomplished by a variety of methods, including photoionisation by the resonant lasers or a separate higher-power laser. The resulting ions are accelerated in an electric field and transmitted through a mass spectrometer with subsequent low background ion counting (Wendt et al. 2000).

RIMS is useful for studying the electronic structure of atoms or molecules and to make quantitative measurements of analyte concentrations.
$^{90}Sr$ was determined by RIMS in collinear geometry on a fast atomic beam (Monz et al. 1993, Wendt et al. 1997, Zimmer et al. 1994), offering detection limits for $^{90}Sr$ down to 2 mBq per sample. Coherent multi-step RIMS (Bushaw and Cannon 1997, Bushaw and Nörtershäuser 2000) offers similar detection limits with much lower experimental expenditure.

### 1.1.2.4 Inductively coupled plasma mass spectrometry

This chapter gives an overview about different ICP-MS instrumentation and methods that have been applied for $^{90}Sr$ determination. The principle of ICP-MS is explained in chapter 1.2.

Electrothermal vaporisation (ETV) is a special sample introduction technique for small sample volumes. It offers significant improvement of sample transport efficiency over conventional pneumatic solution nebulisation techniques. This improvement in transport efficiency (> 75%), results in at least an order of magnitude increase in sensitivity, with a corresponding improve of detection limit. The sample is placed in a pyrolytically coated graphite tube. Argon gas is passed through the tube and routed to the plasma. A low electrical current is first passed through the graphite tube, raising its temperature by resistance heating until the sample solvent evaporates, leaving a residue on the surface of the conductor. After the sample has dried, it is rapidly vaporised by the passage through the conductor of a high electrical current. The vaporised sample is transported by the continuous argon gas stream into the plasma, where it is atomised and ionised (Montaser 1998).
ETV-ICP-MS was applied for determination of $^{90}Sr$ by Berryman and Probst (1996) and Grinberg et al. (2007). Grinberg et al. used a combination of ETV-ICP-MS and DRC technology and obtained procedural detection limits as low as 2 to 20 pg $g^{-1}$ depending on the concentrations of Zr and Y in the samples.

Vonderheide et al. (2004) used double-focusing sector field ICP-MS (ICP-SFMS) under cold plasma conditions and a mass resolution $m/\Delta m = 4000$ for $^{90}Sr$ determination in water and urine samples. The Sr concentration in urine was about 5 ng $g^{-1}$ and the Zr concentration was 25 pg $g^{-1}$. An instrumental detection limit of 3 pg $L^{-1}$ was achieved for $^{90}Sr$ in water samples and an abundance sensitivity of $6 \times 10^{-7}$ for $^{88}Sr$ on mass 90 was reported. Zoriy et al. (2005) used the same approach for separation of Zr in groundwater samples and reported a detection limit of 11 pg $L^{-1}$ for $^{90}Sr$. Sample preparation included acidification and concentration by evaporation, but no further chemical separation was conducted. Natural Sr concentration ranged from 2.2 to 6.0 ng $g^{-1}$ and Zr concentration was below 3 ng $g^{-1}$ in groundwater samples.

Applying selective gas-phase reaction, Vonderheide et al. (2004) achieved a detection limit of 2 ng $L^{-1}$ for $^{90}Sr$ in water samples by using a quadrupole-based ICP-MS equipped with a hexapole collision cell (Platform) and oxygen as reaction gas. Isnard et al., (2006) employed a similar approach for analysing $^{90}Sr$ in spent nuclear fuel samples. These samples are rich in $^{90}Sr$ and the ratio of $^{90}Sr$ to $^{90}Zr$ is 4:1, so that $^{90}Sr$ could be directly analysed using a multi collector-ICP-MS (MC-ICP-MS) with a collision-reaction cell without foregoing liquid separation. Taylor et al. (2007) determined $^{90}Sr$ in water, plant and sediment samples using oxygen as reaction gas in a quadrupole ICP-MS equipped with a dynamic reaction cell. Method detection limits were 0.1 pg $g^{-1}$ (0.5 Bq $g^{-1}$), 0.04 pg $g^{-1}$ (0.2 Bq $g^{-1}$) and 3 pg $L^{-1}$ (0.5 Bq $L^{-1}$) for $^{90}Sr$ in sediments, plant and water samples, respectively. Abundance sensitivity was reported to be less than $10^{-10}$ which is competitive with AMS and RIMS.

### 1.1.2.5 Method comparison

Beta counting allows minimum detectable activity in urine samples of about 0.07 Bq $L^{-1}$ to 0.1 Bq $L^{-1}$ (Alvarez et Navarro, 1996; Shiraishi et al. 2006). However, this approach is time-consuming (Herranz et al., 2001). Especially in cases of a nuclear accidents it is important to know the degree of contamination as quickly as possible e.g. for screening of possibly contaminated food products. After the Chernobyl reactor accident several weeks passed by before the first $^{90}Sr$ results were available. Hence more rapid methods for the determination of $^{90}Sr$ in environmental samples are clearly advantageous. In general, mass spectrometric techniques have a good potential for a prompt determination of long-lived radionuclides and play an increasingly important role in environmental monitoring complementary to radio analytical techniques (Becker 2005). The application of mass spectrometry for determination of relatively low contents of $^{90}Sr$ in environmental samples is limited by isobaric interferences with $^{90}Zr$ and by peak tailing originating from stable $^{88}Sr$ isotope. Both Zr and Sr in environmental samples are usually by 6 to 9 orders of magnitude more abundant than $^{90}Sr$.

AMS and RIMS allow high elemental and isotopic selectivity and thus are suitable for determination of $^{90}Sr$ with detection limits down to 2 mBq per sample (Wendt et al. 2000). However AMS and RIMS are generally much less readily available than ICP-MS. Reason can be found in the high technological complexity of AMS and RIMS instrumentation.

ICP-MS offers excellent sensitivity and accuracy and allows fast and relatively cost-effective isotope analysis at trace and ultratrace concentration levels in different kinds of samples (Becker 2005). Disadvantages of this method consist of limited abundance sensitivity and

potential isobaric interferences. Isobaric interference causes degradation of detection limits and decrease of quantitative analysis (Nelms 2005). Potential isobaric interferences by naturally occurring isotope and molecule ions at *m/z* = 90 and mass resolutions required for separating them from $^{90}Sr^{+}$ are listed in tab. 1. Mass resolution represents the ability to separate two ions with different masses and is calculated as m / Δm. The main interference is produced by the relatively high amount of $^{90}Zr$ in soil samples. A mass resolution of ~ 30 000 would be needed to separate $^{90}Sr$ (89.907738 u) and $^{90}Zr$ (89.904703 u). This resolution is not achievable with common instruments. Therefore, analyte/matrix separation is a prerequisite for accurate determination. Analyte/matrix separation applies Sr specific resin which is commonly used for a wide range of environmental and technological samples (Horwitz et al., 1991).

**Tab. 1** Isobaric Interferences at *m/z* = 90 (N.N. 2007b)

| Interference | Mass | Isotopic abundance [%] | Mass resolution |
|---|---|---|---|
| $^{38}Ar$-$^{52}Cr$ | 89.9032 | 0.06 - 83.79 | 19999 |
| $^{90}Zr$ | 89.9047 | 51.45 | 29620 |
| $^{36}Ar$-$^{54}Fe$ | 89.9072 | 0.34 - 5.85 | 155550 |
| $^{40}Ar$-$^{50}Ti$ | 89.9072 | 99.60 - 5.18 | 159921 |
| $^{40}Ar$-$^{50}Cr$ | 89.9084 | 99.60 - 4.35 | 129906 |
| $^{40}Ar$-$^{50}V$ | 89.9095 | 99.60 - 0.25 | 49766 |
| $^{89}Y$-$^{1}H$ | 89.9137 | 100 - 99.99 | 15146 |
| $^{74}Ge$-$^{16}O$ | 89.9161 | 36.28 - 99.76 | 10762 |
| $^{74}Se$-$^{16}O$ | 89.9174 | 0.89 - 99.76 | 9316 |
| $^{72}Ge$-$^{18}O$ | 89.9212 | 27.54 - 0.21 | 6659 |
| $^{180}Hf$++ | 89.9733 | 35.08 | 1372 |
| $^{180}W$++ | 89.9734 | 0.12 | 1370 |
| $^{180}Ta$++ | 89.9737 | 0.01 | 1362 |

The aim of this work was development of a rapid method for the determination of $^{90}Sr$ in contaminated soil samples collected in Chernobyl vicinity by using ICP-MS. In comparison to the previously reported samples, including urine, water and spent fuels, analysis of soil samples from Chernobyl vicinity requires a high decontamination factor from $^{90}Zr$ (about $10^{6}$ and higher). Therefore, a particular focus was placed on improving the Zr/Sr separation procedure for $^{90}Sr$ determination. Moreover, the interference (peak tailing) by $^{88}Sr$ was studied in detail as the previous publication (Taylor et al., 2007) does not provide any detail about how the abundance sensitivity of less than $10^{-10}$ can be achieved with a conventional quadrupole-based ICP-MS.

## *1.2 ICP-QMS*

Chapter 1.2 explains the basic operation principle of the instrumentation which has been applied in this work for determination of $^{90}Sr$. A MC-ICP-MS (multicollector inductively coupled plasma mass spectrometer, NU Instruments, Wrexham, UK) using a magnetic sector field as mass separator was applied for IDMS analysis. This instrument is described in detail elsewhere (Albarède et al. 2004, Belshaw et al. 1998).

### 1.2.1 Principle

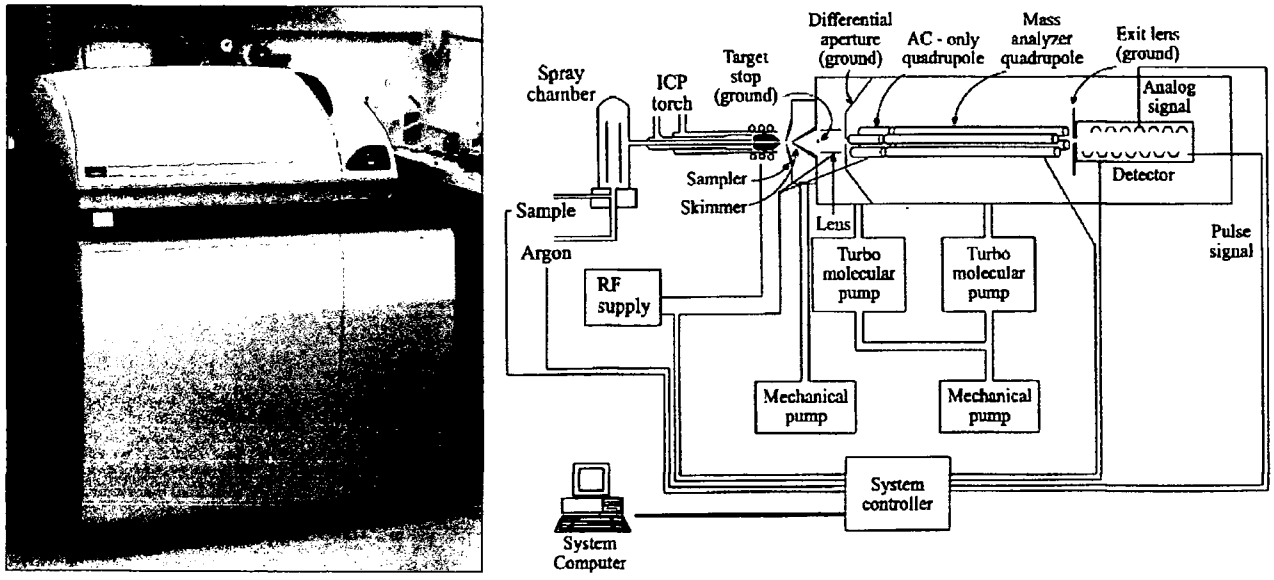


**Fig. 1** a) ELAN DRC II; b) Scheme of a quadrupole ICP-MS (ELAN 6000) (source: Montaser 1989, p.9)

The method was development on the Elan DRC II (Fig. 1), a quadrupole based instrument. Therefore, the principle and the different parts of an ICP-MS instrument are explained by means of this instrument.

The three main parts of a mass spectrometer are the ion source, the mass analyser and the detector. In ICP-MS, inductively coupled plasma serves as the ion source. A high-temperature plasma discharge is used to generate positively charged ions. A liquid sample is pumped through the sample introduction system, nebulised and delivered with nebuliser gas to the plasma as aerosol. In the plasma, the aerosol is vaporised, atomised and ionised. Produced in ICP ions enter the interface region. Then the ion optics focuses the ions into the mass analyser, while photons and neutrals are distracted. After separation in the mass analyser (according to their mass to charge ratios) the ions finally reach the detector. In the Elan DRC II, a dynamic reaction cell is placed before the mass analyser.

### 1.2.2 Sample introduction system

A variety of sample introduction devices can be coupled to an ICP-MS for gaseous, liquid or solid samples (Montaser 1998). The sample introduction system for liquid samples is aimed at converting the sample into a fine-droplet aerosol, suitable for ionisation in the plasma. It principally consists of a nebuliser and a spray chamber. The nebuliser generates the aerosol and the spray chamber selects the droplets. The nebuliser is either self-aspiring or the sample has to be pumped to the nebuliser with a peristaltic pump. After the sample enters the nebuliser, the liquid is broken up into a fine aerosol by the pneumatic action of the nebuliser gas flow, smashing the liquid into tiny droplets. The droplet selection has two purposes. The primarily function of the spray chamber is to allow only the small droplets to enter the plasma, because the plasma discharge is inefficient at dissociating large droplets. The secondary purpose is to smooth out pulses that occur during the nebulisation process, mainly because of the peristaltic pump. (Thomas 2001). Additional to standard sample introduction systems, like PFA nebuliser and cyclonic spray chamber, also high efficiency sample introduction systems are available, like ultrasonic nebuliser and Apex-IR High-Sensitivity Inlet System.

Fig. 2 displays the schematic of an ultrasonic nebuliser. A peristaltic pump introduces liquid sample across an oscillating piezoelectric transducer. The oscillations disperse the sample into a fine aerosol, which is swept out of a spray chamber by a flow of argon gas (nebuliser gas) from the host ICP-MS instrument. The aerosol passes through a heated tube and a cooled condenser. An integrated drain pump removes the condensed sample solvent and any excess sample liquid from the spray chamber. After the condenser, the dried aerosol particles are swept by the nebuliser gas to the ICP instrument for analysis (CETAC U5000AT$^+$ Technical Note). An optional membrane desolvator can be used for further removal of sample solvent. Higher nebulisation efficiency and thus increased sensitivity compared to standard introduction systems is reached by producing very fine aerosol which is more easily ionised. 10 – 15 % of the liquid sample is converted into usable aerosol, compared to 2 – 3 % with conventional pneumatic nebulisers, resulting in analyte signal improvement of ten times and more.

Fig. 3 displays the schematic on an Apex High-Sensitivity Inlet System. The Apex consists of a heated cyclonic spray chamber and a Peltier-cooled multipass condenser and is equipped with a self-aspiring PFA nebuliser. Argon gas is used to sweep the aerosol to the plasma. An optional membrane desolvator can be used for further removal of sample solvent. The Apex-IR has a quartz flow path and includes an additional mixing chamber giving the most stable

signal, ideal for isotope ratio measurements. Sensitivity is improved 3 – 15 times through removal of water from the sample.

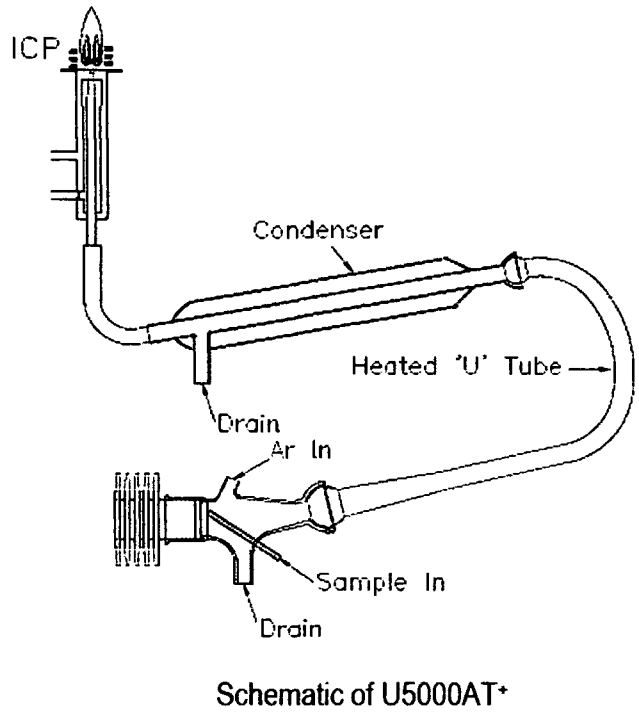


**Fig. 2** Schematic of an ultrasonic nebuliser

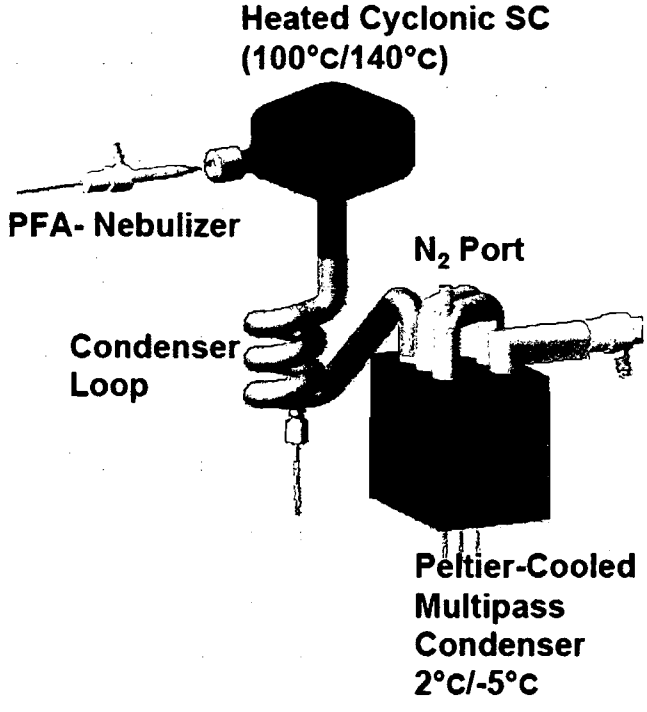


**Fig. 3** Schematic of an Apex sample introduction system

### 1.2.3 Plasma generation

The plasma is the ion source in ICP-MS. It is produced by inductive coupling inside the torch, an assembly of quartz glass tubes. The inductively coupled plasma in an electrode-less discharge in a gas at atmospheric pressure, maintained by energy coupled to it from a radio frequency (RF) generator. Argon is mostly used as plasma gas. A high-temperature plasma discharge is used to generate positively charged ions.

### 1.2.4 Interface region and ion optics

The ions, produced in the plasma, are introduced into the vacuum through a sampler and a skimmer cone. The cones are typically made of nickel and have orifices of about one mm diameter letting the ions into the vacuum system where an ultrasonic jet forms and is led to the mass spectrometric analyser. The function of the interface region is a stepwise reduction in pressure. The pressure of the interface region is $10^{-3}$ bar, whereas the plasma works under atmospheric pressure (1 bar) and the mass analyser under vacuum ($10^{-6}$ - $10^{-7}$ mbar).
The function of the ion optics is to focus the ion beam and direct it into the mass analyser, whereas photons and neutrals are distracted in order to reduce background signal. Instead of bending the ion beam numerous times using complex multi-component lens systems to prevent uncharged species from entering the quadrupole, the ELAN DRC II uses a simple, grounded Shadow Stop, which is positioned before a single ion lens.

### 1.2.5 Mass analyser

The purpose of the mass analyser is the mass separation. Most common ICP-MS instruments use a quadrupole or a magnetic sector field. Mass analyser like time-of-flight, ion cyclotron and ion trap are rarely used.
In a quadrupole ICP-MS, the separation of the ions according to their *m/z* values is performed by a quadrupole mass filter consisting of four straight metal rods placed parallel and equidistant from the axis with applied RF and DC voltages. The introduced ions enter the quadrupole structure at velocities determined by their energy and mass. The applied RF voltages of one rod pair deflect all the ions into oscillatory paths through the rods. If the RF and DC voltages are selected properly, only ions of a given *m/z* ratio will have stable paths and emerge from the other end of the quadrupole system and enter the detector. The stability is defined by the Mathieu equations (Equ. 1)

$$a_U = a_X = -a_Y = 4eV_{dc}/m\omega^2 r_O^2 \qquad q_U = q_X = -q_Y = 2eV_{rf}/m\omega^2 r_O^2 \qquad (1)$$

The quadrupole mass analyser is operated under vacuum ($10^{-6}$ - $10^{-7}$ mbar) in order to avoid distracting collisions of analyte ions with gas molecules.

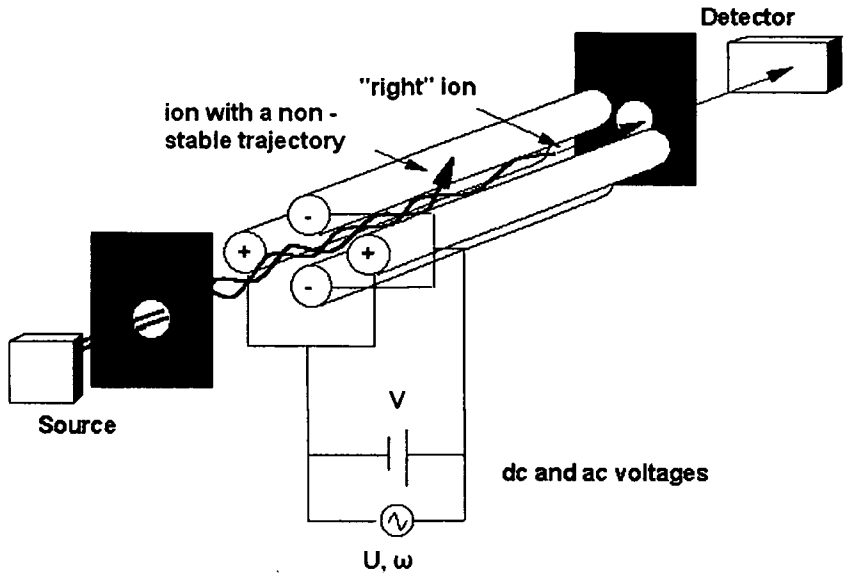


**Fig. 4** Stable and unstable trajectories in a quadrupole

### 1.2.6 Detector

Final detection of the ions is accomplished by an electron multiplier in the quadrupole based instrument Elan DRC II,. A positive ion leaving the mass analyser is being attracted to the negative potential at the detecting cone, hits the surface and secondary electrons are being ejected. These secondary electrons are emitted resulting in a discrete pulse at the collector (Jarvis et al. 1992).

## *1.3 Reduction of spectral interferences in ICP-MS*

Isobaric interferences represent a significant problem in ICP-MS because they degrade detection limits and decrease analytical accuracy. These interferences may come from the sample matrix or the plasma itself. There are different ways to reduce particular interferences including special sample separation procedures and sample introduction systems, cold plasma conditions as well as recently introduced ICP-MS with collision and reaction cells.

### 1.3.1 Cold Plasma

The operation of the mass spectrometer under cold plasma conditions is an attempt to overcome isobaric interferences. Cold plasma conditions mean that lower forward power (RF power) is used for plasma generation in order to suppress the ionisation of elements with higher ionisation potential. Under conventional operation conditions (hot plasma) the Ar-

derived ions $^{38}Ar^1H^+$, $^{40}Ar^+$, $^{40}Ar^1H^+$, $^{40}Ar^1H_2$+, $ArO^+$, ArN+, $ArOH^+$ and $Ar_2^+$ are isobaric interferences of the isotopes of Ca, K, Fe and Se. Cold plasma inhibits the formation of argon-based polyatomic ions, spectral interferences from the plasma (Murphy et al. 2002), by reducing ionisation of Ar. Moreover, increase of nebuliser gas flow rate causes additional cooling of the plasma and improves reduction of Ar-based interferences (Vanhaecke et al. 2000). Addition of oxygen to the nebuliser gas can also create cold plasma conditions (Edlund et al. 2002). However, cold plasma conditions promote formation of matrix induced polyatomic ions. These matrix effects can be reduced by chemical separation prior to measurement.

Muprhy et al. (2000) successfully determined K and Ca isotopes with a forwarded power of 630 W. Kehm et al. (2003) used cold plasma for determination of Ar-interfered Fe isotopes. Whereas cold plasma is usually used to reduce molecular ion formation (Fietzke et al. 2004, Wollenweber et al. 1999), it can also be applied for separation of isobars with different ionisation potential. In the case of Sr, which has an ionisation potential of 5.7 eV, lower forward power is suggested to suppress the ionisation of Zr, with its ionisation potential of 6.8 eV. This approach is not commonly used for determination of radionuclides, but has been applied in a few cases (see 1.1.2.4).

Other elements in the lower mass region also profit from cold plasma conditions, even when they are not interfered in normal plasma mode. The limits of detection are improved due to reduced background noise level and enhanced ion transmission. Especially the improvement for Li and other low mass elements is caused by improved ion transmission efficiency due to the reduced space charge in cold plasma mode (Tanner 1995). Elements of higher mass generally show higher (worse) detection limits compared to normal plasma mode (Wollenweber et al. 1999).

Cold plasma can be used in the semiconductor industry for analysis of high purity reagents.

### 1.3.2 Collision and reaction cells

Recently, collision and reaction cells have become a common method in ICP-MS for elimination of isobaric interferences. Thus, ICP-MS Elan DRC II employs a dynamic reaction cell (DRC) which is situated before the mass analyser (fig. 5). The cell can be operated in standard mode or in pressurised (DRC) mode. In the standard mode, no gas is added to the cell and the reaction volume is evacuated through additional apertures (Cell Vent) into the high vacuum region of the analyser quadrupole. In this mode, the cell quadrupole acts as an rf only ion guide with a wide transmission bandpass. In the pressurised mode, the cell vent is closed and the target gas is added. The functions of a pressurised multipole in ICP-MS are ion focusing and guiding, gas phase ion-molecule reactions and energy focusing.

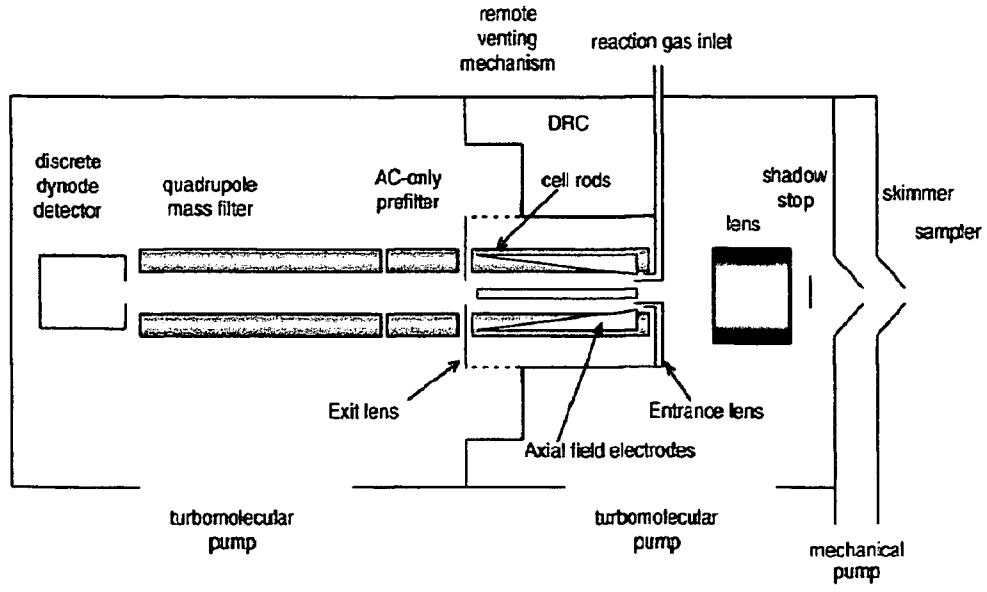


**Fig. 5** Schematic of ICP-QMS instrument with DRC

### 1.3.2.1 Fundamentals

Resolution or reduction of isobaric interference can be achieved by the use of chemical reactions (gas-phase reactions) in the analyte ion beam to selectively remove the interference ions by shifting them to another *m/z* ratio or generate a new analyte ion, which has a different mass. This is called chemical resolution. Therefore, collision and reaction cells have become a common method in ICP-MS for elimination of isobaric interferences. When choosing a reaction gas, different aspects have to be considered. The atomic or molecular mass of the gas should be relatively low to reduce the effects of collisional scattering (Tanner et al. 2002) and the reaction between reaction gas and analyte or reaction gas and interference should be highly efficient. As a basic principle, the reactivity of the reaction gas has to be totally different for the interfering ion and the analyte ion. Either the interference ion is removed by chemical reaction or the analyte ion is shifted to another mass to charge ratio, which can be analysed without interference. The reaction gas has to be highly pure but even in high purity gases impurities can be found that may form interferences in the cell (Yamada et al. 2002). Oxide ions are the most common challenge, due to high abundance of oxygen.

Reported work on gas phase ion-molecule reaction for elimination of isobaric interferences started in 1989 (Douglas, Rowan and Houk) and in 1997 collision and reaction cell ICP-MS was commercially introduced. Currently available quadrupole-based ICP-MS instruments that use collision cells and reaction cells are the Platform™ (GV Instruments), the ELAN® DRC™-e and ELAN® DRC™-II (Perkin Elmer-SCIEX), the X Series ICP-MS (Thermo Electron Corp.)

and the Agilent 7500cs and 7500ce systems. Whereas the analyser is a quadrupole, the collision/reaction cell can be any kind of multipole, a quadrupole, a hexapole or an octapole. A collision cell is used in place of an electrostatic analyser on the double focusing mass analyser of the multi collector sector field IsoProbe Instrument. A main difference of these instruments, besides the multipole type, is the way of controlling unwanted side reactions in the reaction cell and their interfering products. Post-cell kinetic energy discrimination (KED) is used in hexapole and octapole cell instruments to suppress the transport of unwanted in-cell products to the analyser. Selection of an appropriate mass bandpass of the quadrupole is applied for quadrupole cells, which is made possible by their unique stability characteristics, in order to suppress the formation of unwanted side products. (Nelms 2005)

The Mathieu stability diagram (fig. 6) visualises an (a,q) space, for which ions of mass *m* and charge *e* will have finite (stable) trajectory through the ideal infinite length quadrupole. The Mathieu parameters a and q are given in equation 1. Ions that are within the enclosed region are considered to be stable, while ions that are outside of this region are considered to be unstable. When a quadrupole is used as mass filter, the parameters a and q have to be near the apex of the stability diagram in order to achieve unit mass resolution, but when the quadrupole is used as collision/reaction cell, unit mass resolution is not necessary and the parameters can be lower. (Nelms 2005)

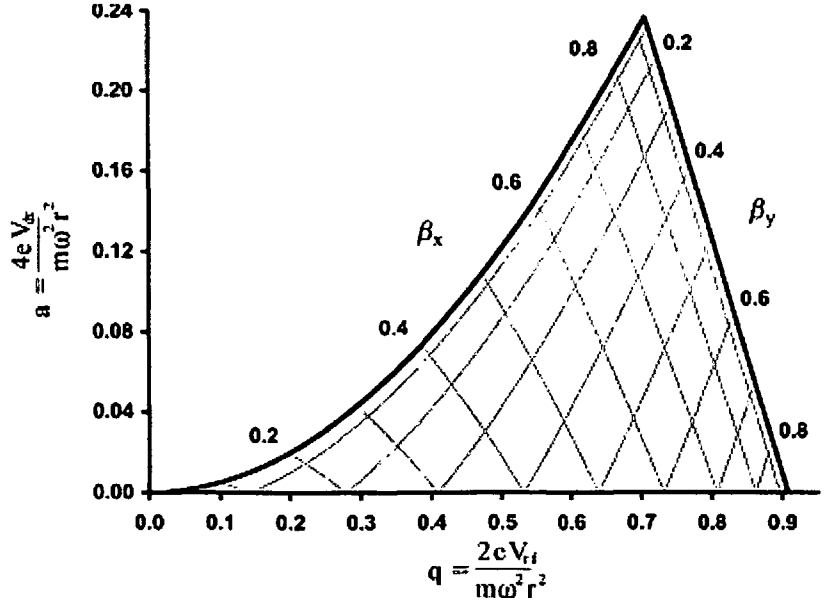


**Fig. 6** Stability diagram for a quadrupole (source: Tanner and Baranov 1999)

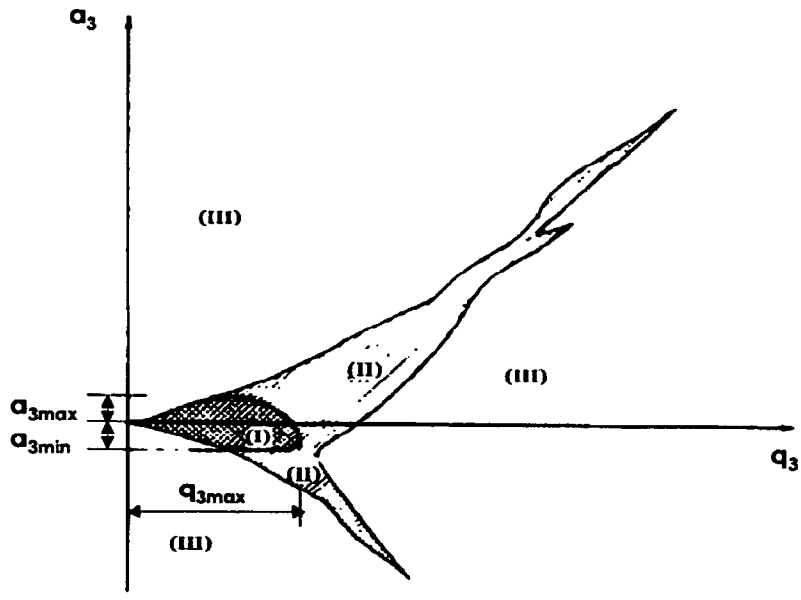


**Fig. 7** Stability diagram for a hexapole (source: Hagg and Szabo 1986)

Fig. 7 shows the stability diagram for a hexapole and represents that higher order multipoles lack stability boundaries. Three areas of stability are shown: I is stable, II is partially stable and III is unstable. The stability diagram for an octopole shows similarities.

Processes induced by collisions between ions and target gas atoms/molecules (neutrals) can be differentiated into

- collisional processes (momentum and energy transfer processes) and
- ion-molecule reactions (particle transfer processes).

### 1.3.2.2 Collisional processes

Unlike ion-molecule reactions, collisional processes do not change the identity of an ion, but may lead to damping of the ion kinetic energy, collisional focusing and excitation of the internal degrees of freedom of the ion or the neutral. Excitation can further lead to collision induced dissociation (CID) of an ion or a neutral. Collisions can cause ions to be lost from the ion beam, which is called scattering loss.

Multiple collisions of the ion result in a sequential loss of kinetic energy and reduce the width and magnitude of the kinetic energy distribution, which is called collisional energy relaxation or energy damping (Douglas et French 1992). Consequences are:

- increase in collision cross section and increase in probability of ion-molecule reactions,
- collisional focusing of ion trajectories toward the axis of an ion guide (rf-multipole),
- an increase in space charge density in the cell,
- an increase in ion transit time through the multipole and a

- temporal homogenisation of ion density fluctuations.

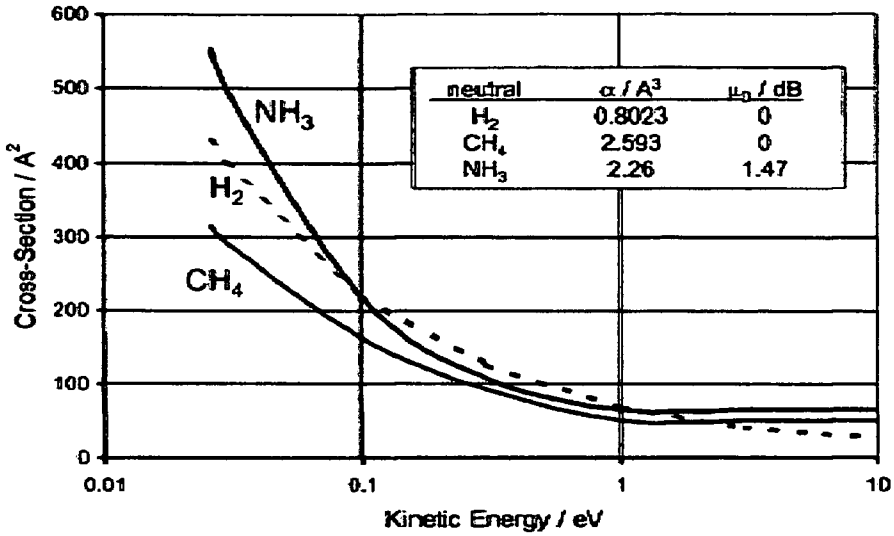


**Fig. 8** Calculated collision cross sections as a function of ion kinetic energy (source: Nelms 2005, p.359)

Fig. 8 shows that the collision cross section increases with reduction of ion energy, what leads to a higher number of collisions and therefore a higher reaction efficiency.

Collisional focusing leads to improvement of ion transmission. This effect strongly depends on the characteristics of the ion beam extracted from the plasma. The larger the energy spread of the beam, the greater the improvement in transmission will be. A further effect can be the improvement of the abundance sensitivity of the quadrupole analyser (Boulyga and Becker 2002).

Through energy damping, the time distribution of ion arrival at the detector can be changed, resulting in collisional broadening of transient signals. The degree of this collisional broadening depends on the pole bias, the entrance and exit aperture potentials, the Mathieu parameter q of the quadrupole and the properties of the target gas. Polyatomic gases produce more significant broadening. The broadening (temporal homogenisation) improves the precision of isotope ratio measurements (Bandura et al. 2000). The problem of using atomic gases for collisional homogenisation is that the number of collisions needed for temporal homogenisation leads to scattering losses of the ion signal. This may inhibit the improvement of ratio precision compared to non-pressurised cells. The use of a polyatomic gas for the chemical resolution of isobaric interferences offers the most practical case of collisional homogenisation. For example, the reactive gas $NH_3$ can be used for removing isobaric interferences and collisional homogenisation of the analyte ion populations. Non-reactive buffer gas, like Ne, can be used in addition to reaction gas to increase the degree of temporal homogenisation, when the optimal cell gas flow is too low for efficient temporal

homogenisation. Temporal homogenisation causes that rapid fluctuations of the ion intensities in the plasma are averaged out by mixing ions sampled at slightly different moments. Consequently, the influence of plasma flicker on the ratio of the sequentially measured intensities of the ion beams corresponding to different isotopes is reduced (Moens et al. 2001). The mass analyser rod offset potential should be negative relative to the DRC rod offset potential for efficient plasma noise damping. Otherwise the ions that are retained in the cell for the longest time, and are thus temporally homogenised and have lower kinetic energies, are otherwise rejected by KED (Bandura et al. 2000).

After collisional damping, the ion transmission depends mostly on the gas drift through the cell. The flow of gas can provide an axial flow that assists with ion penetration in the cell. Moreover, ion penetration into the cell and exit from the cell are assisted by axial electric fields established by the entrance and exit aperture potentials. Whereas the field in the entrance region is retarding for the positive ions inside the cell, at the exit it is accelerating. The combined axial field is defined by entrance and exit potential and space charge potential. (Nelms 2005)

Increase in transit time through the cell is one of the effects of slowing the ions by collisions. This can increase the settling time. Through energy damping, space charge density is dramatically increased in the cell and due to high ion current, space charge has a significant effect on ion transmission. When the cell electric parameters are abruptly changed, the space charge distribution in the cell may change and need to be re-established to a new steady state in order for ion transmission to stabilise. That means when a low *m/z* ratio is measured after a high *m/z* ratio, the cell needs some time to stabilise. For example, when jumping from *m/z* = 238 to *m/z* = 24, the $^{24}Mg^{+}$ signal is significantly suppressed at short dwell times, because the time is insufficient to re-establish the ion distribution within the cell. Longer dwell time means longer time for stabilisation of the ion distribution in the cell and eliminates signal suppression. But auxiliary electrodes for axial field generation (fig. 5) reduce the time needed for recovery following a mass jump from high mass. Consequently, the cell can be operated with a settling time similar to that of the quadrupole analyser and short dwell time. With the additional axial field produced by these electrodes, the ion distribution within the cell is rapidly re-established and the measured signals are largely independent of the dwell time. The main advantages of a DC axial field are

- compression of transit time distribution, which enables more rapid scanning,
- suppression of clustering reactions, because these reactions are very sensitive to the effective collision temperature and
- an increase of the space charge limit (Bandura et al. 2002).

Because these additional axial field electrodes have little effect on the stability characteristics of the r.f. fied of the pressurised quadrupole cell (Tanner et al. 2002), the bandpass control of sequential chemistry in a quadrupole reaction cell is not compromised.

A thermal condition is one under which an ensemble of particles has a Maxwell–Boltzmann energy distribution which has the same temperature in all degrees of freedom. A non-thermal condition is one under which an ensemble of particles has a non-Maxwell–Boltzmann energy distribution in one or more degrees of freedom. An example of a non-thermal ensemble is an ion beam (Tanner et al. 2002). To thermalize a system is to convert a nonthermal ensemble into a thermal ensemble, usually by means of spontaneous energy redistribution (equilibration). Thermalization in the case of an ion beam injected into a pressurized multipole can be achieved (to some extent) by means of multiple collisions with a buffer gas under thermal conditions (Tanner et al. 2002). Under thermalized conditions, the ion energy is defined by the cell bias potential, as the ions 'forget' the energy that they had at the ion source. Thermalization means thermal equilibrium with the environment.
Collisional energy damping refers to the loss of axial ion energy and the reduction of the width of the ion energy distribution towards thermalization with a collision gas.
Reaction enthalpy, which is important for ion-molecule reactions, is defined for thermalized ions and neutrals. Ion-molecule reactions occur under near-thermal conditions.

### 1.3.2.3 Ion - molecule reactions used in ICP-MS

Chemical resolution via ion-molecule reaction is the most universal method for interference suppression in ICP-MS. It facilitates resolving of atomic and polyatomic interferences and can be more specific compared to application of energy and momentum transfer processes (Nelms 2005).
Argide ions ($Ar^+$ and $ArX^+$) cause the most abundant interferences in ICP-MS. Since the corresponding neutrals will have relatively high ionisation potentials, charge transfer of the following type is the most useful type of reaction:

$$A^+ + B \rightarrow B^+ + A \qquad (Ar^+ + NH_3 \rightarrow NH_3^+ + Ar) \qquad (2)$$

For argide ions, this reaction is exothermic for a wide variety of neutrals. It is essential, that the ionisation potential of the reaction gas is higher than that of the analyte but lower than that of the interference. But there are cases for which no appropriate reaction gas is available for interference elimination by charge transfer. In such a case, another type of reaction can be applied, for example several forms of hydrogen-containing particle transfer:

Proton transfer:

$AH^+ + B \rightarrow BH^+ + A$ $\quad (ArH^+ + H_2 \rightarrow H_3^+ + Ar)$ (3)

Hydrogen atom transfer:

$A^+ + BH \rightarrow AH^+ + B$ $\quad (CaO^+ + CH_4 \rightarrow CaOH^+ + CH_3)$ (4)

Hydride ion ($H^-$) transfer:

$A^+ + BH \rightarrow B^+ + AH$ $\quad (Br^+ + CH_4 \rightarrow CH_3^+ + HBr)$ (5)

Another possibility is use of 'condensation reactions'. They involve transfer of other atoms than hydrogen and often result in rearrangement to a thermodynamically stable form. Due to selectivity and speed, oxidation reactions are promising:

$A^+ + BO \rightarrow AO^+ + B$ $\quad (Ba^+ + N_2O \rightarrow BaO^+ + N_2)$ (6)

Oxidising reaction gases are $O_2$, NO, $N_2O$, $NO_2$ and $CO_2$. $O_2$ reacts selectively with $Zr^+$ and $Y^+$, while it does not react with $Sr^+$ (Eiden et al. 1997, Favre et al. 2007). This makes $^{90}Sr$ measurement possible in the presence of $^{90}Zr$ and $^{90}Y$. Otherwise, $N_2O$ selectively oxidises $Sr^+$. This makes determination of $^{87}Sr^+$ in form of $^{87}SrO^+$ in the presence of $^{87}Rb$ possible. Reaction of $N_2O$ with $Ba^+$ is used for separation of $^{135,137}Cs/^{135,137}Ba$ and reaction of NO with $Hf^+$ is used for $^{176}Lu/^{176}Hf$ separation.

Another O-atom transfer reaction is O-atom abstraction of the type:

$AO^+ + B \rightarrow A^+ + BO$ $\quad (ArO^+ + CO \rightarrow Ar^+ + CO_2)$ (7)

Isotope ratio measurements of product oxide ions are complicated because oxygen is not monoisotopic. An alternative is selective reaction of $Sr^+$ with $CH_3F$. $Sr^+$ reacts to $SrF^+$, while the isobaric interference $^{87}Rb$ does not react. $^{19}F$ is monoisotopic and makes the measurement of the isotopic pattern of Sr possible (Moens et al. 2001).

In general, clustering reactions, for example of $NH_3$ or $H_2O$, have a negative role in reaction cell ion chemistry. But in a few cases clustering reactions help to measure an interfered analyte ion as cluster ion on another *m/z* ratio, which is less interfered. For example, Ti an Zn were measured as $TiNH^+ \cdot (NH3)$ at *m/z* = 114 and $Zn^+ \cdot (NH3)$ at *m/z* = 115. KED does not differentiate between unwanted in-cell formed polyatomic ions and desired product ions in respect of discrimination. It suppresses both. So for the procedure of measuring an analyte as product ion, the cell has to be operated under non-KED conditions. That means the quadrupole bias potential has to be set more negative than the collision cell bias. But without energy barrier, also other ion products may reach the analyser and probably increase the background at the *m/z* ratio of the analyte product. (Nelms 2005)

Bandpass tuning and kinetic energy discrimination are both techniques for suppression of unwanted in-cell produced polyatomic ions. While bandpass tuning avoids formation of interfering ions, the KED hinders the formed interfering ions from entering the mass analyser. Hattendorf and Günther (2004) found bandpass tuning to be the more efficient solution.

### 1.3.2.4 Dynamic bandpass control of unwanted cell chemistry

The Mathieu parameters (a,q) of the quadrupole field (given in equation 1) of the cell define a certain mass bandpass. By setting the DRC parameters Rpa and Rpq, which correspond to the Mathieu parameters a and q, to certain values, one can define which masses are stable in the quadrupole and which masses are not stable and therefore ejected from the field. By changing the wide open bandpass to a narrower bandpass, only a small mass range is stable, which averts formation of new unwanted ions in the cell. The narrower band pass mode can influence the analyte transmission and lead to 3- to 10-fold suppression of the analyte signal (Tanner et Baranov 1999, Hattendorf et Günther 2004), but collisional focusing might partly compensate for this losses. Bandpass tuning means the transmission window of the reaction cell quadrupole is narrowed in order to achieve certain *m/z* cut-off. Dynamic bandpass denotes that the mass bandpass is changed along with the mass scan of the analysing quadrupole.

The mass cut-off can be calculated using equation 1 and the stability diagram of the quadrupole (fig. 5). The parameter q controls the low mass cut-off for ions entering the cell, and the parameter a the high mass cut-off (Tanner et al. 2002). For example, measuring *m/z* = 90 with a = 0 and q = 0.6 results in no high mass cut-off and low mass cut-off of *m/z* = 60. By insertion of the measured mass-to-charge ratio and the q value in equation 1, one can calculate the value of $4V_{dc}/\omega^2 r_0^2$. Then, by insertion of another mass-to-charge ratio, like 60 for example, one can calculate the parameter a and q for this mass and have a look at fig. 5 if the mass is in the stability region or not. For *m/z* = 60, q is calculated to be 0.9 in this case. (0, 0.9) is at the brink of the stability diagram.

### 1.3.2.5 Kinetic energy discrimination

Kinetic energy discrimination (KED) is used in hexapole and octapole cell instruments to suppress the transport of the products of the side reactions to the analyser, whereas selection of an appropriate mass bandpass of the quadrupole is applied for quadrupole cells to suppress the formation of unwanted side products. Collision induced dissociation (CID) and KED are supra-thermal processes that are used for suppression of unwanted ions. These processes take place before thermalization occurs due to relaxation of ion kinetic energies. In-

cell produced ions have a potential that is close to the cell rod bias ($V_{CRO}$) and have little residual kinetic energy. The idea of KED is to set the analyser (quadrupole) rod bias ($V_{QRO}$) to a high enough value to stop in-cell formed ion from being transmitted through the analyser. Important for KED is a low number of collisions. Otherwise energy damping (thermalization) occurs and analyte and interference ions can no longer be distinguished on the basis of their energy differences. In other words, ion thermalization should not occur, or separation by post-cell energy barrier is not possible. An example of application of CID and KED is the suppression of $^{16}O_2^+$ interference on $^{32}S^+$ (Pröfrock et al. 2003). Suppression is achieved by use of xenon as collision gas, use of a 37 eV post-cell energy barrier between the analyser quadrupole and the cell multipole and charge transfer between $O_2^+$ and xenon. High efficiency in respect of energy damping of certain reaction gases, like $CH_4$, limits the usability of KED (Tanner et al. 2002). A different form of KED was discussed by Bandura et al. (2002) and is based on establishing a continuous retarding field inside the pressurised cell. The effects are deceleration and scattering of slower polyatomic ions, before the energies of the analyte ions are equilibrated by collisions and the analyte and in-cell produced ions are no more distinguishable. (Nelms 2005)

Further information about collision and reaction cells can be found in Nelms (2005) and in a review about collision and reaction cells in ICP-MS by Tanner et al. (2002). Information about method development concerning dynamic reaction cell (DRC) is provided by Tanner et al. (2002), Hattendorf and Günther (2003) and Olesik and Jones (2006).

# 2 Experimental

## *2.1 Sample preparation*

### 2.1.1 Samples

Three soil samples, KRA, RAD and MAS, were collected from the upper 0 - 1 cm soil layer in the Chernobyl vicinity by Dr. Sergei Boulyga. The soil was collected using a coring device that was specially designed to cut 1 cm thick soil layers down to a depth of 20 cm. The samples analysed represent upper (0 - 1cm) soil layer only. The samples were homogenised, ashed and $^{90}Sr$ activities were measured by beta-spectrometry in 1996. Remaining homogenised, ashed sample fractions were used within this work. The reference soil material IAEA-375 originates from a farm in Russia Brjansk and was certified after drying and homogenisation by interlaboratory comparison in 1990 (Mewis 2004). It has a certified $^{90}Sr$ activity of 108 ± 6 Bq

$kg^{-1}$ (IAEA 2003). An uncontaminated loamy soil sample from Austria, Mag 5_2, was used as control sample. This sample was not ashed.

### 2.1.2 Ashing

Ashing of the samples is no prerequisite for this method, but may facilitate the Sr/matrix separation.

The sample KRA, RAD and MAS had already been ashed when received. The uncontaminated soil sample Mag 5_2 was not ashed. At the beginning, IAEA-375 was not ashed, but after reproducible clogging of the columns during sample separation, it was ashed assuming this would put an end to this problem.

Therefore, three crucibles had to be glow to weight constancy. They were weighed, put into a muffle furnace (Medlin Naber GesmbH, Vienna, Austria) for four hours at 550°C, cooled down overnight in an exsiccator and weighed. The procedure was repeated with heating and cooling time reduced to one hour. Weight constancy was reached and the sample could be weighed into the crucibles. 5 g IAEA-375 were distributed into the three crucibles, ashed for four hours, cooled down overnight in the exsiccator and weighed. The loss of weight was 12%.

### 2.1.3 Sample digestion

Microwave digestion was performed using a high performance microwave digestion unit (MLS1200 mega, Milestone-MLS GmbH, Leutkirch, Germany). The first challenge was to optimise the digestion method for soil samples. At first, 0.4976 g IAEA-375 were digested with 4 mL $HNO_3$ and 1.5 mL $H_2O_2$. This procedure is used for environmental samples (Adout et al. 2007). 2 mL aqua regia (3:1, subboiled HCl and double-subboiled $HNO_3$), 1 mL HF and 1 mL $HClO_4$ had to be added after microwave-digestion for total digestion. Then 0.227 g IAEA-375 were digested using a digestion method for soil samples (Milestone 1996) using 4 mL HF + 1 mL $HClO_4$. Following microwave programme was used:

**Tab. 2** Time and power program of high performance microwave digestion unit

| time | power |
|---|---|
| 5 min | 250 W |
| 5 min | 400 W |
| 10 min | 600 W |
| 5 min | 250 W |

A larger sample volume had to be digested due to expected low activity for determination of $^{90}Sr$ activity in the soil samples. 1 g ashed soil was split into three fractions, which were

combined again after the microwave digestion. Each soil fraction was weighed into a teflon bomb and digested with 4.8 mL HF and 1.2 mL $HClO_4$. Then the three fractions were combined in PFA vessels and evaporated to near dryness using a hot plate (150°C). Then 3 mL aqua regia were added and the sample was heated in closed PFA vessels for 1-2 hours at 100°C. Subsequently remaining liquid was evaporated and the sample was filled up with 8 M $HNO_3$ to a weight of 10 g (1:10 dilution of the sample) for further matrix separation.

### 2.1.4 Sr/matrix separation

Sr-specific resin (EIChroM Industries Inc., Darien, IL, USA) with a particle size of 100-150 µm was used for Sr/matrix separation. It is a cation exchange resin and consists of crown ether (bis-t-butyl-cis-dicyclohexano-18-crown-6) absorbed on an inert substrate (EIChrom 2007). A vacuum sample processing manifold (VacMaster 10, Biotage, Uppsala, Sweden) was used to facilitate the passage of the sample through the resin. 2 mL of resin were packed in a column and conditioned with 5 mL 8 M $HNO_3$ after washing with water and 1% $HNO_3$. Then 2 mL of the sample were loaded onto the resin. The column was washed 30 times with 0.5 mL 8 M $HNO_3$. Sr was eluted with 10 times 0.5 mL subboiled $H_2O$. The aqueous samples were acidified with double-subboiled $HNO_3$ to a concentration of 1% (w/w) $HNO_3$. The solution was evaporated to 2 mL on a heating block, finally resulting in a 1:10 dilution of the original soil.

## *2.2 Reagents and standards*

Sr carbonate standard with defined Sr isotope composition (NIST SRM 987) and $^{86}Sr$ isotope spike were used for IDMS in order to determine the total natural Sr amount of the soil samples The concentration of the $^{86}Sr$ spike was determined by reverse IDMS with a Sr standard solution (CertiPUR®, ICP Standard, Merck, Darmstadt, Germany). Reagents used for the digestion of the soil samples were 48% ultrapur HF (Merck, Germany), 70% suprapur $HClO_4$ (Merck, Germany), 37% analytical grade HCl (Riedel-de Haën, Seelze, Germany) and 65% analytical grade $HNO_3$ (Merck, Germany). Solutions of Rb, Sr, Y and Zr were diluted from 1000 $mgL^{-1}$ stock solutions (Merck, Germany). All solutions were prepared in 1% $HNO_3$.

HCl was purified by single subboiling distillation and $HNO_3$ was purified by double subboiling distillation (Milestone-MLS GmbH, Leutkirch, Germany). Water was purified in a three step process by reverse osmosis followed by a laboratory-reagent grade water system purification (F+L GmbH, Vienna, Austria) and final subboiling distillation (Milestone-MLS GmbH, Germany).

IAEA-375 (International Atomic Energy Agency, Analytical Quality Control Services, Radionuclides in Soil, 250 g) was used as soil reference material.

Sr-specific resin (EIChroM Industries Inc., Darien, IL, USA) with a particle size of 100-150 µm was used for Sr/matrix separation.
Polyethylene flasks, tubes and pipet tips used for sample preparation and measurement process were successively cleaned with $HNO_3$ (10% w/w) and $HNO_3$ (1% w/w) and rinsed with deionised water before use.

## *2.3 ICP-MS instrumentation and measurement procedure*

A double-focusing sector field MC-ICP-MS instrument (Nu Plasma HR, Nu Instruments, Wrexham, Wales, UK) with a desolvating membrane nebuliser (DSN 100, Nu Instruments, UK) was used for determination of stable Sr concentrations in soil samples by isotope dilution mass spectrometry (IDMS). MC-ICP-MS possesses significantly higher precision of isotopic measurements than an ICP-MS with a single ion detector does and thus, allows obtaining more accurate concentrations when measured by IDMS. The concentration of the $^{86}Sr$ spike was determined by reverse IDMS with a Sr standard solution (1000 $mgL^{-1}$ Sr, Merck, Germany). The samples were spiked to an optimum $^{88/86}Sr$ ratio (blend ratio $R_B$) of 1:1, to minimise dead time effects (Prohaska et al. 2000), prior to digestion.

The concentration of Rb, Y and Zr in the contaminated soil samples and the separation efficiency of Sr/matrix separation were determined using an Element 2 (ThermoFinnigan, Bremen, Germany) HR-ICP-MS, because this instrument offers higher sensitivity compared to ELAN, which was favourable due to low concentrations to be measured. Calibration standards of 0.1, 0.2, 0.5, 1 and 2 ng $g^{-1}$ Rb, Sr, Y and Zr have been used for calibration. No internal standard was used.

The method for determination of $^{90}Sr$ was developed on a quadrupole ICP-MS instrument with dynamic reaction cell (ELAN DRC II, Perkin Elmer, Ontario, Canada). Oxygen (Linde AG, Höllriegelskreuth, Germany) with purity 5.0 (≥ 99.999 %) was introduced into the dynamic reaction cell as reaction gas. A second quadrupole ICP-MS with dynamic reaction cell (ELAN DRC-e, Perkin Elmer, Ontario, Canada) was employed for comparative determination of abundance sensitivity and for determination of background equivalent concentration. (The latter instrument is basically identically with the DRC II except for the capabilities of using $NH_3$ as reaction gas, which was not used within this work.) A cyclonic spray chamber (CPI International, Amsterdam, The Netherlands) in combination with a PFA nebuliser (solution uptake rate 0.94 g $min^{-1}$), an ultrasonic nebuliser (USN) "U-6000AT$^+$" (CETAC Technologies, Omaha, NE, USA) and Apex-IR (Elemental Scientific Inc., Omaha, NE, USA) high efficiency sample introduction system in combination with two different PFA nebuliser (solution uptake

rate 0.1 and 0.5 g $min^{-1}$) have been compared within this study. Instrumental parameters of the Elan DRC II are listed in tab. 3.

Isotopic ratio measurements on the Elan DRC ICP-MS were performed in dual detector mode. The $^{90}Sr^{+}$ ion intensities were acquired in pulse mode and the $^{86}Sr^{+}$ intensities were acquired in analogue mode. The analogue mode was calibrated against the pulse mode by sequential measurement of the isotopic ratio of $^{86}Sr/^{88}Sr$ in a 10 ng $g^{-1}$ solution in pulse mode and in 100 ng $g^{-1}$ solution by using pulse mode for $^{86}Sr^{+}$, and analog mode for $^{88}Sr^{+}$.

**Tab. 3** Parameters of ICP-DRC-MS with Apex-IR optimised for $^{90}Sr$ determination

| | |
|---|---|
| Radiofrequency power | 1300 W |
| Nebuliser gas flow rate | 1.14 L $min^{-1}$ |
| Auxiliary gas flow rate | 1.3 L $min^{-1}$ |
| Plasma gas flow rate | 14.25 L $min^{-1}$ |
| Cell gas ($O_2$) flow rate | 2.4 mL $min^{-1}$ |
| Lens Voltage | 6.1 V |
| RPq | 0.6 |
| Quadrupole rod offset | -7 V |
| Cell rod offset | -2 V |
| Cell path voltage | -28 V |
| Axial field voltage | 220 V |
| Number of sweeps | 50 |
| Number of readings | 1 |
| Number of replicates | 6 |
| Dwell time | 50 ms (m=86; 88; 89,5; 90,5)<br>200 ms (m=90; 92) |
| Total analysis time | ~ 4 min |

## *2.4 Isotope Dilution*

Isotope dilution (ID) is used to quantitatively determine the amount of analyte by adding an enriched isotopic spike of the same element to the sample containing an unknown amount of analyte (with usually natural isotopic composition) and by measuring the isotopic ratios of the diluted sample. It represents a method to measure an amount content based on the comparison of amounts of isotopes. The material enriched in one particular isotope is called spike material. If this spike is not certified for its isotopic composition or concentration, it must be quantified using a certified material. This material should be the element or a chemical compound of the element in the sample with known purity, and should preferably have the same (usually natural) isotopic composition as the element in the sample. This method is called reverse IDMS.

IDMS is a primary method of measurement, values are directly traceable to SI units and allow a closed uncertainty chain (Prohaska 2006, lecture: Chemisch Rechnen II).
The elemental amount is calculated with the IDMS equation.

$$C_X = C_Y \cdot \frac{m_Y}{m_X} \cdot \frac{R_Y - K_{R_B} \cdot R_B}{K_{R_B} \cdot R_B - K_{(R_i)_X} \cdot R_X} \cdot \frac{\sum\left(K_{(R_i)_X} \cdot (R_i)_X\right)}{\sum (R_i)_Y}$$

**Equ. 8** IDMS equation

| | |
|---|---|
| $C_X$ | concentration in the sample |
| $C_Y$ | concentration in the spike |
| $m_X$ | amount of sample (weighing) |
| $m_Y$ | amount of spike (weighing) |
| $R_X$ | ratio in the sample |
| $R_Y$ | ratio in the spike |
| $R_B$ | blend ratio |
| $R_{ix/y}$ | isotopic ratios in the sample/spike |
| K | correction factors (mass discrimination) |

## *2.5 External Calibration*

External calibration is a method for the determination of concentrations via calibration curves. The calibration curves in ICP-MS are in general linear over several orders of magnitude. This is a time-saving method for large sample numbers. Matrix and drift effects can be corrected via internal normalisation even though not all effects can be taken into account.

# 3 Results and Discussion

## *3.1 Concentration of Rb, Sr and Zr in soil samples*

### 3.1.1 IDMS results

Beside blank correction it is important to correct for isobaric interferences. Blank correction was done by manually subtracting the blank values from the sample values. The isobaric interference from $^{87}$Rb was corrected mathematically via the isotopic abundance of $^{85}$Rb. Therefore, $^{85}$Rb was measured to calculate the signal intensity of $^{87}$Rb with account to the corresponding natural isotopic abundances ($^{85}$Rb 72.165% and $^{87}$Rb 27.835%, KAERI 2000). The calculated $^{87}$Rb intensity was mass bias corrected applying the exponential mass fractionation law (Albarède et al. 2004). This intensity was subtracted from the blank-corrected $^{87}$Sr intensity. The reference material NIST SRM 987 (NIST 2007) was used for

calculation of the fractionation factor. The certified values are $^{86}Sr/^{88}Sr$ = 0.11935 +/- 0.00325, $^{87}Sr/^{86}Sr$ = 0.71034 +/- 0.00026 and $^{84}Sr/^{86}Sr$ = 0.05655 +/- 0.00014.

Fractionation factor:

$$F = \log (R_{Std,(86/88)} / R_{meas,(86/88)}) / \log (m_{86} / m_{88}) \quad (9)$$

$^{87}Sr$ - Rb corrected:

$$I_{87Sr\text{-}Rb\ corr} = I_{87Sr} - (A_{87Sr} / A_{85Rb}) * I_{85Rb} * (m_{87} / m_{85}) \wedge F \quad (10)$$

| | |
|---|---|
| F | mass bias per mass unit |
| $R_{Std,(86/88)}$ | certified value of $^{86}Sr/^{88}Sr$ ratio of SRM 987 |
| $R_{meas,(86/88)}$ | measured $^{86}Sr/^{88}Sr$ ratio |
| $m_{88}$ | molar mass of $^{88}Sr$ ($m_{88}$ = 87.905619) |
| $m_{87}$ | molar mass of $^{87}Sr$ ($m_{87}$ = 86.90918) |
| $m_{86}$ | molar mass of $^{86}Sr$ ($m_{86}$ = 85.909267) |
| $m_{85}$ | molar mass of $^{85}Rb$ ($m_{85}$ = 84.91180) |
| $I_{87Sr\text{-}Rb\ corr}$ | Rb corrected intensity of $^{87}Sr$ |
| $A_{87Sr}$ | abundance of $^{87}Sr$ ($A_{87Sr}$ = 27.8346 %) |
| $A_{85Rb}$ | abundance of $^{85}Rb$ ($A_{88Rb}$ = 72.1654 %) |

Concentrations and the total combined uncertainties were calculated with the GUM-workbench (Metrodata GmbH, Grenzach-Whylen, Germany) using the IDMS equation (Equ.8). The variable K, the correction factor for mass bias, was neglected, because the unspiked and the spiked samples were measured in the same run. Results of the IDMS are given in tab. 4. The Sr concentrations in the three soil samples were 16.36 ± 0.10, 63.93 ± 0.40 and 19.18 ± 0.12 µg $g^{-1}$, respectively.

**Tab. 4** Total natural Sr amount of the spike and the contaminated soil samples

| Sample | Sr conc [µg $g^{-1}$] | Uncertainty | coverage factor | coverage (normal) |
|---|---|---|---|---|
| $^{86}Sr$ spike | 106.95 | 0.64 | 2 | 95% |
| IAEA-375 | 99.05 | 0.61 | 2 | 95% |
| KRA | 16.36 | 0.10 | 2 | 95% |
| RAD | 63.93 | 0.40 | 2 | 95% |
| MAS | 19.18 | 0.12 | 2 | 95% |

### 3.1.2 External Calibration results

External calibration was performed in order to determine the total Rb, Y and Zr concentration of the contaminated soil samples in order to asses the separation factors of Zr which are required for determination of $^{90}Sr$. Results are listed in tab. 5. The Zr concentration amounted to 74, 86 and 64 µg $g^{-1}$ in the three soil samples, respectively. That corresponded to the

concentrations of 6-9 μg $g^{-1}$ Zr it the soil digests as soil samples were diluted by about ten fold after digestion. Total Sr concentration determined by external concentration is 27 – 39 % lower than determined by IDMS, probably due to high dilution of the samples. Only the Sr concentration of the sample RAD is higher by 6 % when determined by external calibration. Accordingly, the other elemental concentrations might also differ from their real values. No internal standard was used. The measurement was performed to get a rough estimation of the order of magnitude of Zr present in those soil samples.

The results for calculating the separation efficiency of Sr/matrix separation by measuring separated and unseparated samples are given in chapter 3.3.1.

**Tab. 5** Elemental concentrations in soil samples in μg $g^{-1}$. Standard uncertainty is 20%.

| Sample | Rb | Sr | Y | Zr |
|---|---|---|---|---|
| IAEA - 375 | 25 | 72 | 11 | 390 |
| KRA | 11 | 10 | 1 | 74 |
| RAD | 16 | 68 | 7 | 86 |
| MAS | 13 | 14 | 2 | 64 |

## *3.2 Sensitivity*

Sensitivity is a complex function of different parameters, mainly influenced by the sample introduction on a given system. High sensitivity for Sr detection has been as important as eliminating interferences at *m/z* = 90 for this work. The performance of different sample introduction systems has been compared including a cyclonic spray chamber, an ultra-sonic nebuliser (USN) and an Apex-IR high efficiency sample introduction system. Results of sensitivity studies with these 3 systems are summarised in tab. 6. The highest absolute sensitivity of ~130 counts per fg Sr was achieved with Apex-IR equipped with a PFA 100 nebuliser. The cyclonic spray chamber in combination with PFA 1639 showed the lowest sensitivity of all systems. The USN allowed a significant sensitivity enhancement in comparison to the cyclonic spray chamber, but both sample introduction systems, cyclonic spray chamber and USN, require higher solution uptake rates, which is unfavourable due to the small sample volumes which were available (which are 2 mL). The sample uptake of the USN is 0.5 – 2.5 mL/min, whereas the Apex-IR has a sample uptake of 20 – 600 μL $min^{-1}$. Higher sample volumes increase the costs for sample preparation and small sample volume is favoured since contamination of the instrument and handling of highly active samples are critical issues.

USN and Apex-IR were used without membrane desolvation, because no further drying of the aerosol was necessary. On the contrary, oxide formation through remaining water was favoured. Moreover, wet aerosol conditions increase the cold plasma effect because more

energy is necessary for ionisation. Strong bonds of oxides usually withstand plasma conditions (Jakubowski 1998).

Higher sensitivity compared to standard introduction system is achieved by production of very fine aerosol (USN) and drying of the aerosol (Apex-IR).

The uptake of the sample introduction systems was determined gravimetrically. Therefore, an eprouvette was filled with 1% $HNO_3$ and weighted before and after 10 minutes of measurement on the ELAN DRC II. Solution uptake rates are listed in tab. 6.

USN heater temperature was 140°C and cooler temperature was -4°C.

**Tab. 6** Absolute sensitivity of Sr achieved with different sample introduction systems.

| Introduction system | Uptake [g $min^{-1}$] | Sr [counts $fg^{-1}$] | Cell gas flow [mL $min^{-1}$] | ELAN instrument | Nebuliser gas flow [L $min^{-1}$] |
|---|---|---|---|---|---|
| Cyclonic spray chamber + PFA 1639 | 0.94 | 5 | 0 | DRC II | not registered |
| USN (pump speed 100) | 0.51 | 26 | 0 | DRC II | 1.15 |
| USN (pump speed 167) | 0.74 | 34 | 0 | DRC II | not registered |
| USN (pump speed 100) | 0.51 | 38 | 2.5 | DRC II | 1.08 |
| USN (pump speed 100) | 0.51 | 40 | 0 | DRC II | 1.05 |
| Apex + PFA 1639 | 0.51 | 54 | 0 | DRC-e | 0.95 |
| Apex + PFA 1639 | 0.51 | 100 | 0 | DRC-e | 1.10 |
| Apex + PFA 100 | 0.10 | 129 | 2.5 | DRC II | 1.10 |

## *3.3 Separation*

### 3.3.1 Sr/matrix separation

Chemical separation of Sr from interfering elements such as Rb, Y and Zr was performed using a Sr-specific resin. 0.5 mL and 2 mL of resin have been used for optimisation of Sr/matrix separation. The recovery rate of Sr was generally close to 100 % in both cases (Tab 7). Only IAEA-375 showed low Sr recovery due to clogging during separation. Sr recovery for IAEA-375 was only about 16% when using 2 mL resin. The cause might be problems during separation procedure (reproducible clogging of the column).

**Tab. 7** Sr recovery in %. Standard uncertainty is 10%.

| | Sr recovery [%] | |
|---|---|---|
| | 0.5 mL resin | 2 mL resin |
| IAEA-375 | 94 | 16 |
| KRA | 108 | 92 |
| RAD | 113 | 98 |
| MAS | 99 | 80 |

Separation in % and separation efficiencies are summarised in tab. 8. The Zr/Sr separation efficiency of the liquid chromatography (LC) procedure is defined as:

$$S_{LC} = (C_{fin}/C_{init})_{Zr}/(C_{fin}/C_{init})_{Sr} \quad (11)$$

$C_{fin}$ finale concentration (concentration after Sr/matrix separation)
$C_{init}$ initial concentration (concentration before Sr/matrix separation)

Zr separation efficiency was generally < 2 x $10^{-4}$ when using 2 mL resin and this approach was therefore used for further separations. However, a separation efficiency of 2 x $10^{-4}$ was still not sufficient for interference-free determination of $^{90}Sr$ in soils as the initial Zr concentration in samples was higher by $10^6$ to $10^7$ times than the expected $^{90}Sr$ concentration.
IAEA-375 shows inferior separation efficiency compared to the other three soil samples.

**Tab. 8** Separation efficiency of liquid chromatography procedure. Standard uncertainty is 10%.

| | Separation [%] | | $S_{LC}$ | |
|---|---|---|---|---|
| | 0.5 mL resin | 2 mL resin | 0.5 mL resin | 2 mL resin |
| | **Rubidium** | | | |
| IAEA-375 | 93 | 96 | 8.2E-02 | 1.6E-01 |
| KRA | 100 | 100 | 2.6E-03 | 1.2E-03 |
| RAD | 99 | 97 | 6.3E-03 | 2.6E-02 |
| MAS | 100 | 100 | 4.3E-03 | 1.3E-03 |
| | **Yttrium** | | | |
| IAEA-375 | 97 | 99 | 3.2E-02 | 5.2E-02 |
| KRA | 98 | 99 | 2.1E-02 | 5.6E-03 |
| RAD | 100 | 100 | 3.4E-03 | 3.9E-03 |
| MAS | 98 | 100 | 1.9E-02 | 3.8E-03 |
| | **Zirconium** | | | |
| IAEA-375 | 100 | 100 | 8.9E-04 | 1.2E-03 |
| KRA | 100 | 100 | 5.9E-04 | 7.9E-05 |
| RAD | 100 | 100 | 2.0E-04 | 1.7E-04 |
| MAS | 100 | 100 | 7.9E-05 | 2.0E-04 |

### 3.3.2 On-line Zr/Sr separation in ICP-MS by using cold plasma condition and gas-phase reaction with oxygen in a DRC

Both the effect of cold plasma conditions and reaction with oxygen in a dynamic reaction cell were investigated for favorably minimising the Zr signal compared to the $^{88}Sr$ signal.
The Zr/Sr separation efficiency of on-line procedure is defined as:

$$S_{online} = {}^{90}Zr/Sr = (I_{Zr\text{-}90}/C_{Zr}) /(I/C)_{Sr} \qquad (12)$$

I intensity
C concentration

This separation factor was introduced to compare different experiments during method development. The lower the separation factor, the better the separation.

#### 3.3.2.1 Cold plasma

Figs. 9 - 20 and A1 – A10 (Appendix) show the effect of Rf power on the intensity of Sr and Zr, the separation factor $^{90}Zr/Sr$ and the oxide formation of Rb, Sr, Y and Zr. Rf power was varied from 600 – 1300 W and experiments were performed with same parameters under different nebuliser gas flow rates. The nebuliser gas flow rate determines the residence time of aerosol in the ICP. Higher nebuliser gas flows are known to cause additional cooling of the plasma (Vanhaecke et al. 2000). Different sample introduction systems have been tested: cyclonic spray chamber + PFA nebuliser (Figs. 9 – 12, A1 – A8), ultrasonic nebuliser (Figs. 13 – 14, A9 - A10) and Apex-IR + PFA nebuliser (Figs. 15 – 20).

Intensity of Sr, Y and Zr, oxide formation and the separation factor $^{90}Zr/Sr$ were studied under varying Rf power from 600 to 1300 W and under different nebuliser gas flow rates. The intensity of Zr (10 ng $g^{-1}$ solution) could be suppressed effectively under cold plasma conditions and the separation factor was improved, but a significant decrease in the intensity of Sr was also observed. Moreover, an increased rate of molecular ions probably formed from matrix elements was observed at several masses including *m/z* =90. This is in contrast with previous studies by Vonderheide et al. (2004) and Zoriy et al. (2005) that used double-focusing sector field ICP-MS with mass resolution of m/Δm 4000, which offered (i) higher sensitivity for Sr at cold plasma conditions and (ii) a possibility to resolve isobaric interferences by molecule ions with $^{90}Sr$. Thus, cold plasma conditions can be employed for $^{90}Sr$ analysis by sector field ICP-MS but such an approach is not very useful in the case of quadrupole ICP-MS, since signal-to-background ratio is not satisfactory in the later case.
These effects are explained in detail for the different nebulising units in the following chapter.

#### *3.3.2.1.1 Cyclonic spray chamber + PFA nebuliser*

Measurements pictured in figs. 9 - 12 and A1 – A8 were performed on the ELAN DRC II, using PFA nebuliser 1639 in combination with a cyclonic spray chamber.

Figs. 9 and 10 demonstrate the effect of Rf power using a nebuliser gas flow rate of 1.1 L $min^{-1}$. Further results of experiments using higher nebuliser gas flow rate of 1.15 $min^{-1}$ are presented in figs. A1 and A2. Oxide formation and separation factor are improved by higher nebuliser gas flow rate, whereas intensities decrease. The highest intensities for Sr ions are achievable using hot plasma conditions.

In fig. 9, a smaller intensity maximum of Sr in the cold plasma area from 600 to 900 W can bee seen at 750 W RF power. A similar effect was seen by Vonderheide et al. (2004) who tested the cold plasma approach for measurement of $^{90}Sr$ in urine. In that work a quadrupole-based ICP-MS instrument with hexapole collision cell (Platform, Micromass Ltd., Manchester, UK) and a double-focusing sector field ICP-MS instrument (Element 1, ThermoFinnigan, Bremen, Germany) in medium mass resolution were used. On the Platform, an $^{88}Sr$ intensity of more than 2.5 x $10^6$ cps was achieved with 900 – 950 W Rf power in a 50 ng $g^{-1}$ Sr solution. On the Element 1, a Sr maximum in the cold plasma area was achieved by tuning the instrument at 750 W. This equated to higher nebuliser gas flow and higher ion focus lens voltage than under hot plasma conditions. The Sr maximum in the cold plasma area is quite low, compared to ICP-CC-MS. This may be due to the additional focusing that occurs with the hexapole of the quadrupole instrument as the cell is still pressurised with gases from the plasma even when not purposely in use (Vonderheide et al. 2004).

Figs. 9, 11, A1, A3, A5 and A7 show a Sr intensity maximum in the cold plasma area, but the intensity achieved is not higher than 1 x $10^5$ in a 10 ng $g^{-1}$ Sr solution and the separation factor is not satisfactorily low.

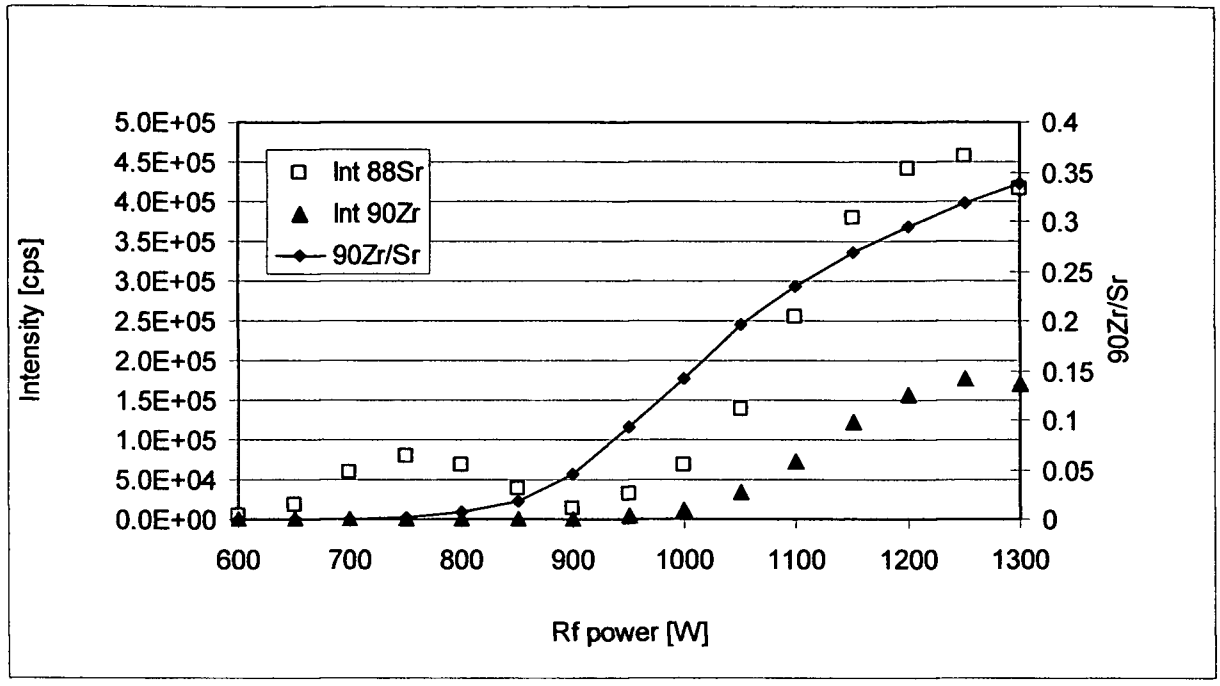


**Fig. 9** Effect of Rf power on the response of $^{88}Sr$ and $^{90}Zr$. Rb, Sr, Y and Zr concentration is 10 ng $g^{-1}$. Nebuliser gas flow rate is 1.0 L $min^{-1}$.

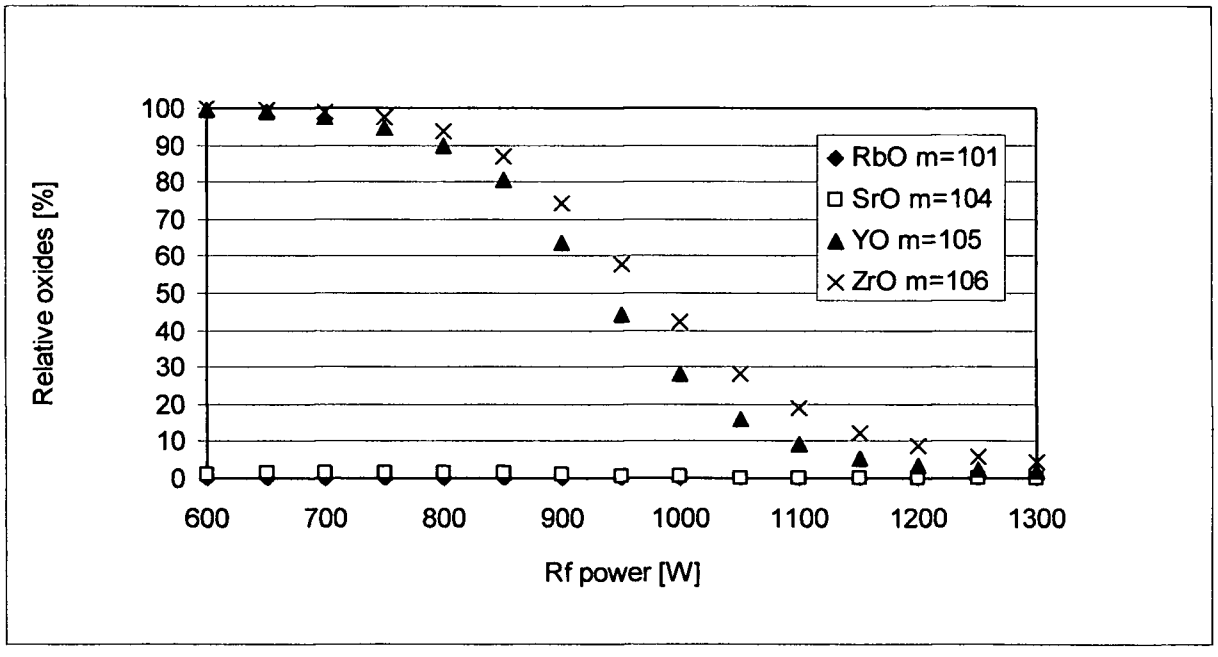


**Fig. 10** Effect of Rf power on the oxide formation of Rb, Sr, Y and Zr. Concentration is 10 ng $g^{-1}$. Nebuliser gas flow rate is 1.0 L $min^{-1}$.

Figs. 11 – 12 and A3 – A8 show the effect of low Rf power under varied nebuliser gas flow rates and auxiliary gas flow rates. Rf power is varied from 650 - 950 W. An increase of the nebuliser gas flow rate from 1.0 L $min^{-1}$ to 1.1 $min^{-1}$ or 1.2 $min^{-1}$ involves improvement of the

separation factor and the oxide formation. The maximum Sr intensity in the cold plasma region is shifted from 700 to 750 W by use of higher nebuliser gas flow rate. This was expected since higher nebuliser gas flow rates lead to additional cooling of the plasma and thus, higher energy is required in order to reach the same conditions as at lower flow rates. There is no significant difference concerning separation factor, intensities and oxide formation in the cold plasma region between use of 1.1 and 1.2 L $min^{-1}$ nebuliser gas flow rate. Increase of the auxiliary gas flow rate from 1.1 to 1.2 L $min^{-1}$ involves improvement of the separation factor.

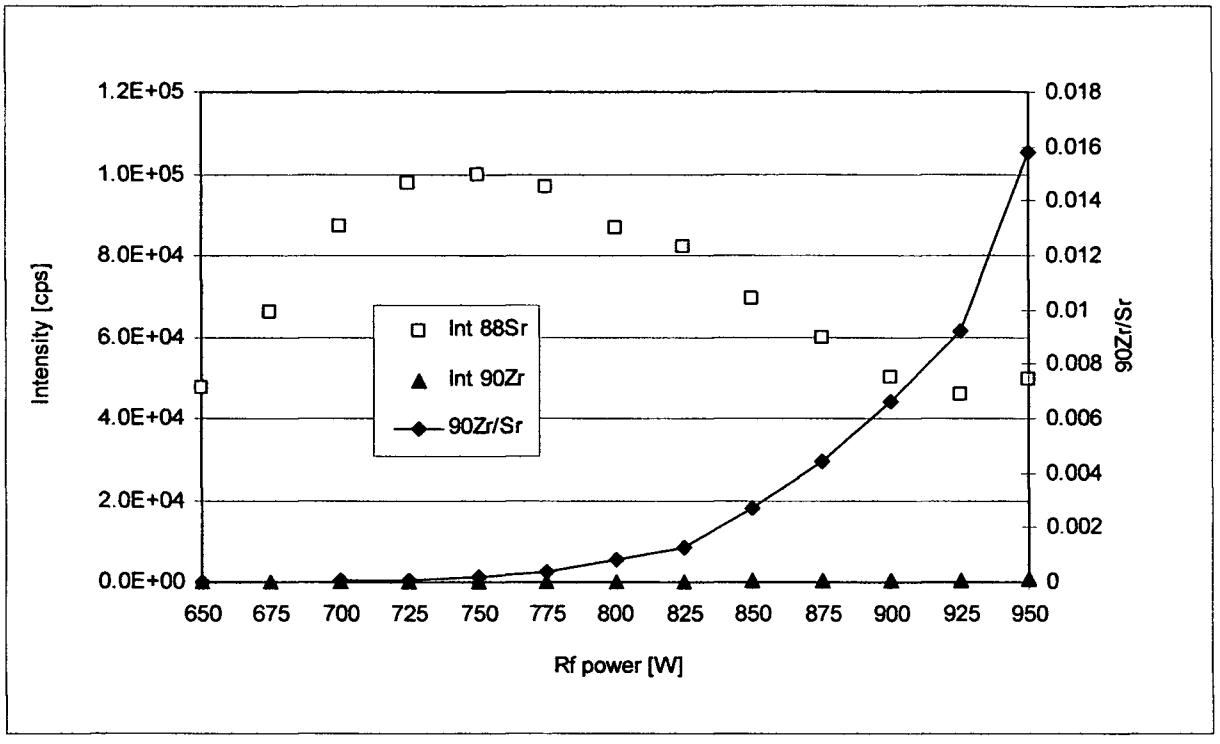


**Fig. 11** Effect of Rf power on the response of $^{88}Sr$ and $^{90}Zr$. Rb, Sr, Y and Zr concentration is 10 ng g-1. Nebuliser gas flow rate is 1.1 L $min^{-1}$ and auxiliary gas flow rate is 1.1 L $min^{-1}$.

Fig. 11 shows the Sr intensity maximum in the cold plasma region that was mentioned before. Sr has a lower ionisation potential than Zr and is therefore more easily ionised than Zr with less energy. The reason for this increase in intensity could be enhanced ion transmission.

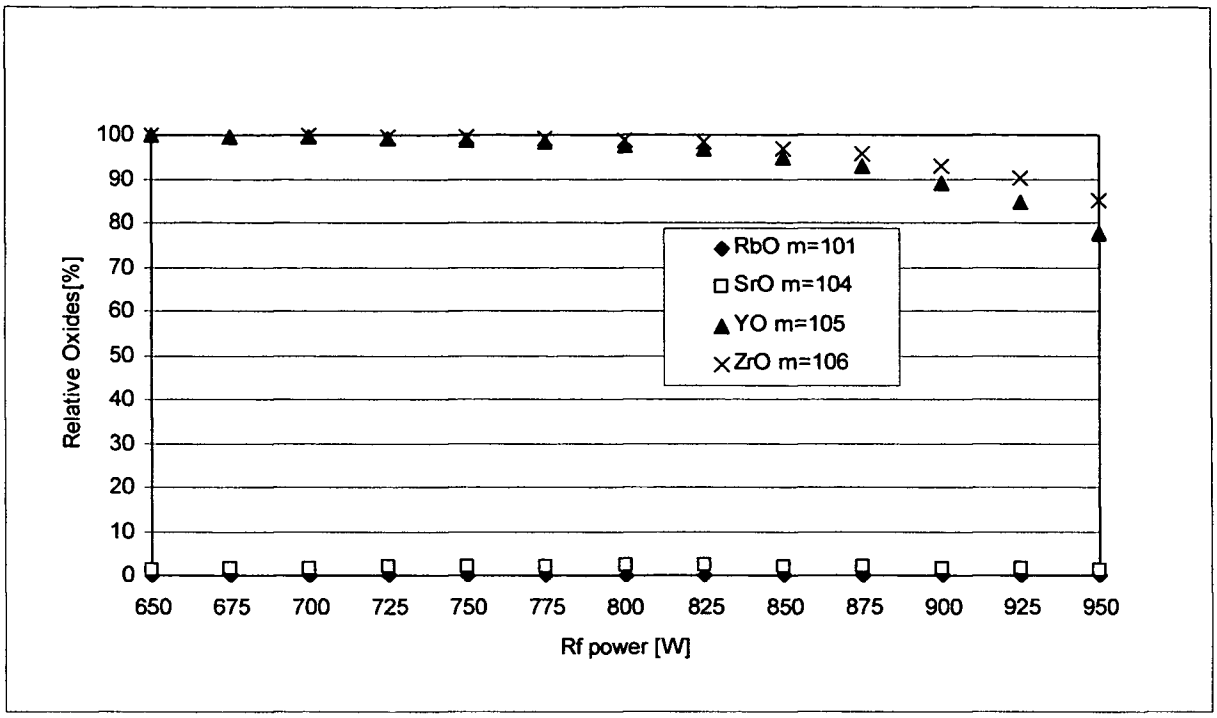


**Fig. 12** Effect of Rf power on the oxide formation of Rb, Sr, Y and Zr. Concentration is 10 ng g-1. Nebuliser gas flow rate is 1.1 L $min^{-1}$ and auxiliary gas flow rate is 1.1 L $min^{-1}$.

### *3.3.2.1.2 Ultrasonic nebuliser*

The USN was used without desolvation membrane unit in order to enhance oxide formation of interfering Zr. The desolvation membrane additionally dries the aerosol, but remaining water is favoured to oxidise Zr and increase the cold plasma effect. Measurements pictured in figs. 13 – 14 and A9 – A10 were performed on the ELAN DRC II, using USN with a sample uptake rate of 500 µL $min^{-1}$. Sr intensity is improved by use of USN compared to use of PFA nebuliser and cyclonic spray chamber, because the USN produces very fine droplets, an aerosol easy to ionise, and dries the aerosol. Figs. 13 and 14 demonstrate the effect of Rf power with a nebuliser gas flow rate of 1.05 L $min^{-1}$. Nebuliser gas flow rate is increased to 1.15 L $min^{-1}$ in figs. A9 and A10.

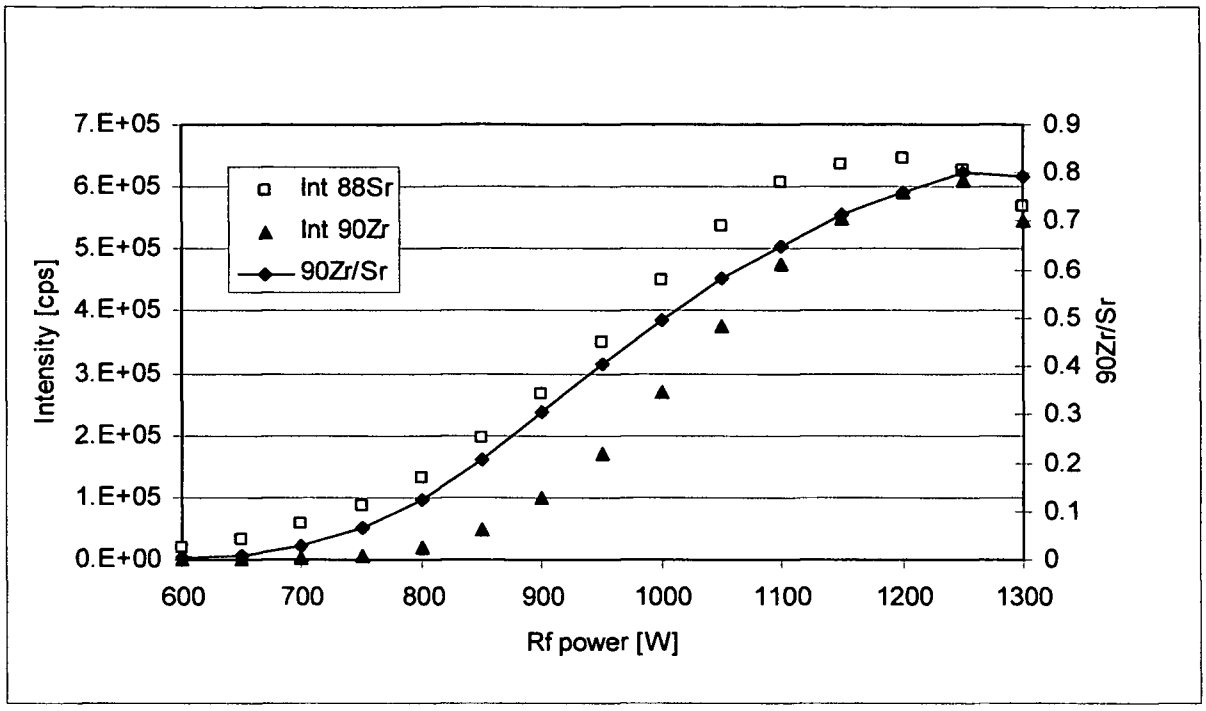


**Fig. 13** Effect of Rf power on the response of $^{88}Sr$ and $^{90}Zr$. Sr, Rb and Y concentration is 2 ng $g^{-1}$ and Zr concentration is 5 ng $g^{-1}$. Nebuliser gas flow rate is 1.05 L $min^{-1}$.

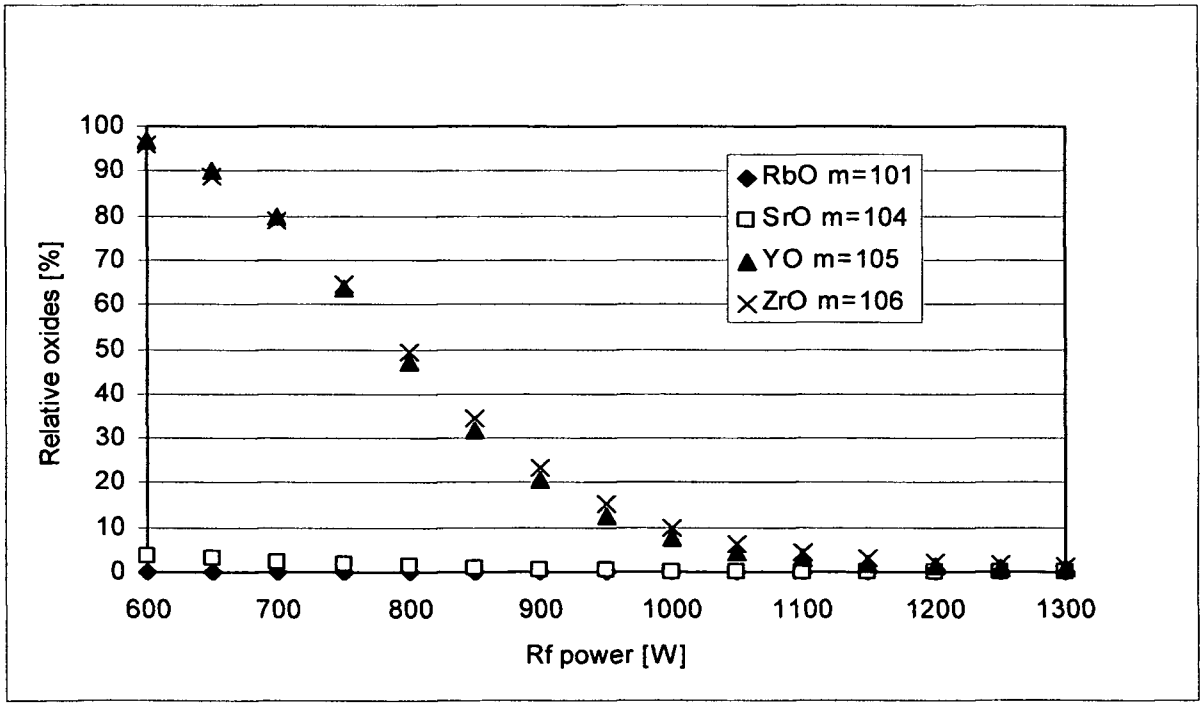


**Fig. 14** Effect of Rf power on the oxide formation of Rb, Sr, Y and Zr. Sr, Rb and Y concentration is 2 ng $g^{-1}$ and Zr concentration is 5 ng $g^{-1}$. Nebuliser gas flow rate is 1.05 L $min^{-1}$.

Higher nebuliser gas flow rate (1.15 compared to 1.05 L $min^{-1}$) improved oxide formation and the separation factor and decreased the intensity of Sr.

There was no increase of Sr intensity in the low Rf power region, when the effect of Rf power was studied using USN, unlike it was observed during application of cyclonic spray chamber with PFA nebuliser.

### *3.3.2.1.3 Apex-IR*

Figs. 15 and 16 picture measurements on ELAN DRC-e using PFA nebuliser 1639, with a solution uptake rate of 500 µL $min^{-1}$. Nebuliser gas flow rate is 1.1 and 0.95 L $min^{-1}$ respectively.

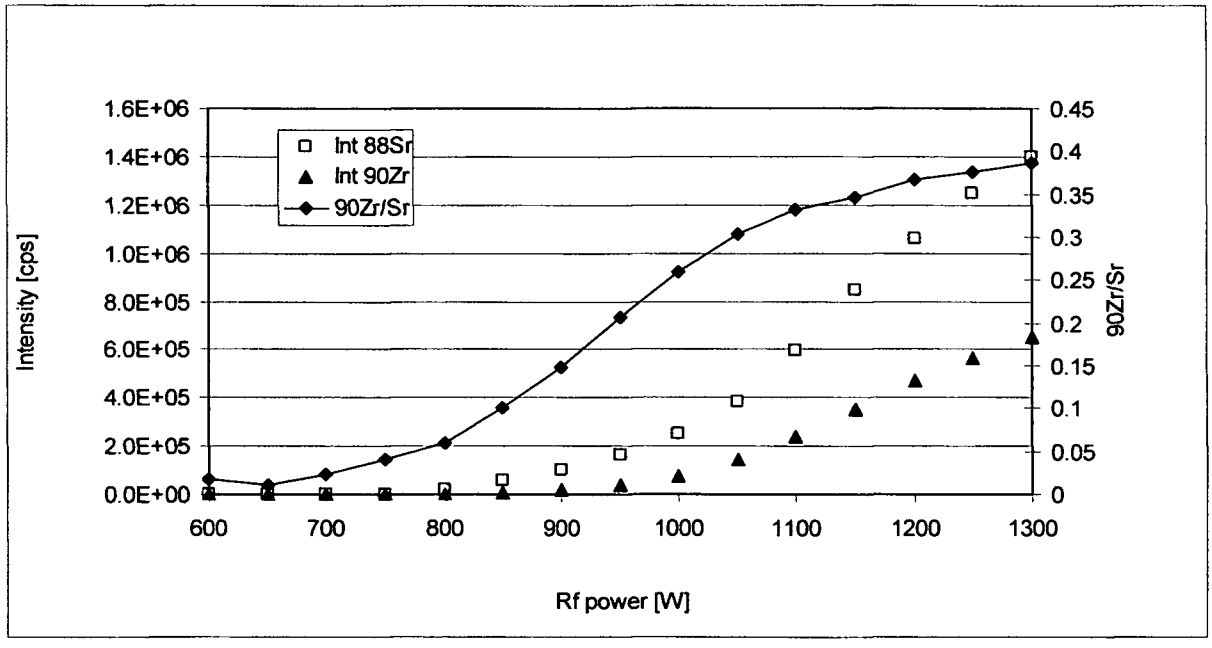


**Fig. 15** Effect of Rf power on the response of $^{88}Sr$ and $^{90}Zr$. Rb, Sr, Y and Zr concentration is 10 ng $g^{-1}$. Nebuliser gas flow rate is 1.1 L $min^{-1}$.

The maximum Sr intensity with a nebuliser gas flow rate of 1.1 lies at 1300 W, while the maximum Sr intensity with a nebuliser gas flow rate of 0.95 lies at 950 W. A lower nebuliser gas flow rate seems to be favourable under cold plasma conditions with regard to intensity of Sr. On the other hand, the separation factor is improved under cold plasma conditions by use of higher nebuliser gas flow rate. The nebuliser gas flow rate has no significant influence on the separation factor under hot plasma conditions.

In Fig. 16 it can be seen that a Sr intensity of more than 1.3 x $10^6$ cps is reached in a 10 ng $g^{-1}$ Sr solution at 950 W, but the separation factor is not very satisfactory.

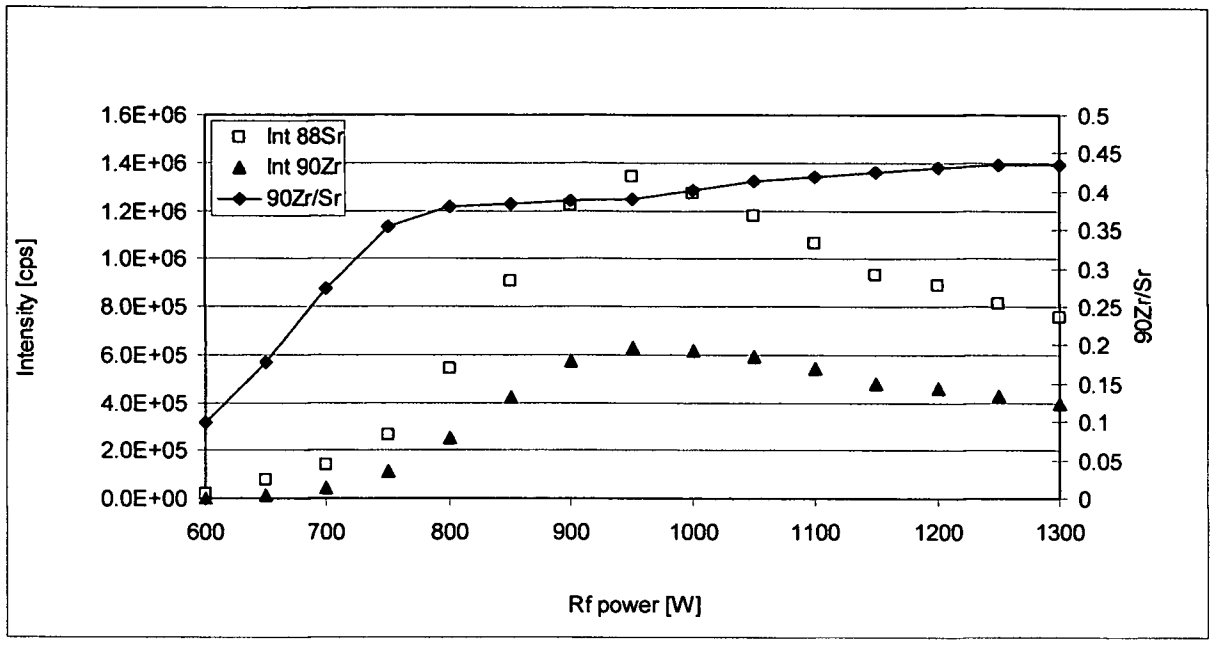


**Fig. 16** Effect of Rf power on the response of $^{88}Sr$ and $^{90}Zr$. Rb, Sr, Y and Zr concentration is 10 ng $g^{-1}$. Nebuliser gas flow rate is 0.95 L $min^{-1}$.

Figs. 17 and 18 show the results of measurements performed on ELAN DRC II using a PFA nebuliser with a sample uptake rate of 100 µL $min^{-1}$ and a nebuliser gas flow rate of 1.15 L $min^{-1}$. Intensity of $^{86}Sr$ is observed instead of $^{88}Sr$, because intensity of $^{88}Sr$ was above the limit of ion counting mode at 1250 and 1300 W Rf power.

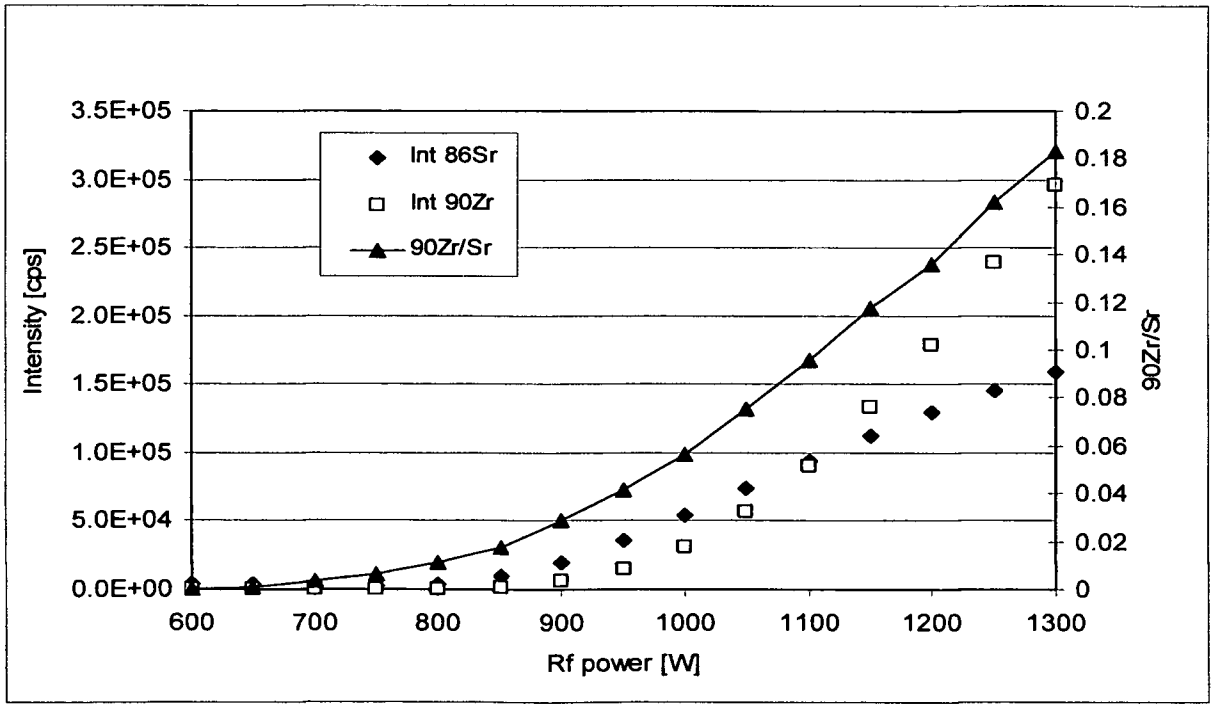


**Fig. 17** Effect of Rf power on the response of $^{86}Sr$ and $^{90}Zr$. Rb, Sr, Y and Zr concentration is 10 ng $g^{-1}$. Nebuliser gas flow rate is 1.15 L $min^{-1}$.

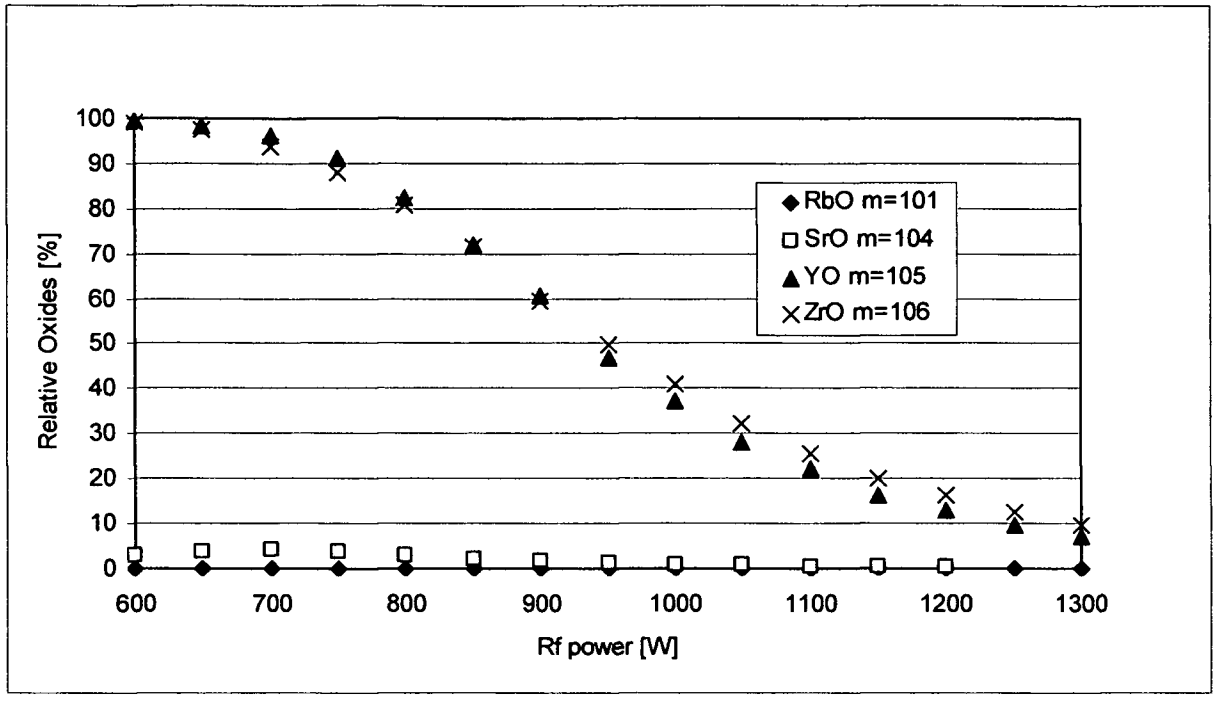


**Fig. 18** Effect of Rf power on the oxide formation of Rb, Sr, Y and Zr. Concentration is 10 ng $g^{-1}$. Nebuliser gas flow rate is 1.15 L $min^{-1}$.

Figs. 19 and 20 show measurement results using an ELAN DRC II equipped with the PFA nebuliser 1639 applying a solution uptake rate of 500 µL $min^{-1}$. Settings are the same as in figs. 17 and 18, nebuliser gas flow rate is 1.15 L $min^{-1}$ and auxiliary gas flow rate 1.1 L $min^{-1}$. A nebuliser with higher solution uptake rate is used and this time Apex-IR is not cooled, in order to enhance the cold plasma effect through wet aerosol. Strontium concentration was reduced to 2 ng $g^{-1}$, compared to previously used 10 ng $g^{-1}$, because $^{88}Sr$ intensity was too high to be measured under hot plasma conditions in counting mode.

An increase of Sr intensity in the cold plasma region, around 700 W Rf power, can be seen in fig. 19 but the intensity is with less 2 x $10^3$ cps rather low. Again, $^{86}Sr$ was monitored.

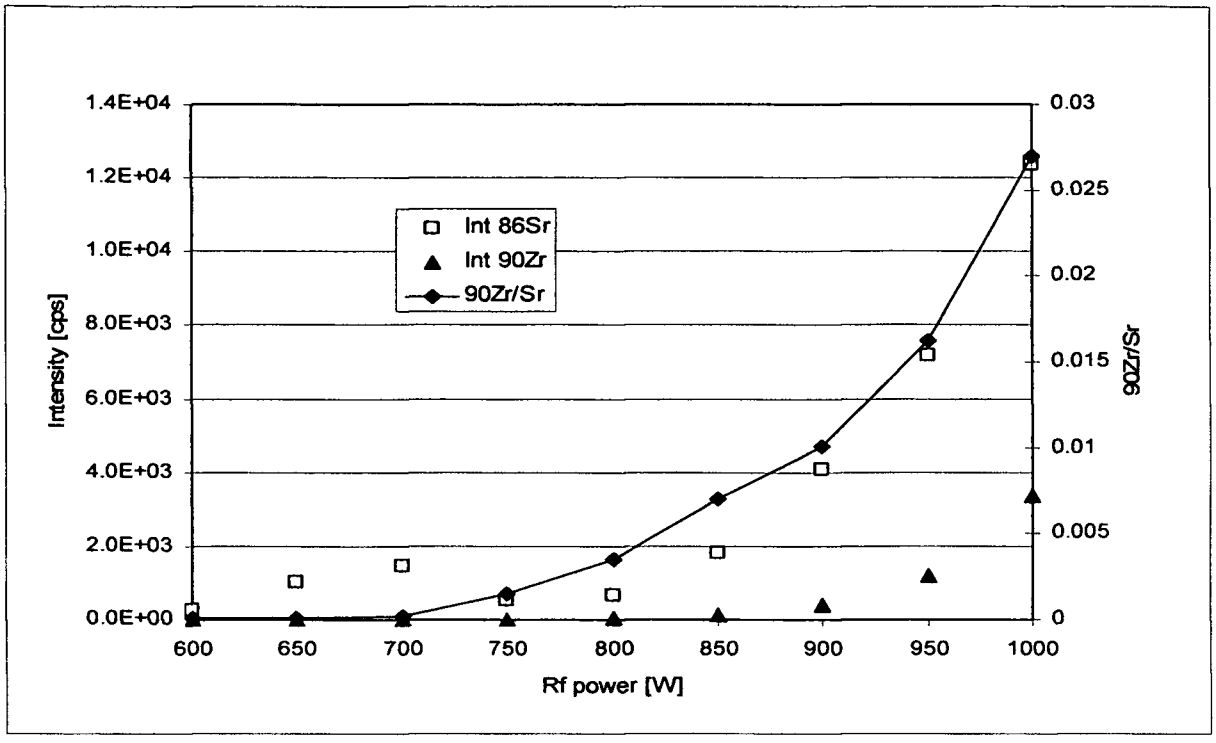


**Fig. 19** Effect of Rf power on the response of $^{86}Sr$ and $^{90}Zr$. Rb, Sr, Y and Zr concentration is 2 ng $g^{-1}$. Nebuliser gas flow rate is 1.15 L $min^{-1}$.

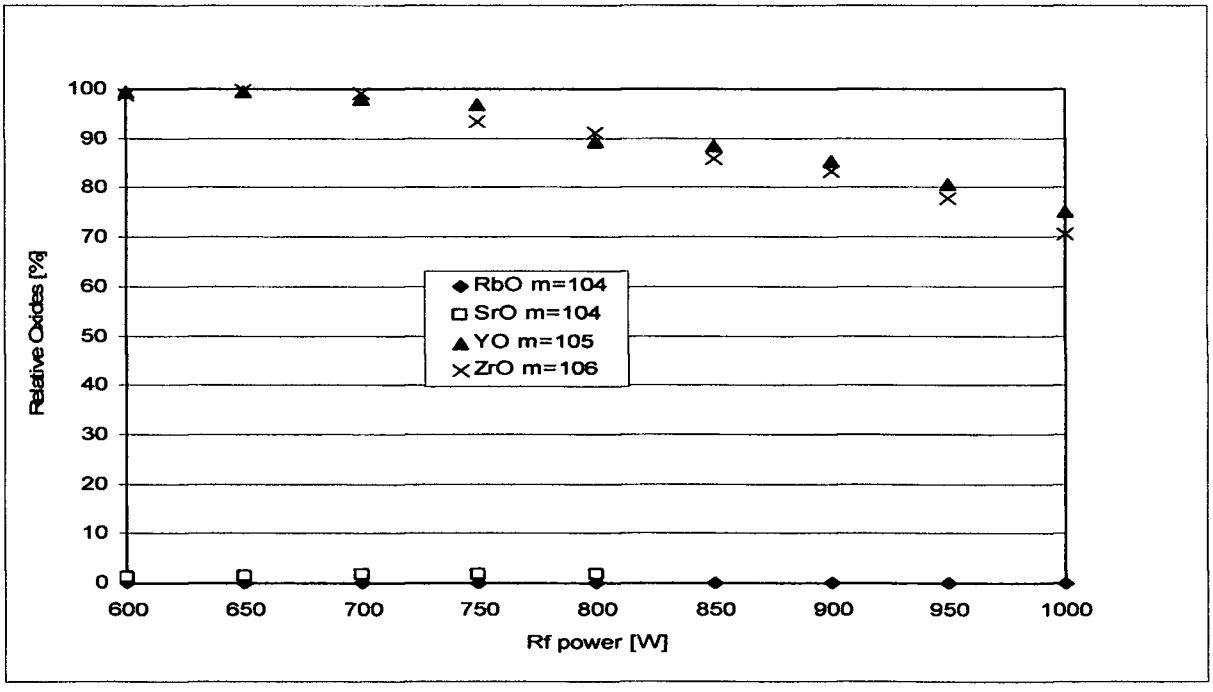


**Fig. 20** Effect of Rf power on the oxide formation of Rb, Sr, Y and Zr. Concentration is 2 ng $g^{-1}$. Nebuliser gas flow rate is 1.15 L $min^{-1}$.

As well as the ultrasonic nebuliser, the Apex-IR offers higher intensity of Sr compared to use of cyclonic spray chamber + PFA nebuliser, due to drying of the aerosol.

### 3.3.2.2 DRC

Apart from the experiments investigating the combined effect of Rf power and reaction gas (3.3.2.2.2), measurements concerning the optimisation of the DRC parameters were performed using Apex-IR introduction system and hot plasma (~ 1300 W Rf power).

#### *3.3.2.2.1 Reaction cell gas*

Oxygen gas flow rate and cell parameters were optimised with respect to high sensitivity for Sr and the most efficient reduction of $^{90}Zr^+$ intensity.
Cell gas flow rate was varied from 0 – 2.5 mL $min^{-1}$ and its effect on the intensities of Sr and Zr, the separation factor and oxide formation of Rb, Sr, Y and Zr was observed.
The relative oxide rates of Y and Zr were nearly 100 % reducing the intensities of $^{90}Zr^+$ and $^{89}Y^+$ ions. Therefore, a separation factor $^{90}Zr/Sr$ better than 5 x $10^{-7}$ could be achieved under the cell gas flow of 2.4 mL $min^{-1}$, whereas the absolute sensitivity for Sr was only slightly deteriorated in comparison to the 'normal' ICP-MS without reaction cell. Figs. A13, 21 and 24 show that in order to achieve the lowest (best) possible separation factor, high concentrations of Sr and Zr have to be applied to demonstrate the full power of the applied gas-phase reaction.

The following paragraphs give the detailed results:

Figs. A11 and A12 show measurements on ELAN DRC-e using PFA nebuliser 1639 (sample uptake rate 500 µL $min^{-1}$). Cell gas flow was varied from 0 – 0.6 mL $min^{-1}$ and elemental concentrations were 10 ng $g^{-1}$. With a cell gas flow of 0.6 mL $min^{-1}$ oxide formation of Y and Zr is almost 100%, whereas Sr and Rb hardly react with the cell gas. Zr intensity drastically increases already with small cell gas flow rates. Sr intensity also decreases with increasing cell gas flow rate, but only marginal compared to Zr. Already small amounts of reaction gas have a huge impact on the separation factor. The separation factor is improved by more than two orders of magnitude by increase of cell gas flow rate to 0.6 mL $min^{-1}$. Further experiments had to be made to explore the full potential of the selective reaction of Zr with oxygen. Higher Sr and Zr concentrations are necessary for accurate determination of the separation factor.

Figs. 21 – 24 and A13 – A14 show measurements on the ELAN DRC II. Cell gas flow rate was varied from 0 – 2.5 mL $min^{-1}$. First, elemental concentration used was 2 ng $g^{-1}$ (figs. A13 and A14). In Fig. A13 the separation factor shows no more improvement from 1.8 mL $min^{-1}$ cell gas flow on, because the whole Zr amount (2 ng $g^{-1}$) is totally oxidised with 1.8 ml $L^{-1}$. It is not possible to determine the separation factor with this low Zr concentration since no satisfactory

count rates could be observed. Thus, the same experiment was performed with higher elemental concentrations in order to achieve higher intensities (figs. 21 and 22). Fig. 21 shows the separation factor determined with 10 ng $g^{-1}$ Zr.

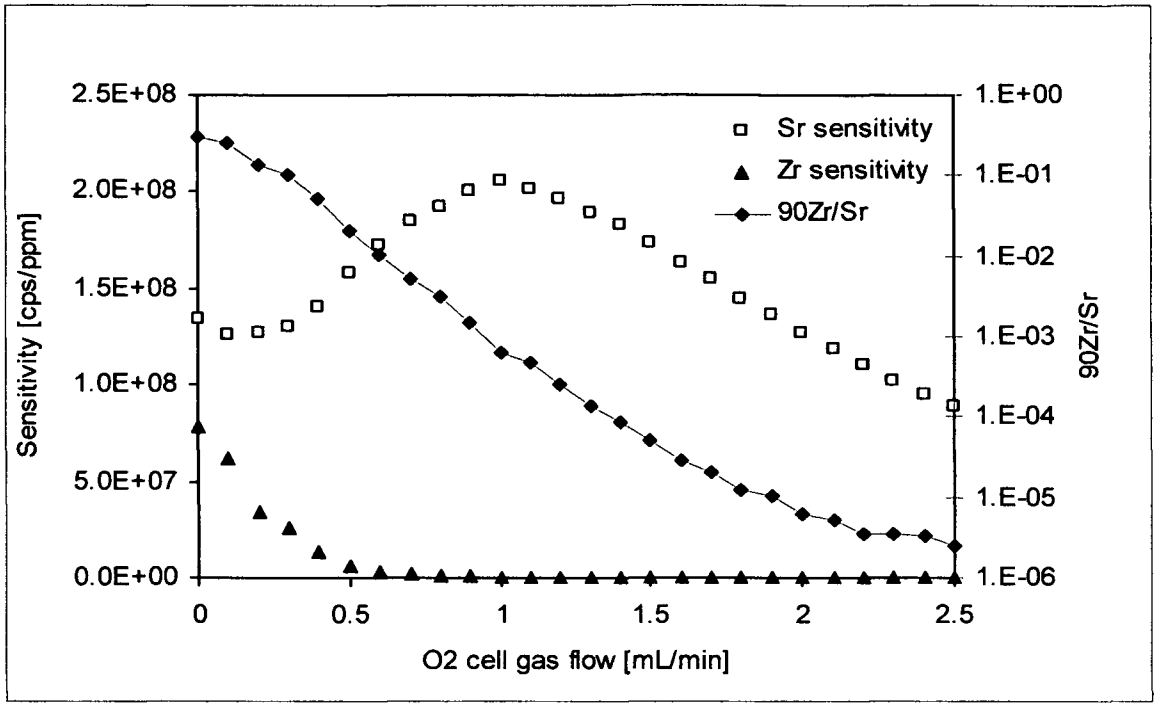


**Fig. 21** Effect of cell gas flow on the sensitivity of Sr and Zr. Sr, Rb, Y and Zr concentration is 10 ng $g^{-1}$.

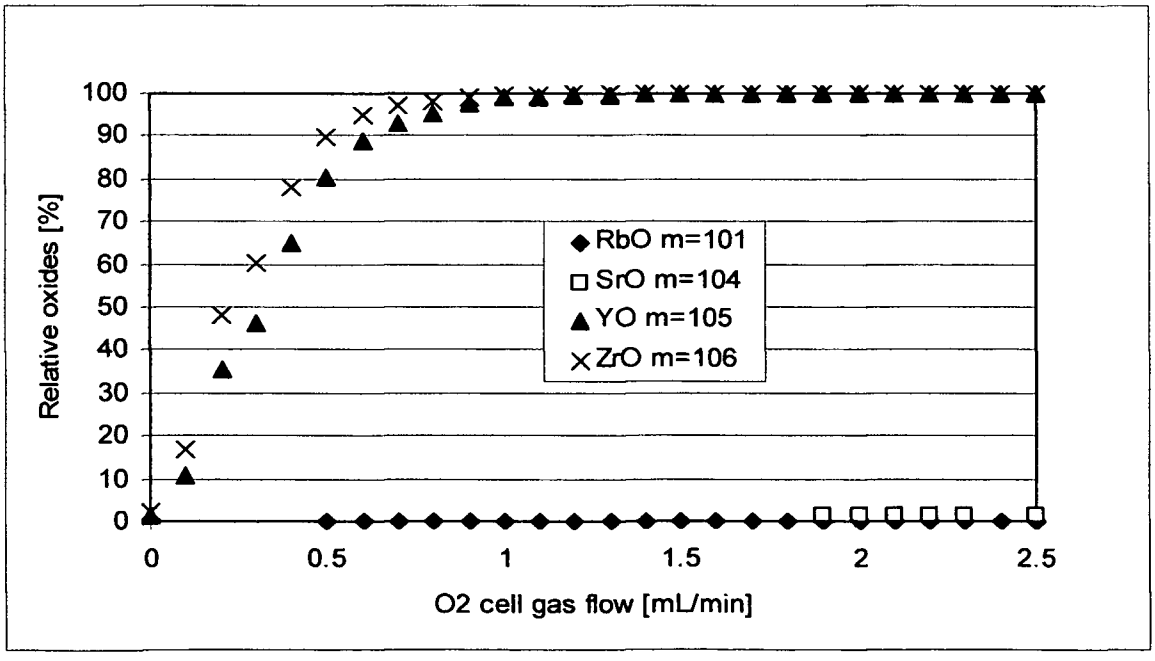


**Fig. 22** Effect of cell gas flow on the oxide formation. Sr, Rb, Y and Zr concentration is 10 ng $g^{-1}$.

Figs. 23 and 24 show the effect of high cell gas flow rate (1.8 – 2.5 mL $min^{-1}$) on the absolute sensitivity of Sr and Zr and the separation factor. RPq value was 0.4, axial field voltage 0 and solution uptake rate 100 µL $min^{-1}$. Fig. 24 shows that the separation factor is finally determined with a ~ 5 µg $g^{-1}$ Zr concentration to be about $10^{-7}$.

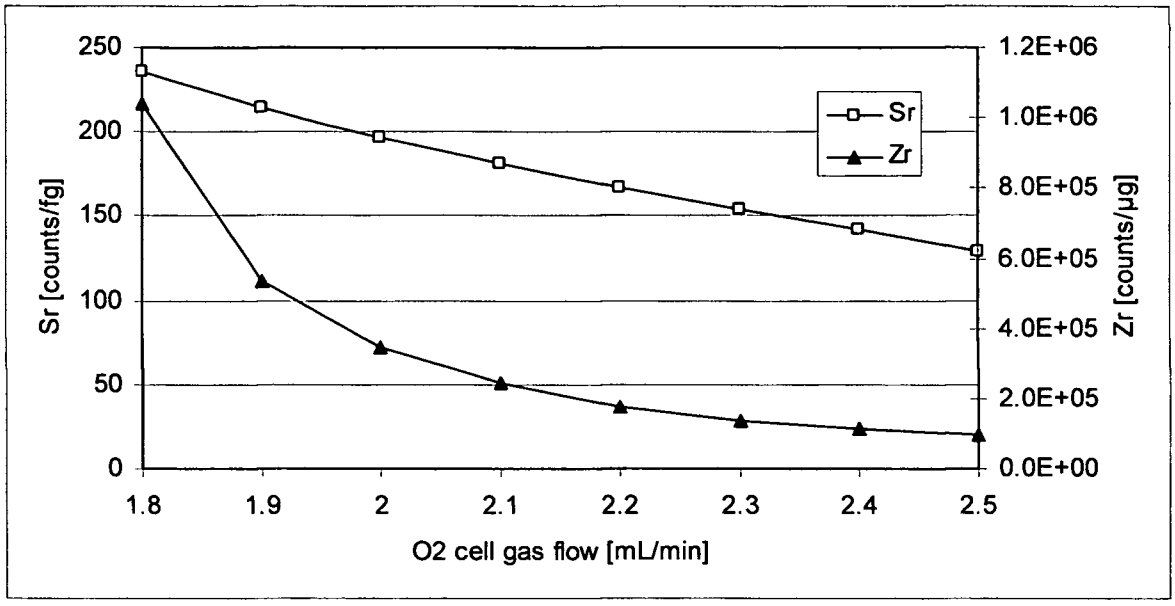


**Fig. 23** Effect of cell gas flow on absolute sensitivity of Sr and Zr. Sr concentration is 5.3 ng $g^{-1}$ and Zr concentration is 4.7 µg $g^{-1}$.

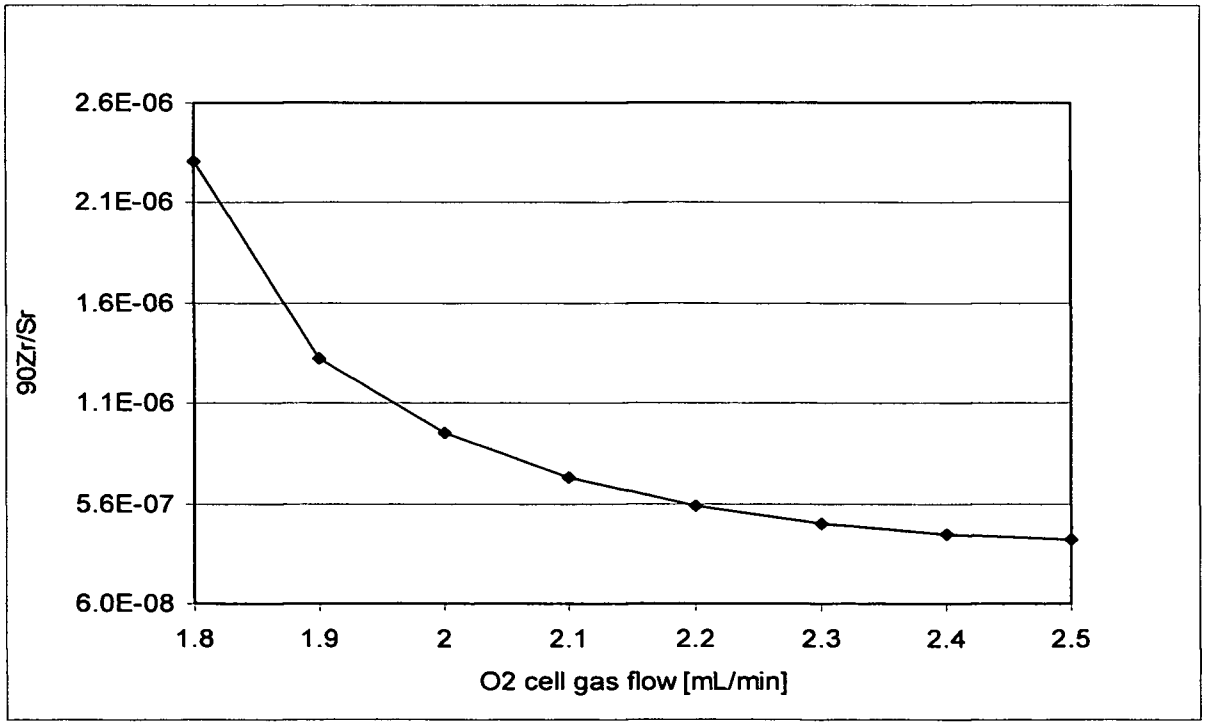


**Fig. 24** Effect of cell gas flow on the separation factor. Sr concentration is 5.3 ng $g^{-1}$ and Zr concentration is 4.7 µg $g^{-1}$.

### *3.3.2.2.2 Combined effect of Rf power and reaction gas*

Additionally, the combined effect of cold plasma and reaction gas was studied. Figs. A15 - A17 show the results of this combined effect on Sr and Zr intensity, oxide formation, absolute intensity and the separation factor $^{90}Zr/Sr$. Zr concentration is 7 µg $g^{-1}$ and Sr concentration is 2 ng $g^{-1}$. Reaction cell gas flow is 2.5 mL $min^{-1}$ and nebuliser gas flow rate is 1.08 L $min^{-1}$. USN was used as sample introduction system.

Fig. A15 shows that Sr intensity decreases with decreasing Rf power. The separation factor has an optimum at 900 W Rf power. Fig. A16 shows almost 100 % oxide formation of 7 µg $g^{-1}$ Zr as well under cold plasma as under hot plasma conditions, due to use of high reaction cell gas flow of 2.5 mL $min^{-1}$. Fig. A17 shows that the absolute sensitivity of Sr and Zr is decreasing with decreasing Rf power.

The best separation factor achieved during cell gas flow optimisation was 3.8 x $10^{-7}$ (fig. 24) with a cell gas flow of 2.5 mL $min^{-1}$ under hot plasma conditions (1300 W). In this combined experiment the separation factor slightly increases under cold plasma conditions with an optimum at 900 W. Separation factor is 2.6 x $10^{-7}$ at 900 W and 7.9 x $10^{-7}$ at 1300 W. The separation factor achieved under combined effect shows no significant improvement compared to solely use of reaction gas. This reflects the previous results, that high reaction cell gas flow has a great impact on the separation factor, unlike cold plasma conditions. Since absolute sensitivity of Sr is decreased from 40 to 15 counts $fg^{-1}$ under cold plasma, the conclusion can be drawn, that for this method, use of reaction gas should be applied under hot plasma conditions.

Nevertheless, 7 µg $g^{-1}$ Zr is suppressed to a $^{90}Zr$ intensity of 228 cps at an Rf power of 900 W with a cell gas flow of 2.5 mL $min^{-1}$. Therefore, this parameter combination was further assayed: Six measurements of a solution containing 2 ng $g^{-1}$ Sr and 7 µg $g^{-1}$ Zr were performed with applied Rf power of 900 W and a reaction cell gas flow of 2.5 mL $min^{-1}$ (Tab. 9).

**Tab. 9** Absolute sensitivity of Sr and Zr and separation factor measured at 900 W with a reaction cell gas flow of 2.5 mL $min^{-1}$.

| | Sr [counts/fg] | Zr [counts/µg] | 90Zr/Sr |
|---|---|---|---|
| 1 | 1.27E+01 | 6.09E+03 | 2.47E-07 |
| 2 | 1.40E+01 | 6.51E+03 | 2.40E-07 |
| 3 | 1.40E+01 | 6.74E+03 | 2.47E-07 |
| 4 | 1.45E+01 | 6.66E+03 | 2.37E-07 |
| 5 | 1.49E+01 | 6.81E+03 | 2.35E-07 |
| 6 | 1.49E+01 | 6.60E+03 | 2.27E-07 |

In order to test the separation efficiency of this combined effect on a real sample, an unseparated uncontaminated soil sample (Mag5_2) was measured (Tab. 10) using the same parameters as before.

**Tab. 10** Measurement of unseparated uncontaminated soil sample. Rf power is 900 W and reaction cell gas flow is 2.5 mL $min^{-1}$.

| Soil sample Mag5_2 | | | | |
|---|---|---|---|---|
| | mass | Intensity [cps] | SD | RSD [%] |
| Rb | 84.91 | 5.9E+06 | 8.6E+05 | 14.5 |
| Sr | 85.91 | 7.0E+05 | 1.4E+05 | 19.6 |
| Sr | 86.91 | 3.2E+06 | 5.3E+05 | 16.4 |
| Sr | 87.91 | 7.4E+06 | 1.5E+06 | 19.8 |
| Y | 88.91 | 2.5E+04 | 3.4E+03 | 13.7 |
| **Zr** | **89.90** | **3.4E+05** | 5.7E+04 | 16.9 |
| Zr | 90.91 | 2.9E+04 | 3.3E+03 | 11.5 |
| Zr | 91.91 | 3.3E+03 | 4.5E+02 | 13.5 |

The high intensity of $^{90}Zr$ measured in the unseparated soil sample shows that the use of high cell gas flow combined with an Rf power of 900 W (cold plasma) does not provide sufficient separation of Zr, nor would cell gas alone. Additional pre-separation of Zr is unavoidable for measurement of $^{90}Zr$ in soil samples. Therefore, off-line separation in form of Sr/matrix separation using Sr-specific resin is essential.

#### *3.3.2.2.3 Cell rod offset*

DRC parameters such as axial field voltage (AFV), cell rod offset (CRO) and quadrupole rod offset (QRO) alter the ion transmission time within the reaction cell, which may result in changing both the sensitivity for $Sr^+$ ions and the overall reaction rate of $Zr^+$ ions with oxygen. Initial experiments investigating the effect of the CRO on the intensities of Sr and Zr, the separation factor and oxide formation were perfomed by using ELAN DRC-e, Apex-IR and PFA nebuliser (sample uptake rate 500 µL $min^{-1}$) (figs. A18 and A19) Quadrupol rod offset (QRO) was always set by 5 V lower than CRO. Reaction cell gas flow was 0.2 mL $min^{-1}$. The cell rod offset does not significantly alter the separation factor in the range from -1 to 3 V, but due to the fact that the sensitivity of Sr decreases, the cell rod offset should be below 1 V. Fig. A19 shows that oxide formation of Y and Zr decreases with decreasing CRO.

Figs. 25 and 26 show the effect of the CRO on the intensities of Sr and Zr, the absolute sensitivity and the separation factor obtained by using ELAN DRC II, Apex-IR and PFA nebuliser (sample uptake rate 100 µL $min^{-1}$). CRO was changed from -4 V to 2 V. Quadrupol rod offset (QRO) was always set 5 V lower than CRO. Cell gas flow rate was 2.1 mL $min^{-1}$, which is the main difference to the previous experiment, with a cell gas flow rate of 0.2 mL $min^{-1}$ (figs. A18 and A19) and results in improvement of the separation factor by 4 orders of magnitude. Sr concentration was 5.3 ng $g^{-1}$ and Zr concentration was 4.7 µg $g^{-1}$.

The cell rod offset was set to -2 V for the final measurement of the soil samples.

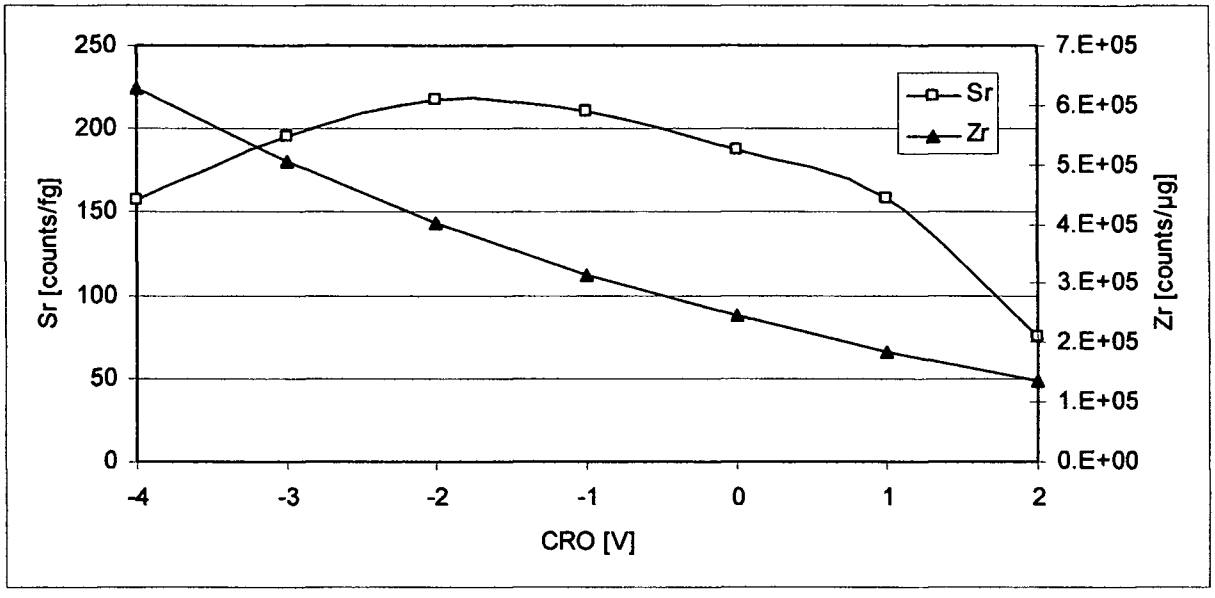


**Fig. 25** Effect of cell rod offset on the absolute sensitivity of Sr and Zr. Sr concentration is 5.3 ng $g^{-1}$ and Zr concentration is 4.7 µg $g^{-1}$. Cell gas flow is 2.1 mL $min^{-1}$.

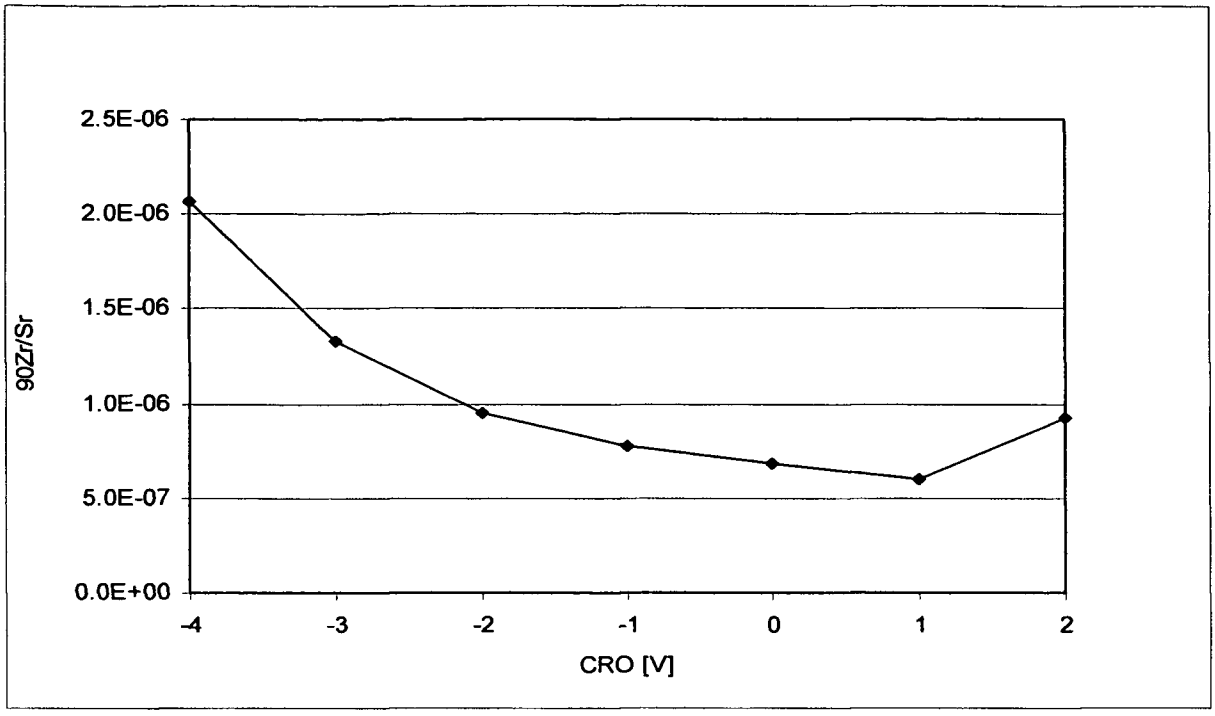


**Fig. 26** Effect of cell rod offset on the separation factor. Sr concentration is 5.3 ng $g^{-1}$ and Zr concentration is 4.7 µg $g^{-1}$. Cell gas flow is 2.1 mL $min^{-1}$.

### *3.3.2.2.4 Axial field*

The absolute sensitivity slightly decreases for both elements with increasing axial field voltage (Fig. 27), whereas an inverse effect was reported by Taylor et al. (2007). In general, particular DRC parameters are interdependent, so that different conditions introduced by a combination of other DRC parameters may alter observed effects. Therefore, also other optimal conditions than those given in tab. 3 can be found. Higher axial field voltages seemed favorable for minimising intensity of Zr, as long as the Sr sensitivity is still appropriate.

Fig. 27 and 28 show the effect of axial field voltage on absolute sensitivity of Sr and Zr and the separation factor. Axial field voltage was changed from -20 to 200 V. ELAN DRC II, Apex-IR and PFA nebuliser (solution uptake rate 100µL $min^{-1}$) were applied for this measurement. Reaction cell gas flow was 2.1 mL $min^{-1}$. Sr concentration was 5.3 ng $g^{-1}$ and Zr concentration was 4.7 µg $g^{-1}$.

Fig. 28 shows that the axial field voltage has no significant impact on the separation factor.

The axial field voltage was set to 220 V for the measurement of the soil samples, which was optimal in connexion with the final parameters given in tab. 3.

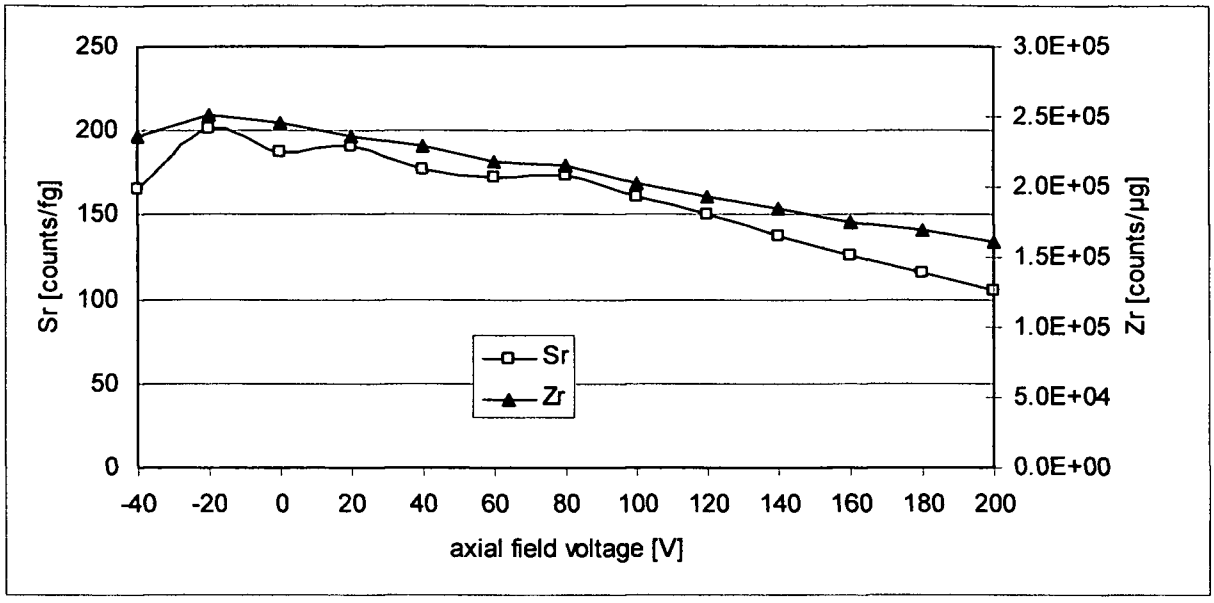


**Fig. 27** Effect of axial field voltage on the absolute sensitivity of Sr and Zr. Sr concentration is 5.3 ng $g^{-1}$ and Zr is 4.7 µg $g^{-1}$. Cell gas flow rate is 2.1 mL $min^{-1}$.

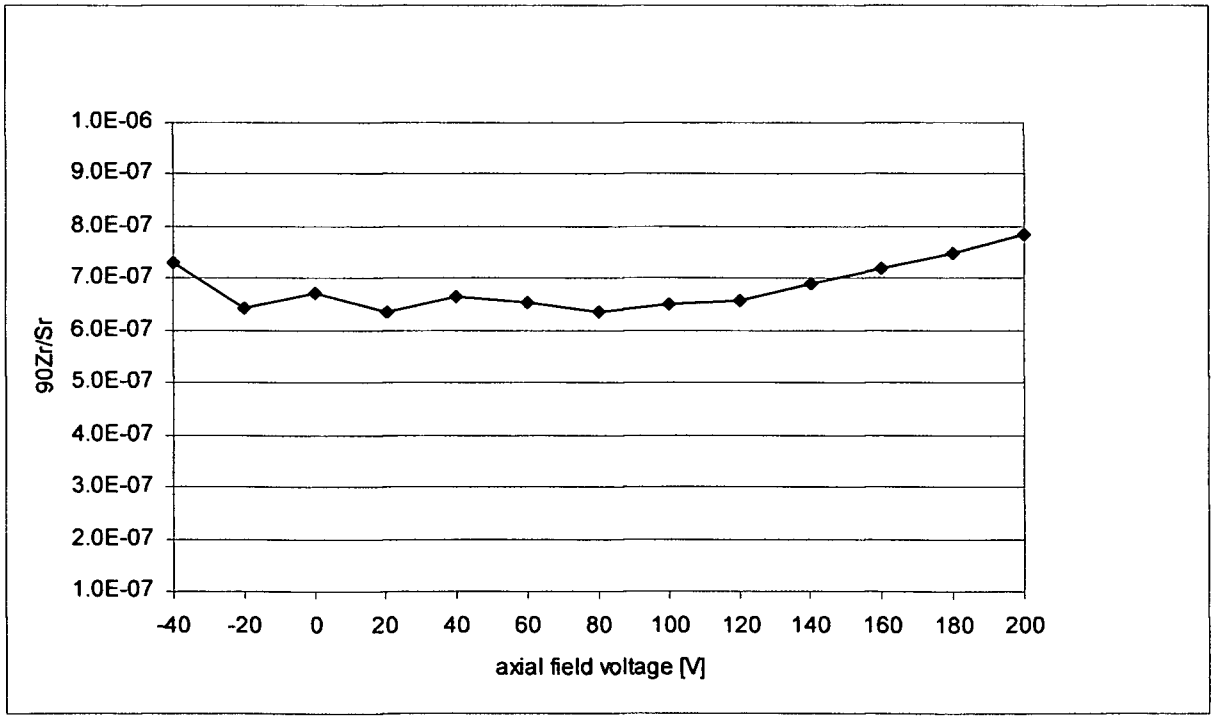


**Fig. 28** Effect of axial field voltage on the separation factor $^{90}Zr/Sr$. Sr concentration is 5.3 ng $g^{-1}$ and Zr is 4.7 µg $g^{-1}$. Cell gas flow rate is 2.1 mL $min^{-1}$.

#### *3.3.2.2.5 RPq value*

A further reaction cell parameter needed to be optimised in order to reduce background at *m/z* = 90 is the RPq value, which correspond to Mathieu parameter q describing ion motion in the DRC (Taylor et al. 2007). This parameter controls the low mass cut-off for ions entering the cell (Tanner et al. 2002) that is particularly useful for filtering away low mass ions which can build molecular ions within DRC representing isobaric interferences with $^{90}Sr$. The RPq value was set to 0.6 (such an RPq value corresponds to a low mass cut off of *m/z* = 60 – for calculation see 1.3.2.4) which resulted in reducing the background signal at *m/z* = 90 from about 200 cps to 0-13 cps in a 2 ppb Sr solution (the final background intensity depended also on other DRC parameters). RPa value (corresponding to the Mathieu parameter a) was set to zero, since no high mass cut-off was necessary.

## 3.3.3 Possible interference by hydrides

### 3.3.3.1 Yttrium hydride

Natural yttrium concentration in the analysed soil samples varied from 1.4 to 7.0 μg $g^{-1}$ (determined using external calibration, tab. 5) and $^{89}Y$, which has an abundance of 100% (KAERI 2000), can interfere with $^{90}Sr$ through a formation of molecule ion $^{89}YH^+$ detected at *m/z* = 90. Chemical separation prior to measurement removed nearly 100 % of Y (tab. 8). Oxide formation of remaining Y was also ~100 %. If $^{89}YH^+$ was formed before entering the reaction cell, it would be detected at *m/z* = 90. The absence of $^{89}YH^+$ interference was proved by measuring a 100 ng $g^{-1}$ Y solution by use of the developed ICP-DRC-MS method. The measurement was performed on the Elan DRC-e and cell gas flow rate was 0.5 mL $min^{-1}$.
Vonderheide et al. (2004) also observed no hydride formation when measuring a 200 ng $g^{-1}$ Y solution.

### 3.3.3.2 Strontium hydride

$^{88}Sr$, which is present in soil samples in high concentration, may form an interfering hydride, $SrH_2$, at *m/z* = 90.
During the method development relatively high Sr concentrations were measured. Therefore, it was important to properly rinse the instrument in between and after the experiments with 1% $HNO_3$. Tab. 11 shows the results of six blank measurements with a cell gas flow rate of 2.1 mL $min^{-1}$ and an RPq value of 0.4. The Sr intensities in this blank may come from residual Sr in the instrument. They can be overcome by blank correction of analysed samples. The actual

question is, if the high blank signal at *m/z* = 90 (3 cps) is caused by molecular interference from $SrH_2$.

**Tab. 11** Average of six blank measurements at a cell gas flow rate of 2.1 mL $min^{-1}$ and RPq = 0.4.

| | Blank | | |
|---|---|---|---|
| | Intensity [cps] | SD | RSD [%] |
| $^{86}Sr$ | 122.8 | 104.2 | 78.5 |
| $^{88}Sr$ | 1189.9 | 719.8 | 61.7 |
| $^{89}Y$ | 1.7 | 0.2 | 13.1 |
| $^{90}Zr$ | 3.2 | 0.5 | 16.2 |

The formation of $SrH_2$ was investigated by measuring increasing concentrations of Sr. If $SrH_2$ was the cause of this interference, the interference would increase with Sr concentration. A blank (1% $HNO_3$), 10 ng $g^{-1}$, 20 ng $g^{-1}$, 100 ng $g^{-1}$, 300 ng $g^{-1}$, 1 µg $g^{-1}$ and 3 µg $g^{-1}$ solutions of Sr were measured. The experiments produced evidence that hydride formation of Sr was not the cause of the interference at *m/z* = 90, because the intensity at *m/z* = 90 did not increase with ascending Sr concentration.

The interference could be caused by molecular ions produced by low mass ions in the DRC and should be eliminated by increasing the RPq value of the DRC (bandpass tuning), as shown in 3.3.2.2.5, filtering low mass ions away. The optimised method was not applied in this particular case.

## 3.3.4 Figures of merit

### 3.3.4.1 Background equivalent concentration

The background equivalent concentration (BEC) was measured on the ELAN DRC-e in 1% $HNO_3$ as blank. A solution of ng $g^{-1}$ Zr was used for evaluation of Zr sensitivity. No reaction cell gas was used. Apex-IR introduction system and PFA nebuliser 1291 with a solution uptake of 100 µL $min^{-1}$ were used. BEC was determined to be 1.4 pg $g^{-1}$ Zr.

### 3.3.4.2 Abundance sensitivity

The isotopic abundance sensitivity is one of the most important figures of merit of a mass spectrometer system describing its ability to differentiate peaks of low-abundant isotopes from the tailing of the directly adjacent major isotope peak. It is normally defined as the intensity at the desired mass (corresponding to a low abundant isotope) originating from the peak tailing of a dominant neighboring isotope divided by the peak height of that dominant isotope. Since the natural Sr concentration in soil is higher than the expected $^{90}Sr$ concentration by several

orders of magnitude, the peak-tailing of $^{88}Sr$, which has a natural abundance of 82.58 %, is a potential interference source at *m/z* = 90.

As the expected abundance sensitivity for $^{90}Sr$ was lower than $10^{-7}$ the intensity of the main isotope must be high enough to produce a well measurable peak tailing at *m/z*=90. The dynamic range of the used ICP-MS covers about 9 orders of magnitude. Therefore, it is impossible to measure directly isotopic ratios lower than $10^{-8}$ with this instrument. Following procedure was applied in this work. A Sr solution with a concentration of 30 µg/g was analysed. As the $^{88}Sr$ intensity was too high for the applied detection system the intensity of this isotope was estimated by measuring $^{86}Sr^{+}$ intensity with account to $^{86}Sr$ and $^{88}Sr$ abundances. In this way, dynamic range of the applied detection system could be extended by about one order of magnitude. In order to avoid any contribution by possible molecular ions (e.g. $^{88}Sr^{1}H_2^{+}$), the peak tail intensity at *m/z* = 90 was determined as the average value of intensities measured at *m/z* = 89.5 and 90.5. Fig. 29 shows the dependence of abundance sensitivity as a function of oxygen cell gas in ICP-DRC-MS. The ratio of the background intensity at *m/z* = 90 to the $^{88}Sr^{+}$ intensity demonstrates the cumulative effect of the peak tailing by $^{88}Sr^{+}$ and potential contribution by residual $^{90}Zr^{+}$ as well as molecular ions. Without the use of oxygen in the reaction cell, the background intensity at m=90 u/$^{88}Sr$ ratio is higher than the contribution of $^{88}Sr$ peak tailing abundance sensitivity by 1-2 orders of magnitude because of the background contribution of residue $^{90}Zr$ on *m/z* = 90. The contribution disappears with increasing cell gas flow, $^{90}Zr$ is oxidised with increasing cell gas flow rate. Background equivalent concentration was found to be 1.4 pg $g^{-1}$ Zr in the blank solution. As seen from Fig. 29 the abundance sensitivity does not change significantly contrary to the previously reported results obtained by using a quadrupole based "Platform" ICP-MS with collision cell (Boulyga and Becker 2002). Very low extraction potentials are used in the Elan DRC II ICP-DRC-MS, and thus the energies of ions entering the mass spectrometer are small. Therefore, further deceleration of ions by collisions in the DRC does not have any significant effect on the abundance sensitivity (Fig. 29). It should also be mentioned, that application of collision gas in the cell increases the pressure within the mass analyser, where residual gas molecules may cause additional scattering of ions within the quadrupole. Blaum et al. (2000) observed deterioration of abundance sensitivity on a higher mass by a factor of three, by artificially increasing the vacuum by an order of magnitude up to $5\times10^{-6}$ mbar. This effect can explain a slight increase of peak tailing at higher cell gas flow rates, observed in fig. 29.

Abundance sensitivity at a cell gas flow of 2.4 mL $min^{-1}$ $O_2$ and an RPq value of 0.6 was found to be $3 \times 10^{-9}$. Comparative measurements were performed by using an Elan DRC-e, where a similar value of $2 \times 10^{-9}$ was found. This finding does not fit in with results by Taylor et al. (2007) who reported an abundance sensitivity value better than $10^{-10}$ measured by introducing

a 100 mg $L^{-1}$ Sr solution on the Elan DRC II using oxygen as reaction gas. Unfortunately, Taylor et al. does not provide any further detail on the measurement procedure applied for the determination of this abundance sensitivity value. In our work introducing 100 mg $L^{-1}$ natural Sr solution resulted in overload of the detector which made accurate determination of the abundance sensitivity impossible.

**Tab. 12** Abundance sensitivity and 90/88 ratio against cell gas flow in 30 µg $g^{-1}$ Sr.

| Cell gas flow [ml $min^{-1}$] | Int 90 [cps] | AS m-1 | 90/88 ratio | AS m+1 | AS m90 |
|---|---|---|---|---|---|
| 2.4 | 5.5 | 2.0E-09 | 2.6E-09 | 2.6E-09 | 2.3E-09 |
| 2.0 | 6.3 | 1.7E-09 | 2.3E-09 | 2.1E-09 | 1.9E-09 |
| 1.6 | 7.0 | 1.5E-09 | 2.0E-09 | 1.9E-09 | 1.7E-09 |
| 1.2 | 7.9 | 1.8E-09 | 1.9E-09 | 2.0E-09 | 1.9E-09 |
| 0.8 | 10.8 | 1.3E-09 | 2.6E-09 | 1.8E-09 | 1.6E-09 |
| 0.4 | 62.1 | 1.4E-09 | 2.1E-08 | 1.4E-09 | 1.4E-09 |
| 0.0 | 354.5 | 2.9E-09 | 1.3E-07 | 1.7E-09 | 2.3E-09 |
| 2.4 | 7.9 | 2.9E-09 | 3.7E-09 | 3.0E-09 | 2.9E-09 |
| 2.4 | 8.4 | 3.1E-09 | 3.9E-09 | 3.6E-09 | 3.4E-09 |
| 2.4 | 7.6 | 3.0E-09 | 3.6E-09 | 3.9E-09 | 3.4E-09 |

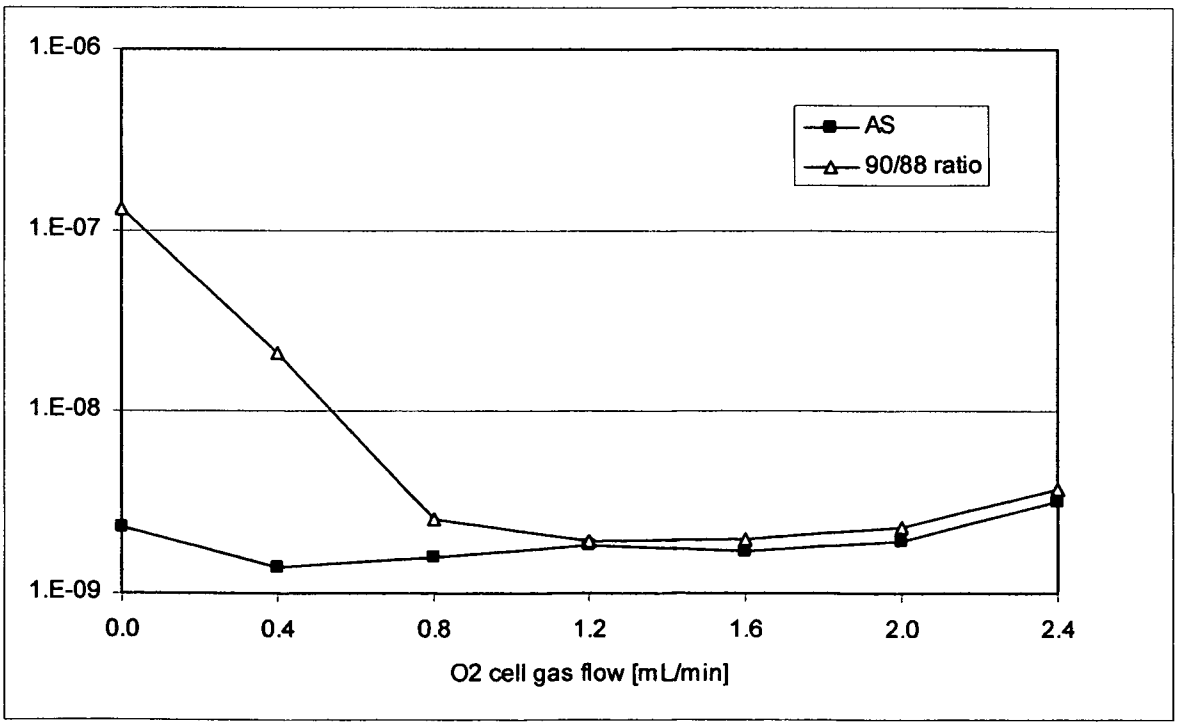


**Fig. 29** Effect of cell gas flow on abundance sensitivity and 90/88 ratio in 30 µg g-1 Sr. Data obtained from Tab. 12.

### 3.3.4.3 Minimum detectable ratio

The minimal detectable ratio was calculated as three times the standard deviation of the background intensity at *m/z* = 90 (inclusively peak tail from $^{88}Sr$, possible molecular ions interference like $^{88}Sr^1H_2^+$ etc.) divided through the $^{88}Sr^+$ intensity ($3s(I_{90u})/I_{88u}$) measured in 30 µg $g^{-1}$ Sr solution. The minimal detectable ratio $^{90}Sr/^{88}Sr$ was $5\times10^{-10}$ under optimised experimental conditions given in tab. 3 and it was deteriorated when reducing cell gas (due to lesser reduction of residue Zr interference) and at lower RPq values (due to increasing interferences by molecular ions produced within reaction cell).

## *3.4 Soil samples*

### 3.4.1 Detection limit

The detection limit of $^{90}Sr$ by ICP-DRC-MS was calculated as three times the standard deviation of the background signal at *m/z* = 90 u divided by the Sr sensitivity. A detection limit of $4 \times 10^{-15}$ g $g^{-1}$ was calculated for an ideal solution (1% $HNO_3$), containing no Zr, in the measured tenfold diluted soil digest, which corresponds to 0.04 pg $g^{-1}$ soil (or specific activity of 0.2 Bq per g soil). A detection limit of 0.2 pg $g^{-1}$ soil (1 Bq $g^{-1}$ soil) was determined for a solution of 5 µg $g^{-1}$ Sr and 50 ng $g^{-1}$ Zr and for real non-contaminated soil samples (after digestion and matrix separation) with account to the residue Zr concentration and background by molecular ions.

### 3.4.2 Determination of $^{90}Sr$ activity in soil samples

The total natural Sr amount in the soil samples was determined by IDMS as explained before. Isotopic ratios of $^{90}Sr/^{88}Sr$ were determined by using ICP-DRC-MS, after liquid Sr extraction from the soil samples. The measured $^{90}Sr$ intensity was corrected with respect to blank intensity, peak tailing originating from $^{88}Sr$ and residue Zr signal at mass 90 u, the later was corrected by measuring $^{92}Zr$ with account to corresponding isotopic abundances ($^{90}Zr$ 51.45% and $^{92}Zr$ 17.15%, KAERI 2000). The $^{90}Sr$ concentrations were then converted into specific activity (Equ. 15). Concentrations, activities and total combined uncertainties were calculated with the GUM-workbench (Metrodata GmbH, Grenzach-Whylen, Germany). $^{90}Sr$ concentrations in the three soil samples KRA, RAD and MAS were 4.66 ± 0.27, 13.48 ± 0.68 and 12.9 ± 1.5 pg $g^{-1}$, respectively which accords to the activities 23.7 ± 1.3, 68.6 ± 3.5 and 65.6 ± 7.8 Bq $g^{-1}$ soil. $^{90}Sr$ activities in the soil samples measured by radiometric method in 1996 were corrected with account to the decay since the analysis time (Equ. 13 and 14) and implicated for validation of the method. The ICP-DRC-MS results showed a satisfactory

agreement with radiometric results with account to the experimental uncertainties of both methods (Tab. 13).

$$A(t) = A_0 * e^{-\lambda t} \quad (13)$$

$$\lambda = \ln 2 / T_{1/2} \quad (14)$$

$A_0$ activity in 1996 [Bq $g^{-1}$]

t 11 years [s]

$$A = \ln 2 / T_{1/2} * N_{1g} \quad (15)$$

**Tab. 13** $^{90}Sr$ concentration and activity in soil samples measured by ICP-DRC-MS (parameter according to Tab. 3) and radiometric method.

| Sample | ICP-DRC-MS | | Radiometric measurement | |
|---|---|---|---|---|
| | [pg $g^{-1}$] | Bq $g^{-1}$ | Bq $g^{-1}$ 1996 | Bq $g^{-1}$ 2007 |
| IAEA-375 | 340.6 ± 2.2 | 1734 ± 11 | | |
| KRA | 4.66 ± 0.27 | 23.7 ± 1.3 | 45 ± 9 | 35 ± 7 |
| RAD | 13.48 ± 0.68 | 68.6 ± 3.5 | 82 ± 16 | 63 ± 13 |
| MAS | 12.9 ± 1.5 | 65.6 ± 7.8 | 99 ± 18 | 76 ± 15 |

IAEA-375 has a certified $^{90}Sr$ activity of 108 ± 6 Bq $kg^{-1}$, while the $^{90}Sr$ activity measured with ICP-DRC-MS is 1734 Bq $g^{-1}$ pointing out a significant interference problem (Tab. 13). This control standard was probably not measurable due to a high Zr concentration of 390 µg $g^{-1}$ (Tab. 5), determined by external calibration, and non-satisfactory separation of soil matrix by liquid chromatography caused by clogging the column, even after this sample was ashed.

The uncontaminated soil sample (Mag 5_2) was measured subsequently to the contaminated soil samples in order to demonstrate the success of the Sr/Zr separation. The intensity at *m/z* = 90 stayed at the blank value in this sample (Tab. 14).

**Tab. 14** Intensity comparison of Mag 5_2 and a sample blank (parameter according to Tab. 3).

| | Mag 5_2 | | Blank RAD | |
|---|---|---|---|---|
| mass | Intensity [cps] | RSD | Intensity [cps] | RSD |
| 90 | 4.1 | 0.6 | 5.3 | 0.1 |
| 92 | 2.2 | 0.3 | 1.6 | 0.1 |

# 4 Conclusion

A rapid method was developed for determination of $^{90}Sr$ in soil samples by ion exchange separation using a strontium specific resin followed by ICP-QMS analysis using oxygen as reaction gas in a DRC. A soil sample can be digested and analysed within two days, with sample preparation being the limiting factor. Zr could be successfully reduced by a factor of $10^7$ after a two step procedure, which are both necessary in order to reach proper separation. The method represents a time- and cost-effective method for determination of $^{90}Sr$ in soil samples down to activity levels of approximately 1 Bq $g^{-1}$.
The soil sample IAEA-375 showed that insufficient sample preparation and liquid separation of matrix lead to incorrect concentration and $^{90}Sr$ activity results.

Although the method is inferior to commonly used radiometric methods as well as RIMS and AMS (see e.g. Paul et al. 1997) with respect to the achievable minimum detectable activity, it represents a step towards fast monitoring of high-level $^{90}Sr$ contamination in environment (e.g. contamination in the vicinity of Chernobyl). The method offers easy sample preparation and short analysis time which is advantageous for the prompt assessing the radio ecological situation in a case of a nuclear accident. Taking into account the relatively low costs of ICP-DRC-MS and its availability in a number of routine laboratories, it is a promising alternative to radiometric techniques for routine analysis of high-level nuclear industrial samples.

Application of a sector-field ICP-MS with special high abundance sensitivity channels could potentially be useful for $^{90}Sr$ determination. It offers superior abundance sensitivity, but does not solve the isobaric interference problem. The upcoming newest development in mass spectrometric techniques, like the invention of Orbitrap MS (Makarov et al. 2006) possessing a principal possibility for resolving isobaric interferences due to significantly higher mass resolution, show a future potential for radioanalytical purposes.

The following diagram gives the stepwise instruction for the procedure.

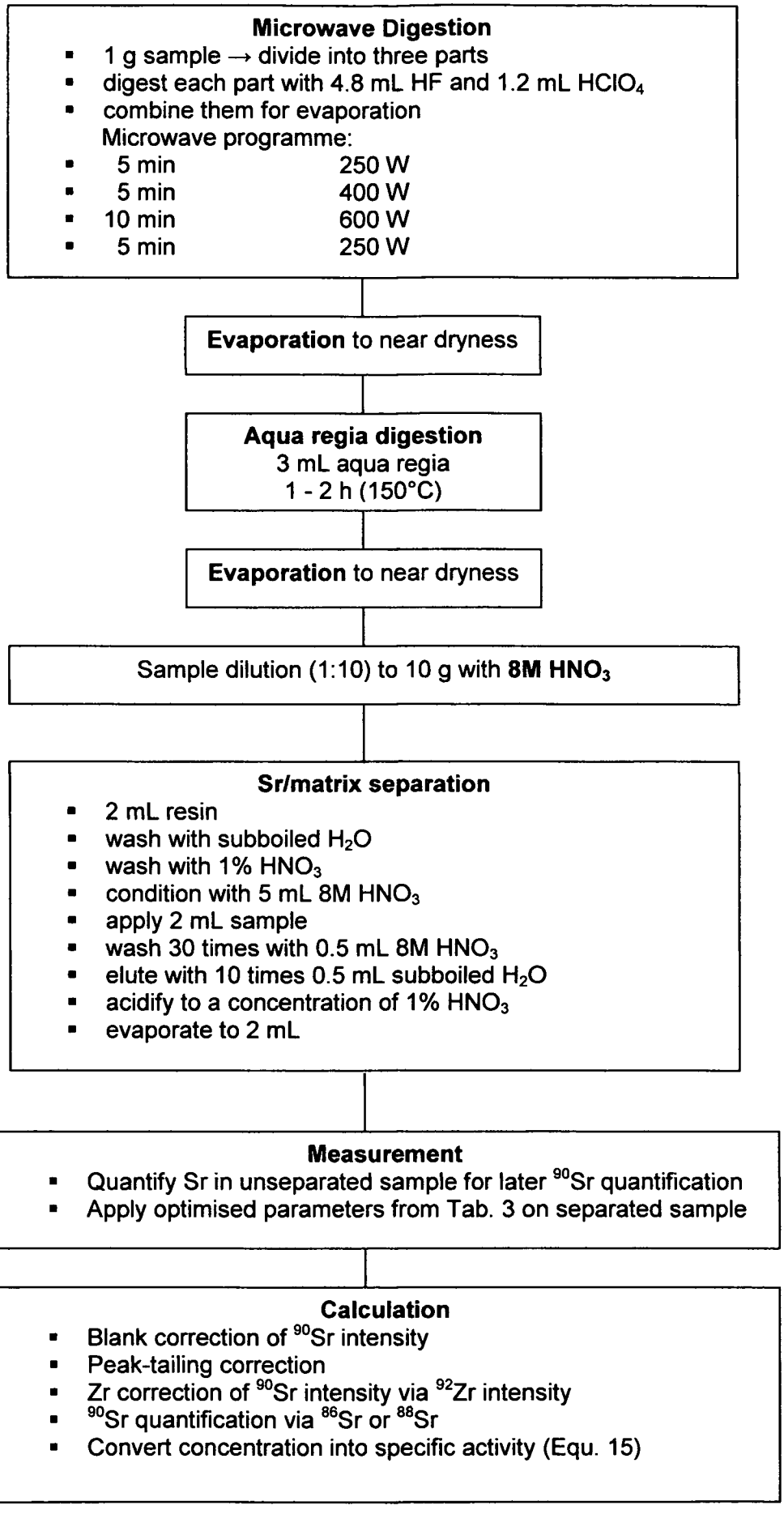
Microwave Digestion
1 g sample → divide into three parts
digest each part with 4.8 mL HF and 1.2 mL $HClO_4$
combine them for evaporation
Microwave programme:
5 min 250 W
5 min 400 W
10 min 600 W
5 min 250 W
Evaporation to near dryness
Aqua regia digestion
3 mL aqua regia
1 - 2 h (150°C)
Evaporation to near dryness
Sample dilution (1:10) to 10 g with 8M $HNO_3$
Sr/matrix separation
2 mL resin
wash with subboiled $H_2O$
wash with 1% $HNO_3$
condition with 5 mL 8M $HNO_3$
apply 2 mL sample
wash 30 times with 0.5 mL 8M $HNO_3$
elute with 10 times 0.5 mL subboiled $H_2O$
acidify to a concentration of 1% $HNO_3$
evaporate to 2 mL
Measurement
Quantify Sr in unseparated sample for later $^{90}Sr$ quantification
Apply optimised parameters from Tab. 3 on separated sample
Calculation
Blank correction of $^{90}Sr$ intensity
Peak-tailing correction
Zr correction of $^{90}Sr$ intensity via $^{92}Zr$ intensity
$^{90}Sr$ quantification via $^{86}Sr$ or $^{88}Sr$
Convert concentration into specific activity (Equ. 15)

# 5 Bibliographies


Acar R., Acar O., **2004**. Determination of $^{90}Sr$ Accumulation in Human Teeth. Turkish Journal of Chemistry 28, 67-74.

Adout A., Hawlena D., Maman R., Paz-Tal O., Karpas Z., **2007**. Determination of trace elements in pigeon and raven feathers by ICPMS. International Journal of Mass Spectrometry 267, 109-116.

Alberède F., Telouk P., Blichert-Toft J., Boyet M., Agranier A., Nelson B., **2004**. Precise and accurate isotopic measurements using multiple-collector ICPMS. Geochimica et Cosmochimica Acta 68, 2725-2744.

Alvarez A., Navarro N., **1996**. Method for Actinides and Sr-90 Determination in Urine Samples. Applied Radiation and Isotopes 47, 869-873.

Arslan F., Behrendt M., Ernst W., Finckh E., Greb G., Gumbmann F., Haller M., Hofmann S., Karschnick R., Klein M., Kretschmer W., Mackiol J., Morgenroth G., Pagels C., Schleicher M, **1994**. $^{14}C$ and $^{90}Sr$ measurements at the Erlangen AMS facility. Nuclear Instruments and Methods in Physics Research B 92, 39-42.

Bandura D.R., Baranov V.I., Tanner S.D., **2000**. Effect of collisional damping and reactions in a dynamic reaction cell on the precision of isotope ratio measurements. Journal of Analytical Atomic Spectrometry 15, 921-928.

Bandura D.R., Baranov V.I., Tanner S.D., **2002**. Inductively coupled plasma mass spectrometer with axial field in a quadrupole reaction cell. Journal of the American Society for Mass Spectrometry 13, 1176-1185.

Bandura D.R., Baranov V.I., Litherland A.E., Tanner S.D., **2006**. Gas-phase ion–molecule reactions for resolution of atomic isobars: AMS and ICP-MS perspectives. International Journal of Mass Spectrometry 255-256, 312-327.

Becker J.S., **2005**. Inductively coupled plasma mass spectrometry (ICP-MS) and laser ablation ICP-MS for isotope analysis of long-lived radionuclides. International Journal of Mass Spectrometry 242, 183-195.

Belshaw N.S., Freedman P.A., O'Nions R.K., Frank M., Guo Y., **1998**. A new variable dispersion double-focusing plasma mass spectrometer with performance illustrated for Pb isotopes. International Journal of Mass Spectrometry 181, 51-58.

Berryman N., Probst T., **1996**. Rapid determination of Sr-90 by electrothermal vaporization inductively coupled plasma mass spectrometry (ETV-ICP-MS). Radiochimica Acta 76, 191-195.

Blaum K., Geppert Ch., Müller P., Nörtershäuser W., Wendt K., Bushaw B.A., **2000**. Peak shape for a quadrupole mass spectrometer: comparison of computer simulation and experiment. International Journal of Mass Spectrometry 202, 81-89.

Boulyga S.F., Becker J.S., **2002**. Improvement of abundance sensitivity in a quadrupol-based ICP-MS instrument with a hexapole collision cell. J. Anal. At. Spectrom. 17, 1202-1206.

Bushaw B.A., Cannon B.D., **1997**. Diode laser based resonance ionization mass spectrometric measurement of Sr-90. Spectrochimica Acta B 52, 1839-1854.

Bushaw B.A., Nörtershäuser W., **2000**. Resonance ionization spectroscopy of stable Sr isotopes and $^{90}Sr$ via $5s^2\ ^1S_0 \rightarrow 5s5p\ ^1P_1 \rightarrow 5s5d\ ^1D_2 \rightarrow 5s11f\ ^1F_3 \rightarrow Sr^+$. Spectrochimica Acta B 55, 1679-1692.

Choi Y.-H., Kang H.-S., Jun I., Keum D.-K., Park H.-K., Choi G.-S., Lee H., Lee C.-W., **2007**. Transfer of $^{90}Sr$ to rice plants after its acute deposition onto flooded paddy soils. Journal of Environmental Radioactivity 93, 157-169.

Douglas D.J., **1989**. Some current perspectives on ICP-MS. Can. J. Spectrosc. 34, 38-49.

Douglas D.J, French J.B., **1992**. Collisional focusing effects in radio frequency quadrupoles. Journal of Analytical Atomic Spectrometry 3, 398-408.

Du Z.Y., Houk R.S., **2000**. Attenuation of metal oxide ions in inductively coupled plasma mass spectrometry with hydrogen in a hexapole collision cell. Journal of Analytical Atomic Spectrometry 15, 383-388.

Edlund M., Visser H., Heitland P., **2002**. Analysis of biodiesel by argon-oxygen mixed-gas inductively coupled plasma optical emission spectrometry. Journal of Analytical Atomic Spectrometry 17, 232-235.

EIChrom **2007**. Product description of Sr spec Resin: http://www.eichrom.com/products/info/sr_resin.cfm

Eiden G.C., Barinaga C.J., Koppenaal D.W., **1997**. Beneficial Ion/Molecule Reactions in Elemental Mass Spectrometry. Rapid Communications in Mass Spectrometry 11, 37-42.

Favre G., Brennetot R., Chartier F., Vitorge P., **2007**. Understanding reactions with $O_2$ for $^{90}Sr$ measurements by ICP-MS with collision-reaction cell. International Journal of Mass Spectrometry 265, 15-22.

Fietzke J., Eisenhauer A., Gussone N., Bock B., Liebetrau V., Nägler Th.F., Spero H.J., Bijma J., Dullo C., **2004**. Direct measurement of $^{44}Ca/^{40}Ca$ ratios by MC-ICP-MS using the cool plasma technique. Chemical Geology 206, 11-20.

Gastberger M., Steinhäusler F., Gerzabek M.H., Lettner H., Hubmer A., **2000**. Soil-to-plant transfer of fallout caesium and Sr in Austrian lowland and Alpine pastures. Journal of Environmental Radioactivity 49, 217-233.

Gastberger M., Steinhäusler F., Gerzabek M.H., Hubmer A., **2001**. Fallout Sr and caesium transfer from vegetation to cow milk at two lowland and two Alpine pastures. Journal of Environmental Radioactivity 54, 267-273.

Goutelard F., Nazard R., Bocquet C., Coquenlorge N., Letessier P., Calmet D., **2000**. Improvement in 90Sr measurements at very low levels in environmental samples. Applied Radiation and Isotopes 53, 145-151.

Grinberg P., Willie S., Sturgeon R.E., **2007**. Determination of natural Sr and $^{90}Sr$ in environmental samples by ETV-ICP-MS. Journal of Analytical Atomic Spectrometry 22, 1409-1414.

Hagg C., Szabo I., **1986**. New ion-optical devices utilizing oscillatory electric fields. II. Stability of motion in a two-dimensional hexapole field. Int. J. Mass Spectrom. Ion Processes 73, 237–275.

Hattendorf B., Günther D., **2003**. Strategies for method development for an inductively coupled plasma mass spectrometer with bandpass reaction cell. Approaches with different reaction gases for the determination of selenium. Spectrochimica Acta B 58, 1-13.

Hattendorf B., Günther D., **2004**. Suppression of in-cell generated interferences in a reaction cell ICP-MS by bandpass tuning and kinetic energy discrimination. Journal of Analytical Atomic Spectrometry 19, 600-606.

Herranz M., Elejalde C., Legarda F., Romero F., **2001**. $^{90}Sr$ content of soils from Biscay (Spain). Applied Radiation and Isotopes 55, 521-525.

Horwitz E.P., Dietz M.L., Fisher D.E., **1991**. Separation and Preconcentration of Sr from Biological, Environmental, and Nuclear Waste Samples by Extraction Chromatography Using a Crown Ether. Analytical Chemistry 63, 522-525.

IAEA, **2003**. http://www-naweb.iaea.org/nahu/nmrm/nmrm2003/material/iaea375.htm

Isnard H., Aubert M., Blanchet P., Brennetot R., Chartier F., Geertsen V., Manuguerra F., **2006**. Determination of 90Sr / 238U ratio by double isotope dilution inductively coupled plasma mass spectrometer with multiple collection in spent nuclear fuel samples with in situ 90Sr / 90Zr separation in a collision-reaction cell. Spectrochimica Acta Part B 61, 150 – 156.

Jakubowski N., Moens L., Vanhaecke F., **1998**. Sector field mass spectrometers in ICP-MS. Spectrochimica Acta B 53, 1739-1763.

Jarvis K.E., Gray A.L., Houk R.S., **1992**. Handbook of Inductively Coupled Plasma Mass Spectrometry. Chapman and Hall, New York.

KAERI (Korea Atomic Energy Research Institute) **2000**. Table of Nuclides. http://atom.kaeri.re.kr/

Kehm K., Hauri E.H., Alexander C.M.O'D., Carslon R.W., **2003**. High precision iron isotope measurements of meteoritic material by cold plasma ICP-MS. Geochimica et Cosmochimica Acta 67, 2879–2891.

Koppenaal D.W., Eiden G.C., Barinaga C.J., **2004**. Collision and reaction cells in atomic mass spectrometry: development, status, and applications. Journal of Analytical Atomic Spectrometry 19, 561-570.

Lariviere D., Taylor V.F., Evans R.D., Cornett R.J., **2006**. Radionuclide determination in environmental samples by inductively coupled plasma mass spectrometry. Spectrochimica Acta Part B 61, 877-904.

Makarov A., Denisov E., Kholomeev A., Balschun W., Lange O., Strupat K., Horning S., **2006**. Performance Evaluation of a Hybrid Linear Ion Trap/Orbitrap Mass Spectrometer. Analytical Chemistry 78, 2113-2120.

Mewis A., **2004**. Dissertation: Sr-90 in der Umwelt: Migrationsverhalten im Boden, Transfer in die Nahrungskette und Strahlenexposition in der nördlichen Ukraine.
Milestone Acid Digestion Cookbook. Report Code 291. Update **1/1/1996**.
Moens L.J., Vanhaecke F.F., Bandura D.R., Baranov V.I., Tanner S.D., **2001**. Elimination of isobaric interferences in ICP-MS, using ion-molecule reaction chemistry: Rb/Sr age determination of magmatic rocks, a case study. Journal of Analytical Atomic Spectrometry 16, 991-994.
Montaser A., **1998**. Inductively coupled plasma mass spectrometry. Wiley-VCH.
Monz L., Hohmann R., Kluge H.-J., Kunze S., Lantzsch J., Otten E.W., Passler G., Senne P., Stenner J., Stratmann K., Wendt K., Zimmer K., **1993**. Fast, low level detection of Sr-90 and Sr-89 in environmental samples by collinear resonance ionization spectroscopy. Spectrochimica Acta 48B, 1655-1671.
MP Biomedicals, **2007**. http://www.mpbio.com/product_info.php?products_id=880020
Murphy K.E., Long S.E., Rearick M.S., Ertas Ö.S., **2002**. The accurate determination of potassium and calcium using isotope dilution inductively coupled "cold" plasma mass spectrometry. Journal of Analytical Atomic Spectrometry 17, 469-477.
Neis P., Hille R., Paschke M., Pilwat G., Schnabel A., Niess C., Bratzke H., **1999**. Sr90 for determination of time since death. Forensic Science International 99, 47-51.
Nelms S., **2005**. Inductively coupled plasma mass spectrometry handbook, Oxford (UK), Blackwell Publishing
NIST **2007**. https://srmors.nist.gov/view_cert.cfm?srm=987
N.N. **2007**. Liquid scintillation counting, in Wikipedia, http://en.wikipedia.org/wiki/Liquid_scintillation_counting, date: 2007-10-15
N.N. **2007a**. http://www.14c.uni-erlangen.de/en/ams.html
N.N. **2007b**. www.webelements.com
Olesik J.W., Jones D.R., **2006**. Strategies to develop methods using ion-molecule reactions in a quadrupole reaction cell to overcome spectral overlaps in inductively coupled plasma mass spectrometry. Journal of Analytical Atomic Spectrometry 21, 141-159.
Paul M., Berkovits D., Cecil L.D., Feldstein H., Hershkowitz A., Kashiv Y., Vogt S., **1997**. Environmental $^{90}Sr$ measurements. Nuclear Instruments and Methods in Physics Research B 123, 394-399.
Pröfrock D., Leonhard P., Prange A., **2003**. Determination of sulfur and selected trace elements in metallothionein-like proteins using capillary electrophoresis hyphenated to inductively coupled plasma mass spectrometry with an octopole reaction cell. Analytical and Bioanalytical Chemistry 377, 132–139.
Prohaska T., Quétel C.R., Hennessy C., Liesegang D., Papadakis I., Taylor P.D.P., Latkoczy., Hann S., Stingeder G., **2000**. SI-traceable cerification of Cu, Cr, Cd and Pb in sediment and fly ash candidate reference material. Journal of Environmental Monitoring 2, 613-620.
Rowan J.T., Houk R.S., **1989**. Attenuation of polyatomic ion interferences in inductively coupled plasma mass-spectrometry by gas-phase collisions. Applied Spectroscopy 43, 976-980.
Schrader H., **2004**. Half-life measurements with ionization chambers - A study of systematic effects and results. Applied Radiation and Isotopes 60, 317-323.
Shen C-C., Chiu H-Y., Chiang H-W., Chu M-F., Wei K-Y., Steinke S., Chen M-T., Lin Y-S., Lo L., **2007**. High precision measurements of Mg/Ca and Sr/Ca ratios in carbonates by cold plasma inductively coupled plasma quadrupole mass spectrometry. Chemical Geology 236, 339-349.
Shiraishi K., Ko S., Arae H., Ayama K., **2006**. Rapid analysis technique for Sr, thorium, and uranium in urine samples. Journal of Radioanalytical and Nuclear Chemistry 273, 307-310.
Tanner S.D., **1995**. Characterization of ionization and matrix suppression in inductively coupled cold plasma mass spectrometry. Journal of Analytical Atomic Spectrometry 10, 905-921.
Tanner S.D., Baranov V.I., **1999**. A Dynamic Reaction Cell for Inductively Coupled Plasma Mass Spectrometry (ICPDRC-MS). II. Reduction of Interferences Produced Within the Cell. American Society for Mass Spectrometry 10, 1083-1094.
Tanner S.D., Baranov V.I., Bandura D.R., **2002**. Reaction cells and collision cells for ICP-MS: a tutorial review. Spectrochimica Acta Part B 57, 1361-1452.
Taylor V.E., Evans R.D., Cornett R.J., **2007**. Determination of 90Sr in contaminated environmental samples by tuneable bandpass dynamic reaction cell ICP-MS. Analytical and Bioanalytical Chemistry 387, 343-350.

Thomas R., **2001**. A beginners guide to ICP-MS Part II: The sample-introduction system. Spectroscopy 16(5), 56-60.

Turner P.J., Mills D.J., Schröder E., Lapitans G., Jung G., Iacone L.A., Haydar D.A. and Montaser A. (**1998**). Instrumentation for low- and high-resolution ICPMS. In: Inductively Coupled Plasma Mass Spectrometry, Chapter 6 (ed. Montaser A.), Wiley-VCH, New York, p. 444.

UNSCEAR **2000**a Report, Annex C, Exposures to the public from man-made sources of radiation: http://www.unscear.org/docs/reports/annexc.pdf

UNSCEAR **2000**b Report, Annex J, Exposures and effects of the Chernobyl accident: http://www.unscear.org/docs/reports/annexj.pdf

U.S. Department of health and human services, Toxicological profile for Sr, April **2004**: http://www.atsdr.cdc.gov/toxprofiles/tp159-p.pdf

Vanhaecke F., Saverwyns S., De Wannemacker G., Moens L., Dams R., **2000**. Comparison of the application of higher mass resolution and cool plasma conditions to avoid spectral interferences in Cr(III)/Cr(VI) speciation by means of high-performance liquid chromatography – inductively coupled plasma mass spectrometry. Analytica Chimica Acta 419, 55-64.

Vonderheide A.P., Zoriy M.V., Izmer A.V., Pickhardt C., Caruso J.A., Ostapczuk P., Hille R., Becker S., **2004**. Determination of $^{90}$Sr at ultratrace levels in urine by ICP-MS. Journal of Analytical Atomic Spectrometry 19, 675-680.

Wendt K., Bhowmick G.K., Bushaw B.A., Herrmann G., Kratz J.V., Lantzsch L., Müller P., Nörtershäuser W., Otten E.W., Schwalbach R., Seibert U., Trautmann N., Walter K., Zimmer K.,**1997** Rapid trace analysis of Sr-89,Sr-90 in environmental samples by collinear laser resonance ionization mass spectrometry Radiochimica Acta 79, 183-190.

Wendt K., Trautmann N., Bushaw B.A., **2000**. Resonant laser ionization mass spectrometry: An alternative to AMS? Nuclear Instruments and Methods in Physics Research B 172, 162-169.

Wollenweber D., Straßburg Silke, Wünsch G., **1999**. Determination of Li, Na, Mg, K, Ca and Fe with ICP-MS using cold plasma conditions. Fresenius' Journal of Analytical Chemistry 364, 433-437.

Yamada N., Takahashi J., Sakata K., **2002**. The effects of cell-gas impurities and kinetic energy discrimination in an octopole collision cell ICP-MS under non-thermalized conditions. Journal of Analytical Atomic Spectrometry 17, 1213-1222.

Yamaguchi N., Seki K., Komamura M., Kurishima K., **2007**. Long-term mobility of fallout $^{90}$Sr in ploughed soil, and $^{90}$Sr uptake by wheat grain. Science of the Total Environment 372, 595-604.

Zimmer K., Stenner J., Kluge H.-J., Lanztsch J., Monz L., Otten E.W., Passler G., Schwalbach R., Schwarz M., Stevens H., Wendt K., Herrmann G., Nieß S., Trautmann N., Walter K., Bushaw B.A., **1994**. Determination of $^{90}$Sr in environmental samples with resonance ionization spectroscopy in collinear geometry. Applied Physics B 59, 117-121.

Zoriy M.V., Ostapczuk P., Halicz L., Hille R., Becker S., **2005**. Determination of $^{90}$Sr and Pu isotopes in contaminated groundwater samples by inductively coupled plasma mass spectrometry. International Journal of Mass Spectrometry 242, 203-209.

# 6 Appendix

## *6.1 Figures*

### 6.1.1 Cold plasma – cyclonic spray chamber + PFA nebuliser

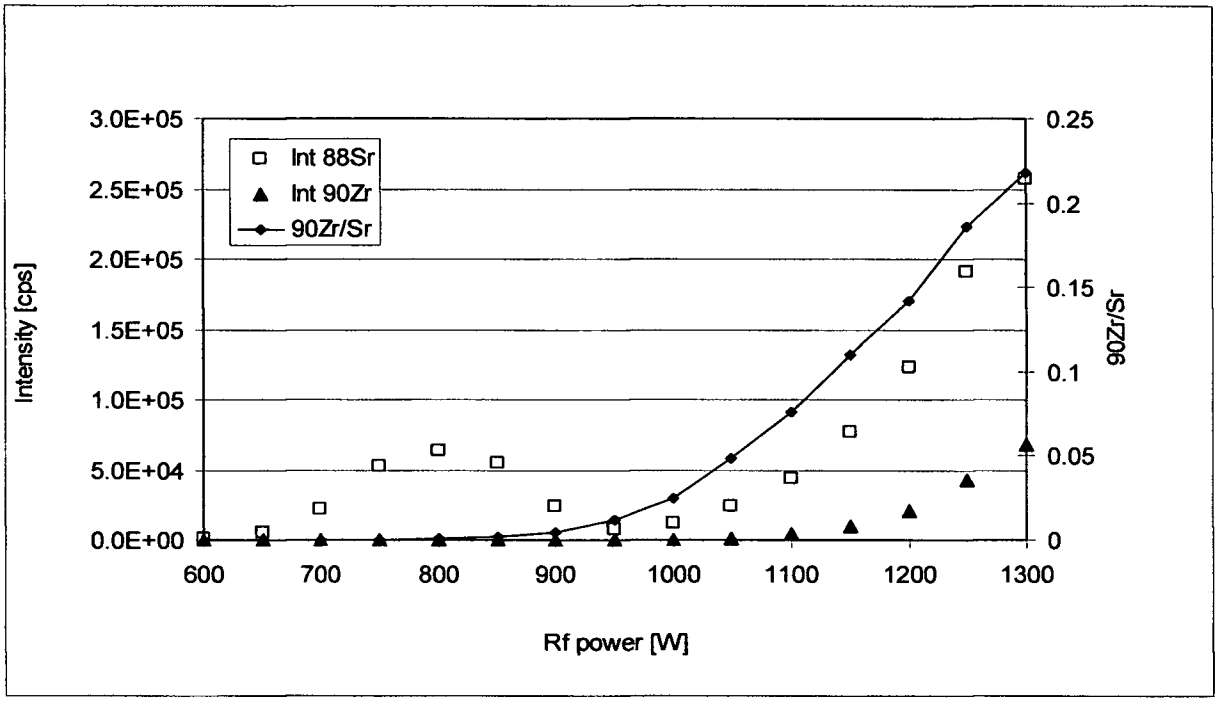


**Fig. A 1** Effect of Rf power on the response of $^{88}Sr$ and $^{90}Zr$. Rb, Sr, Y and Zr concentration is 10 ng $g^{-1}$. Nebuliser gas flow rate is 1.15 L $min^{-1}$.

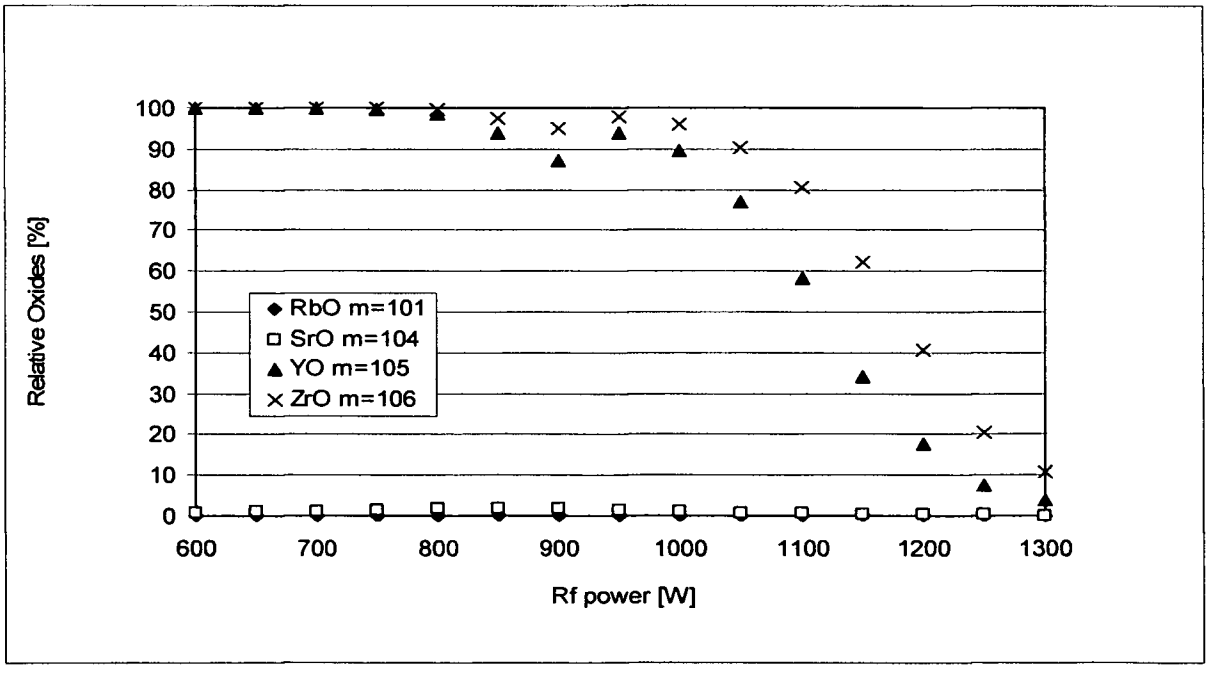


**Fig. A 2** Effect of Rf power on the oxide formation of Rb, Sr, Y and Zr. Concentration is 10 ng $g^{-1}$. Nebuliser gas flow rate is 1.15 L $min^{-1}$.

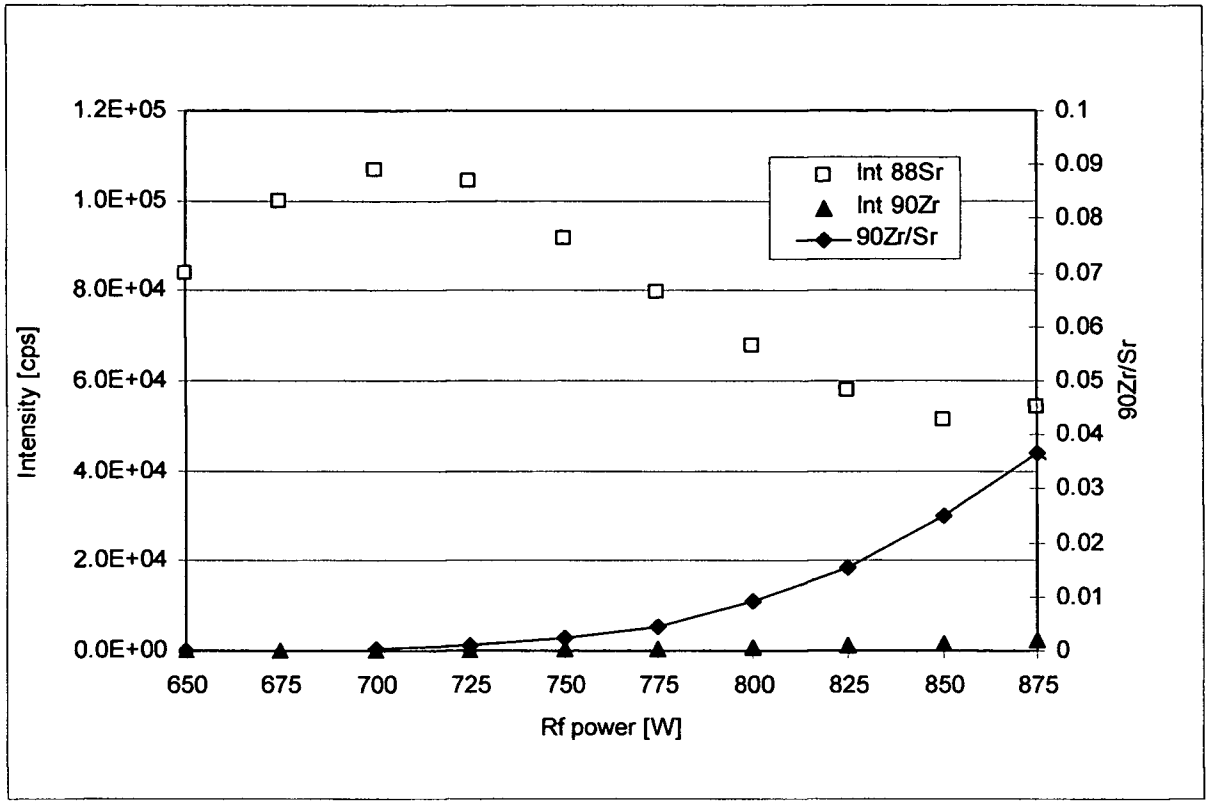


**Fig. A 3** Effect of Rf power on the response of $^{88}Sr$ and $^{90}Zr$. Rb, Sr, Y and Zr concentration is 10 ng $g^{-1}$. Nebuliser gas flow rate is 1.0 L $min^{-1}$ and auxiliary gas flow rate is 1.1 L $min^{-1}$.

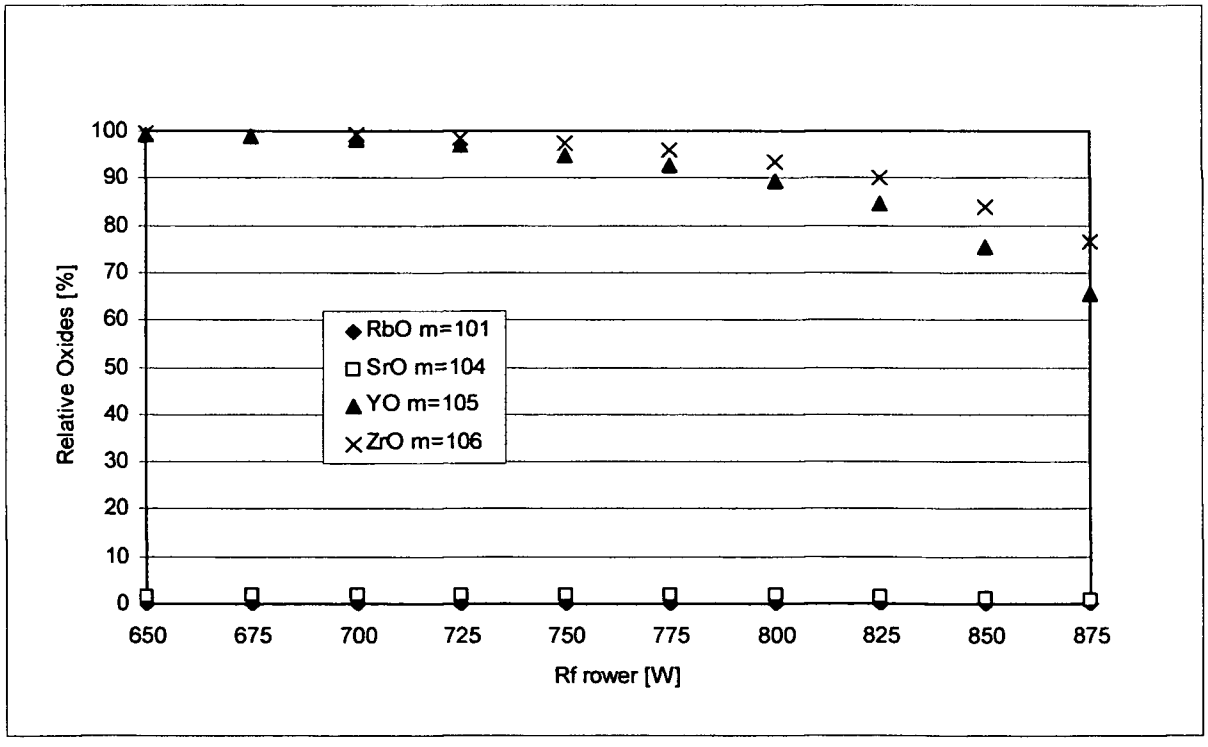


**Fig. A 4** Effect of Rf power on the oxide formation of Rb, Sr, Y and Zr. Concentration is 10 ng $g^{-1}$. Nebuliser gas flow rate is 1.0 L $min^{-1}$ and auxiliary gas flow rate is 1.1 L $min^{-1}$.

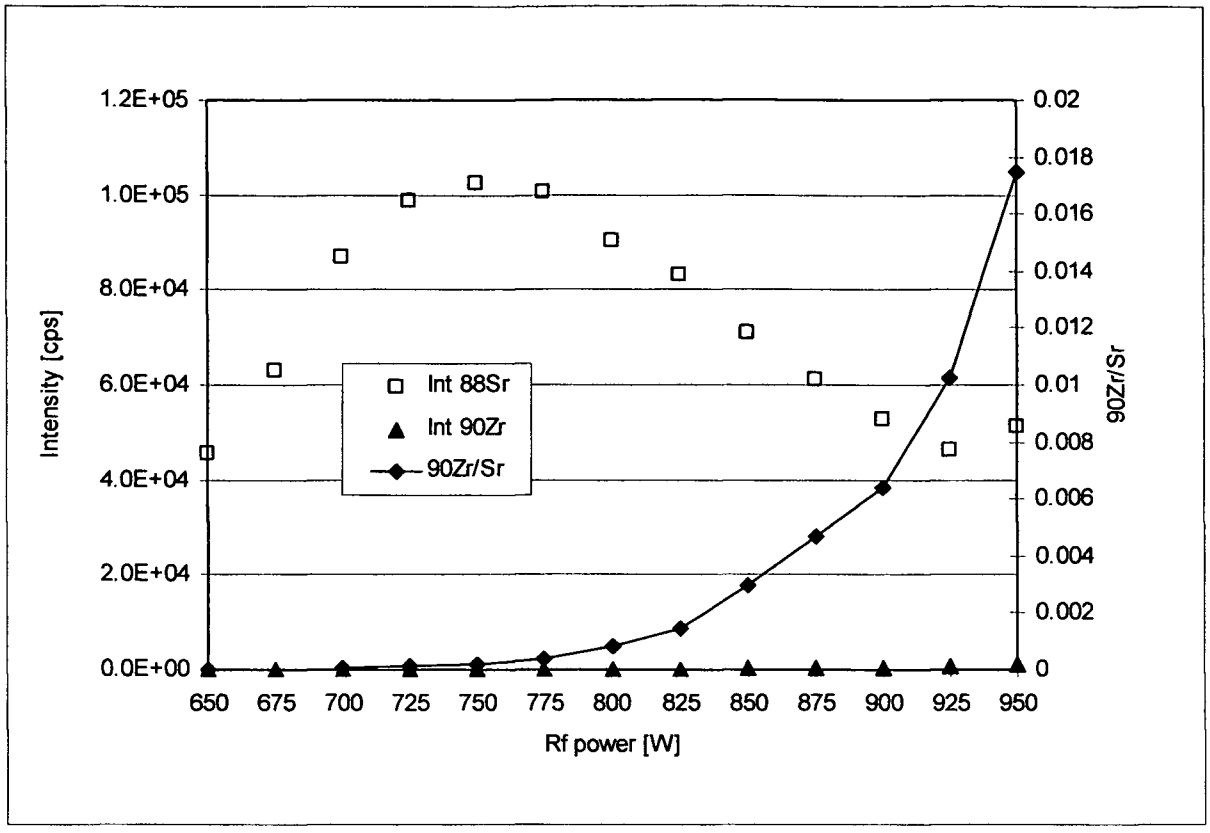


**Fig. A 5** Effect of Rf power on the response of $^{88}Sr$ and $^{90}Zr$. Rb, Sr, Y and Zr concentration is 10 ng $g^{-1}$. Nebuliser gas flow rate is 1.2 L $min^{-1}$ and auxiliary gas flow rate is 1.1 L $min^{-1}$.

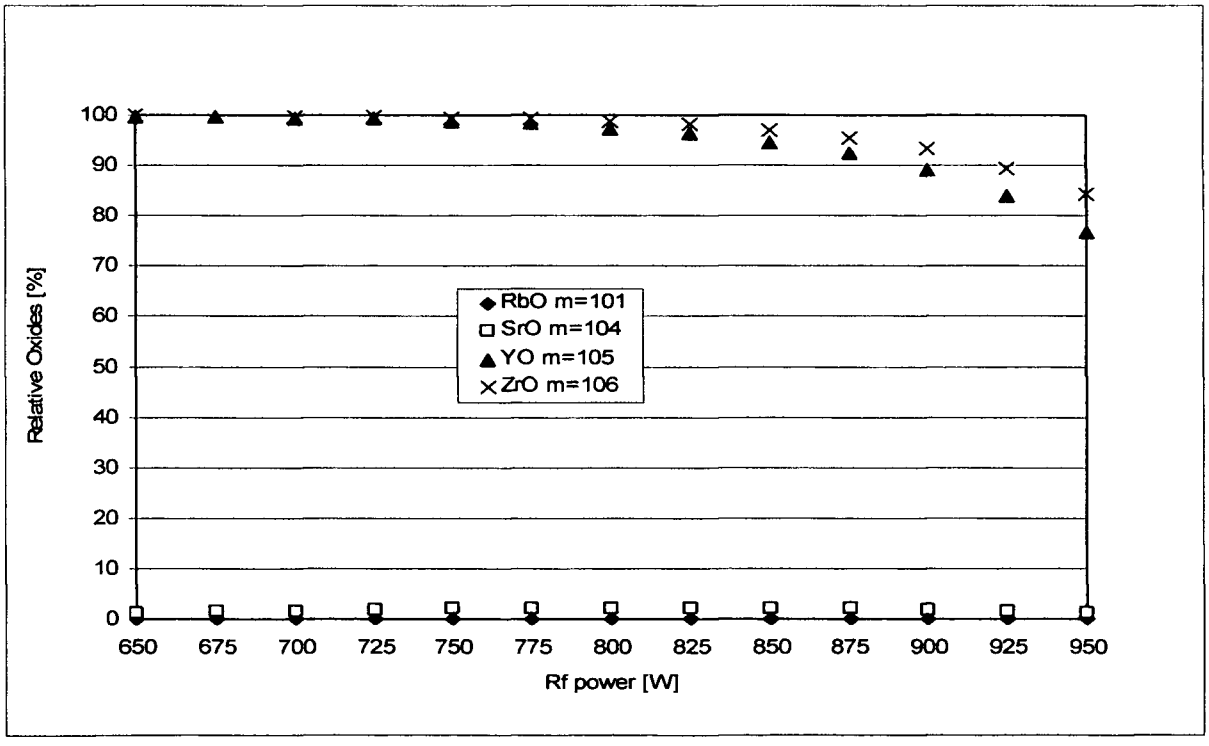


**Fig. A 6** Effect of Rf power on the oxide formation of Rb, Sr, Y and Zr. Concentration is 10 ng $g^{-1}$. Nebuliser gas flow rate is 1.2 L $min^{-1}$ and auxiliary gas flow rate is 1.1 L $min^{-1}$.

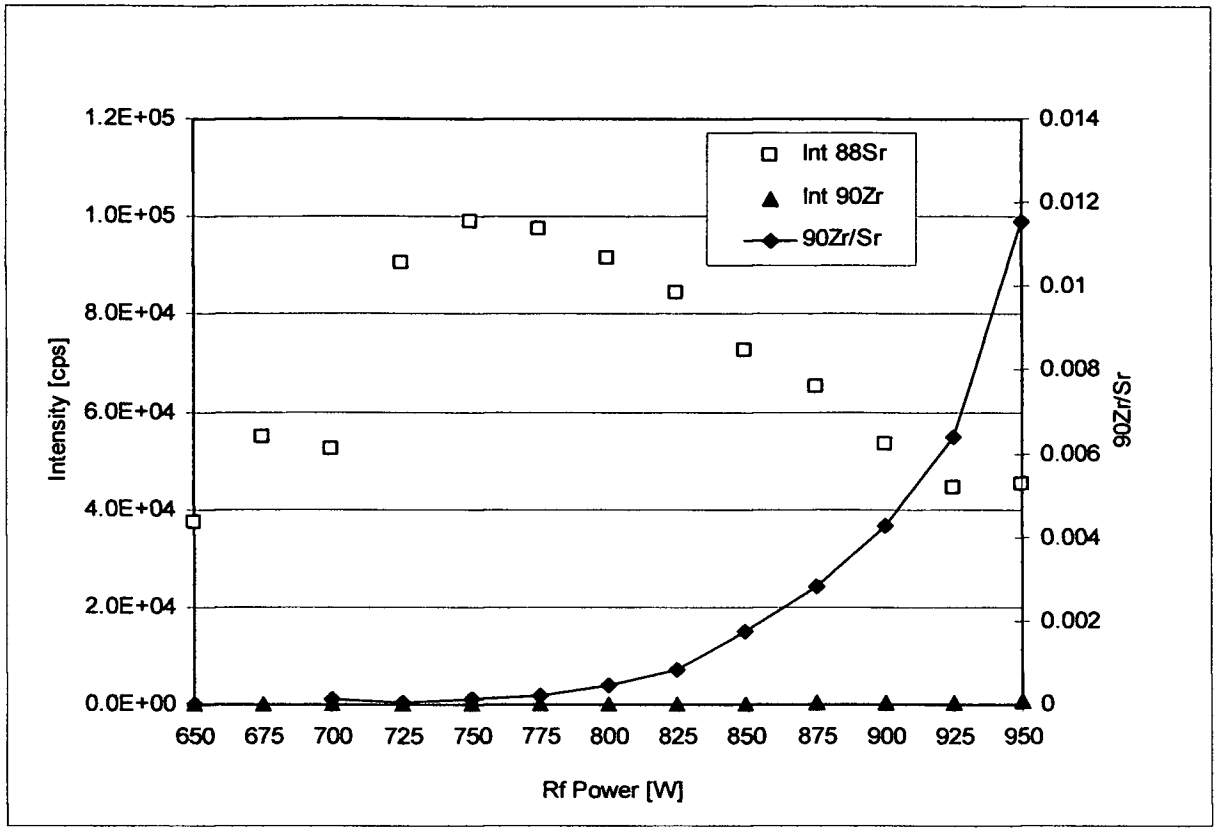


**Fig. A 7** Effect of Rf power on the response of $^{88}Sr$ and $^{90}Zr$. Rb, Sr, Y and Zr concentration is 10 ng $g^{-1}$. Nebuliser gas flow rate is 1.1 L $min^{-1}$ and auxiliary gas flow rate is 1.2 L $min^{-1}$.

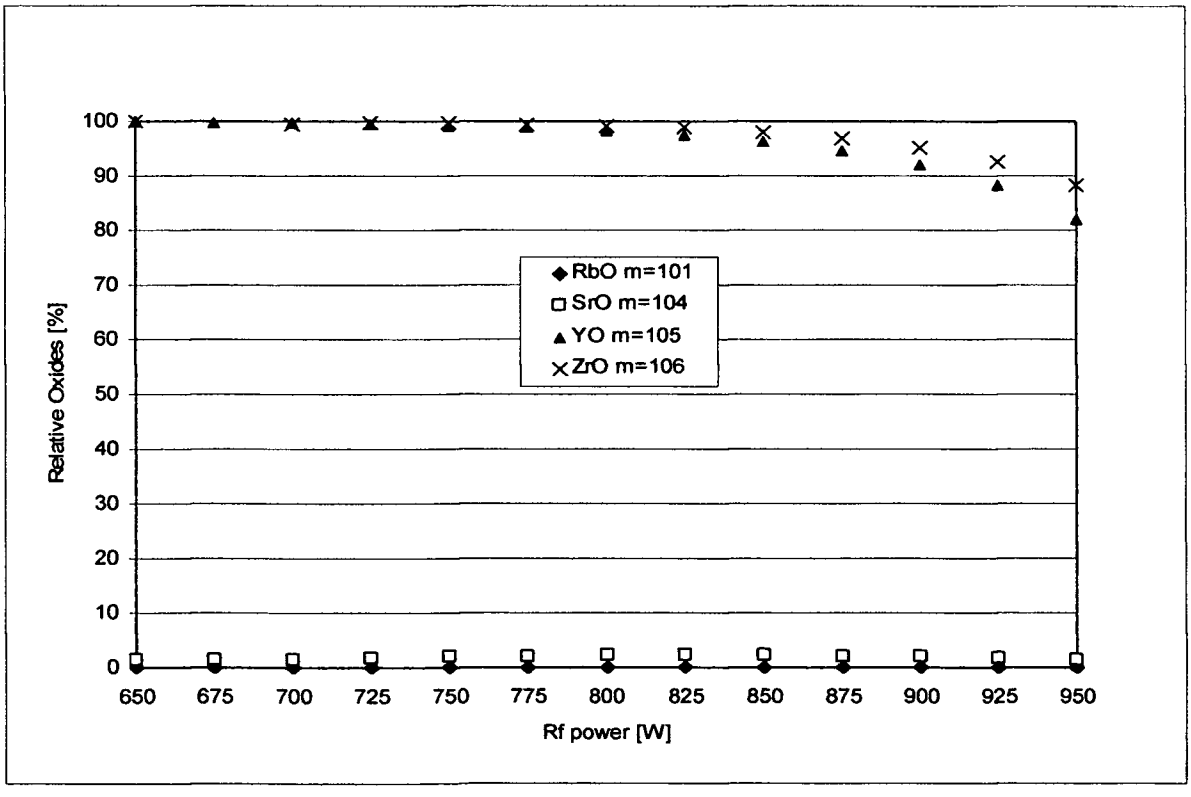


**Fig. A 8** Effect of Rf power on the oxide formation of Rb, Sr, Y and Zr. Concentration is 10 ng $g^{-1}$. Nebuliser gas flow rate is 1.1 L $min^{-1}$ and auxiliary gas flow rate is 1.2 L $min^{-1}$.

## 6.1.2 Cold plasma – ultrasonic nebuliser

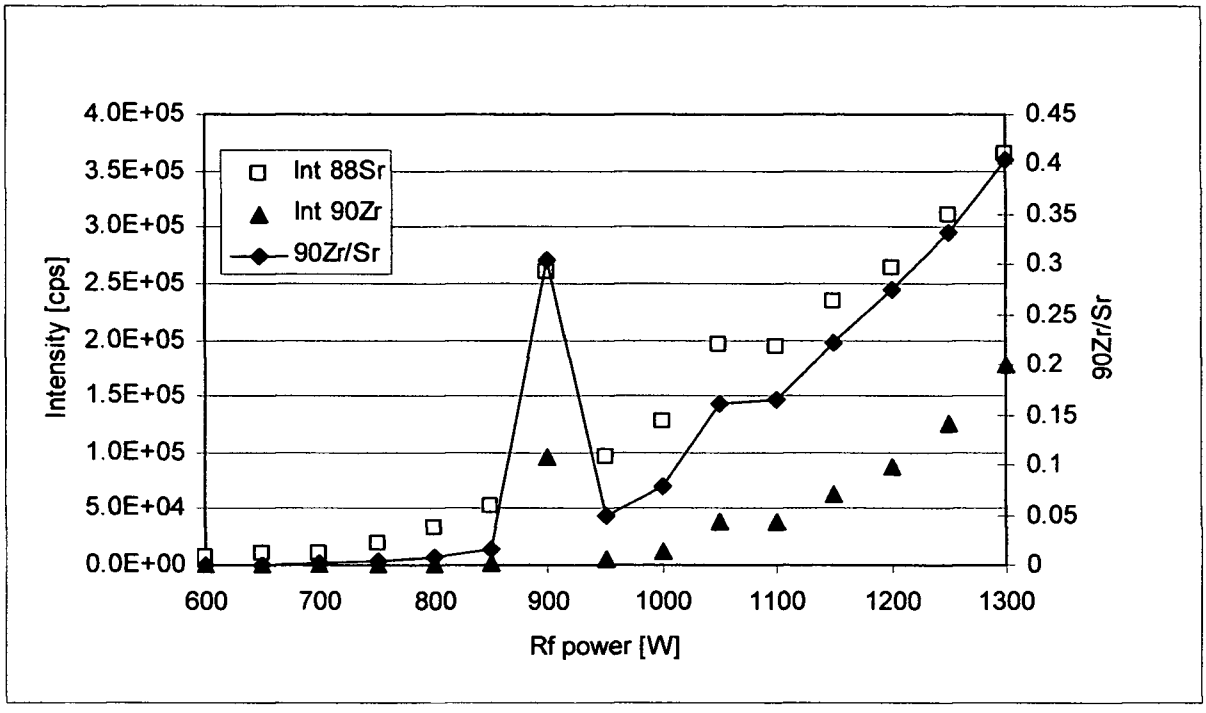


**Fig. A 9** Effect of Rf power on the response of $^{88}Sr$ and $^{90}Zr$. Sr, Rb and Y concentration is 2 ng $g^{-1}$ and Zr concentration is 5 ng $g^{-1}$. Nebuliser gas flow rate is 1.15 L $min^{-1}$. The values at 900 W are outliers.

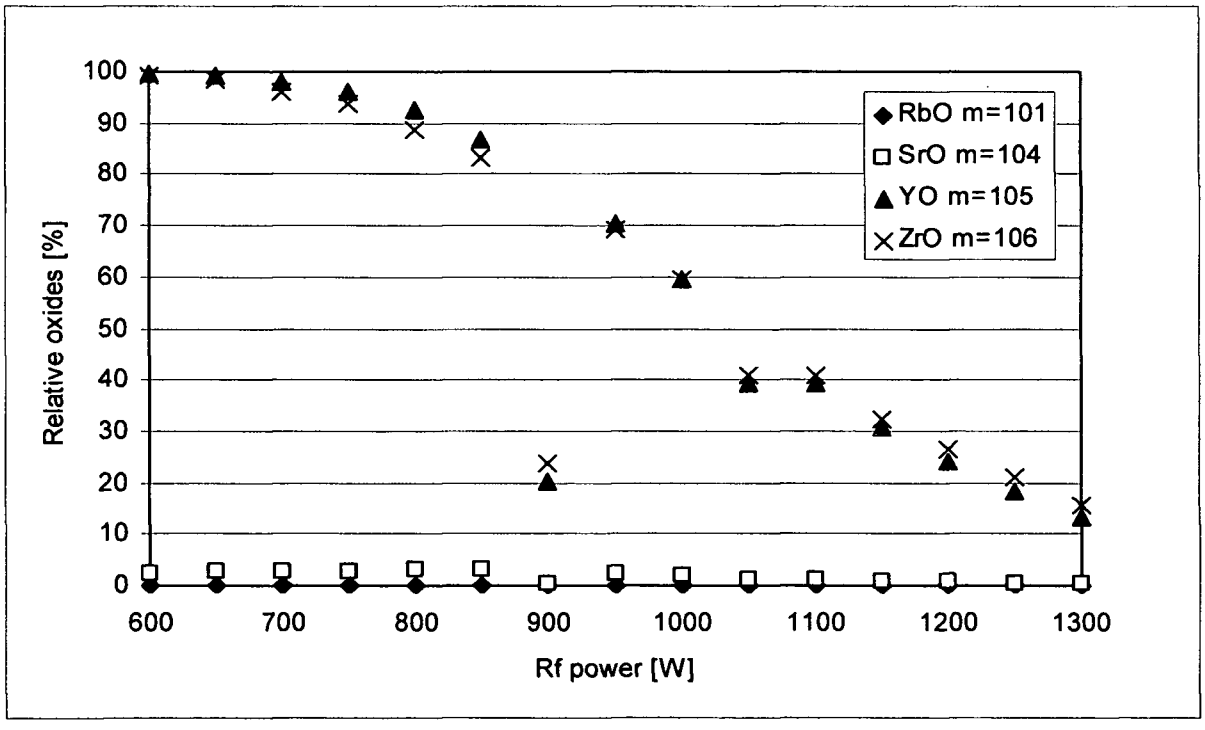


**Fig. A 10** Effect of Rf power on the oxide formation of Rb, Sr, Y and Zr. Sr, Rb and Y concentration is 2 ng $g^{-1}$ and Zr concentration is 5 ng $g^{-1}$. Nebuliser gas flow rate is 1.15 L $min^{-1}$. The values at 900 W are outliers.

## 6.1.3 DRC – Reaction cell gas

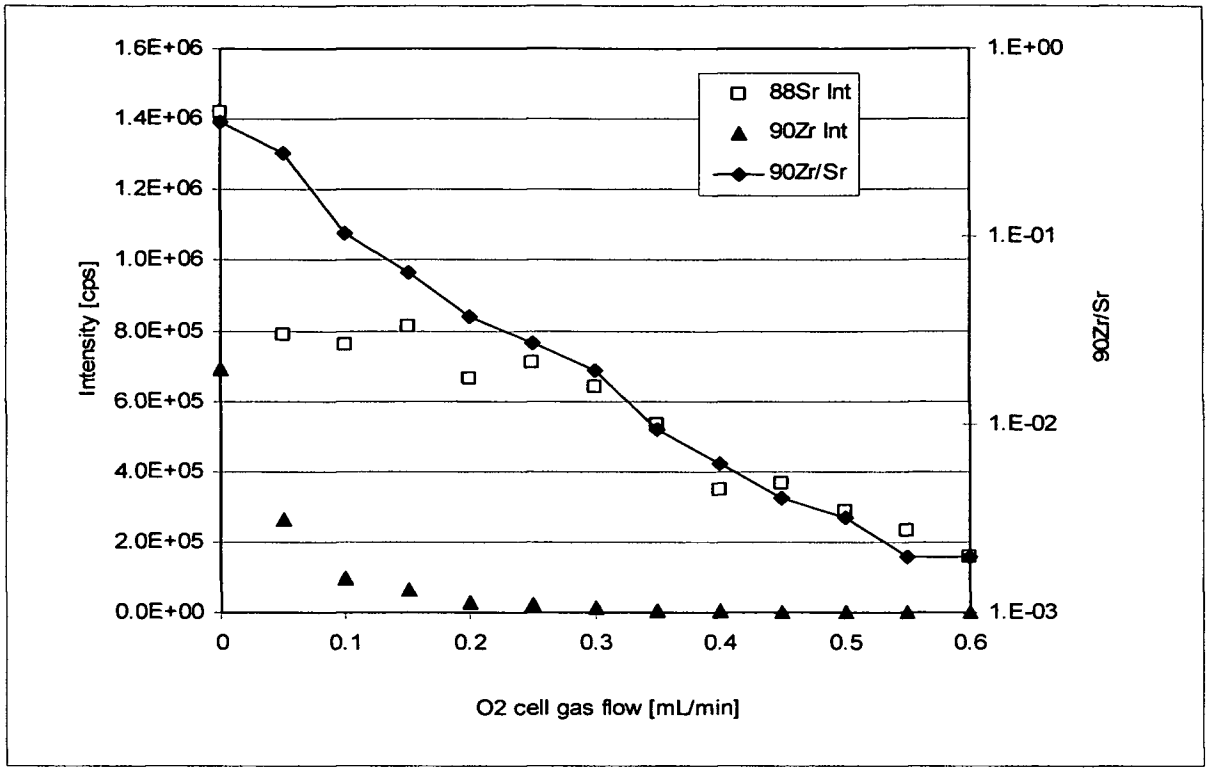


**Fig. A 11** Effect of cell gas flow on the response of $^{88}Sr$ and $^{90}Zr$. Sr, Rb, Y and Zr concentration is 10 ng $g^{-1}$.

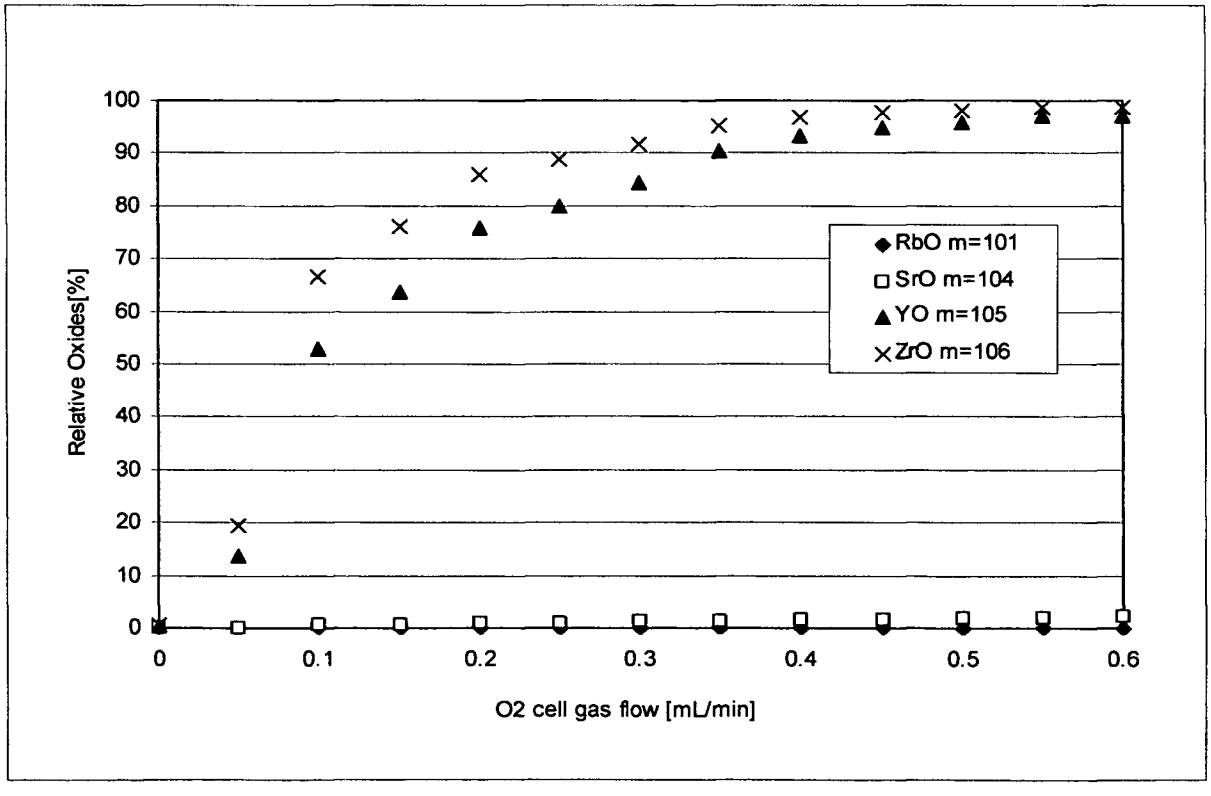


**Fig. A 12** Effect of cell gas flow on the oxide formation. Sr, Rb, Y and Zr concentration is 10 ng $g^{-1}$.

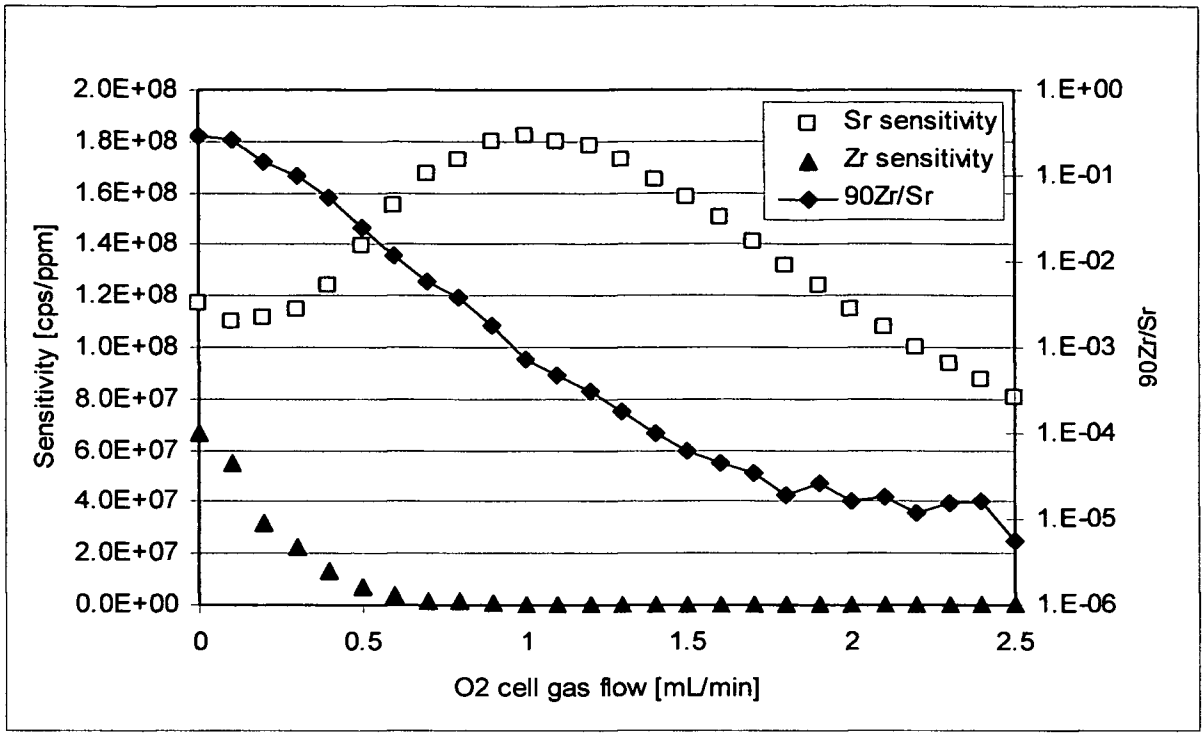


**Fig. A 13** Effect of cell gas flow on the sensitivity of Sr and Zr. Sr, Rb, Y and Zr concentration is 2 ng $g^{-1}$.

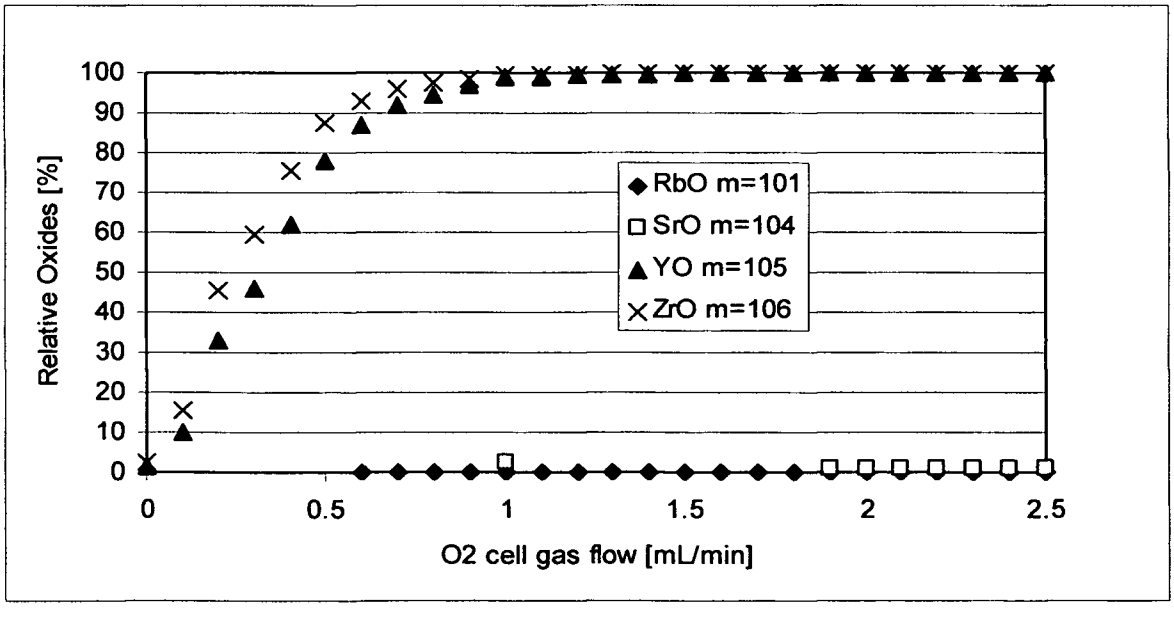


**Fig. A 14** Effect of cell gas flow on the oxide formation. Sr, Rb, Y and Zr concentration is 2 ng $g^{-1}$.

## 6.1.4 Combined effect of cold plasma and reaction gas

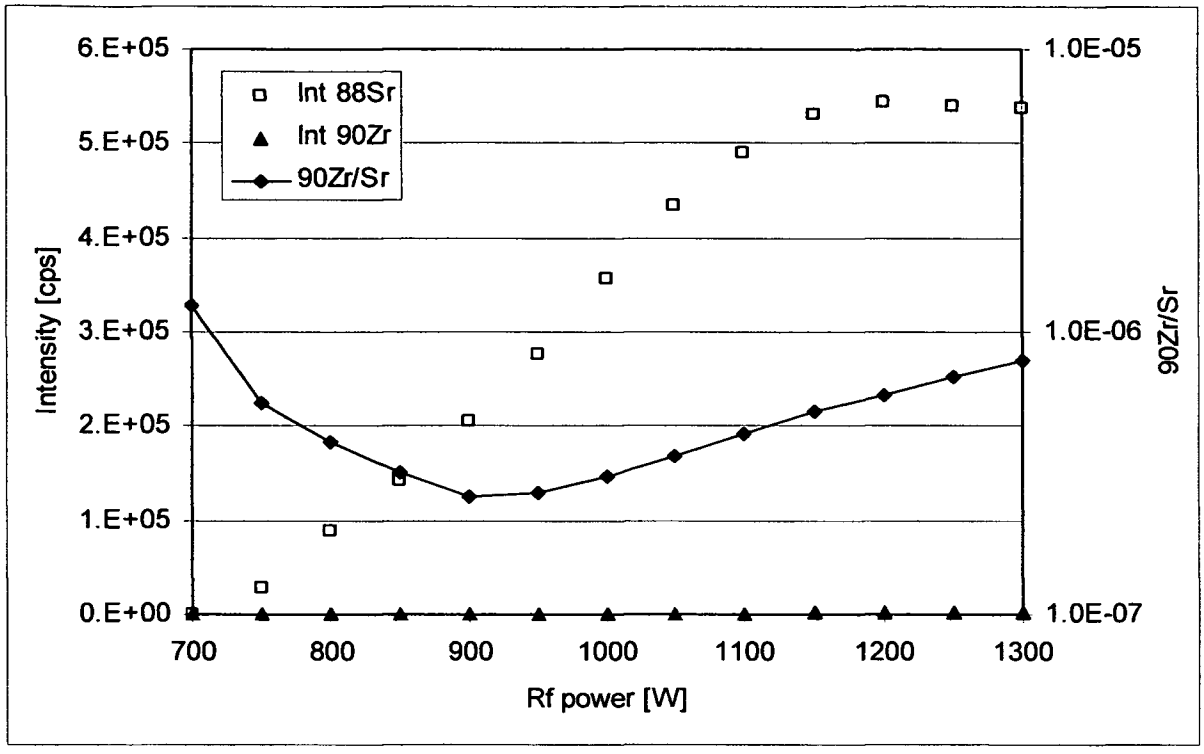


**Fig. A 15** Effect of Rf power on the response of $^{88}Sr$ and $^{90}Zr$. Ultrasonic nebuliser is used, cell gas flow is 2.5 mL $min^{-1}$ and nebuliser gas flow rate is 1.08 mL $min^{-1}$. Concentration of Sr is 2 ng $g^{-1}$ and concentration of Zr is 7 µg $g^{-1}$.

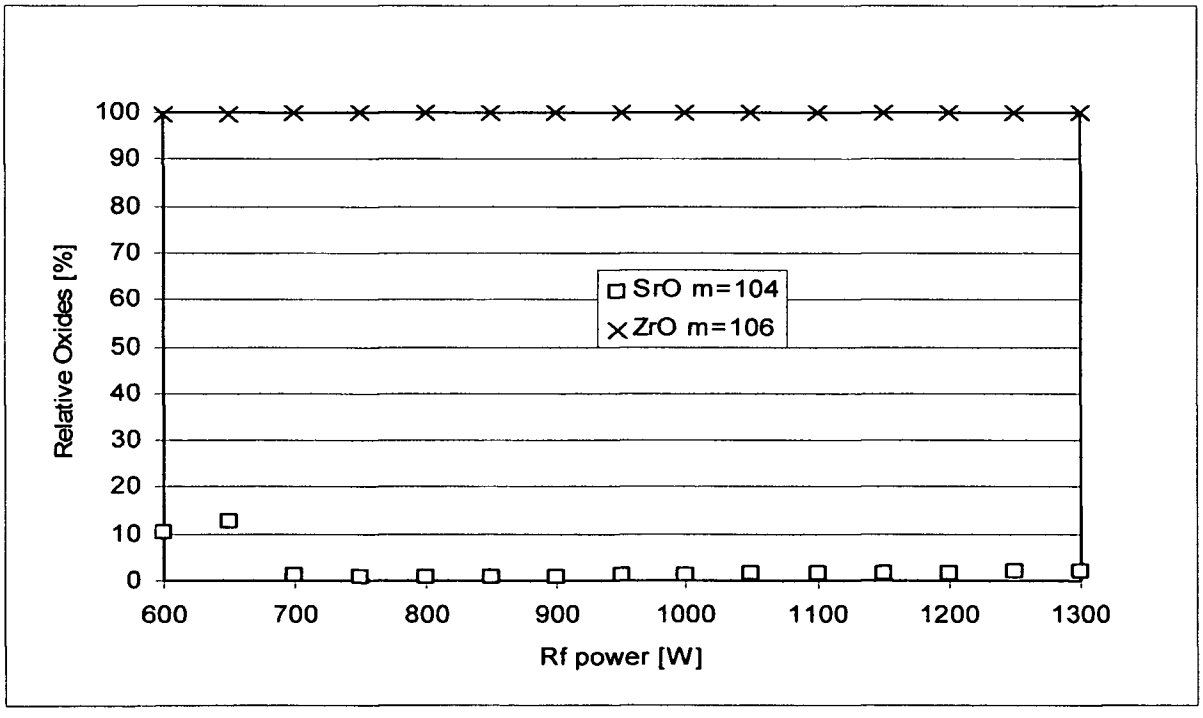


**Fig. A 16** Effect of Rf power and reaction gas on the oxide formation of Sr and Zr. Ultrasonic nebuliser is used, cell gas flow is 2.5 mL $min^{-1}$ and nebuliser gas flow rate is 1.08 mL $min^{-1}$. Concentration of Sr is 2 ng $g^{-1}$ and concentration of Zr is 7 µg $g^{-1}$.

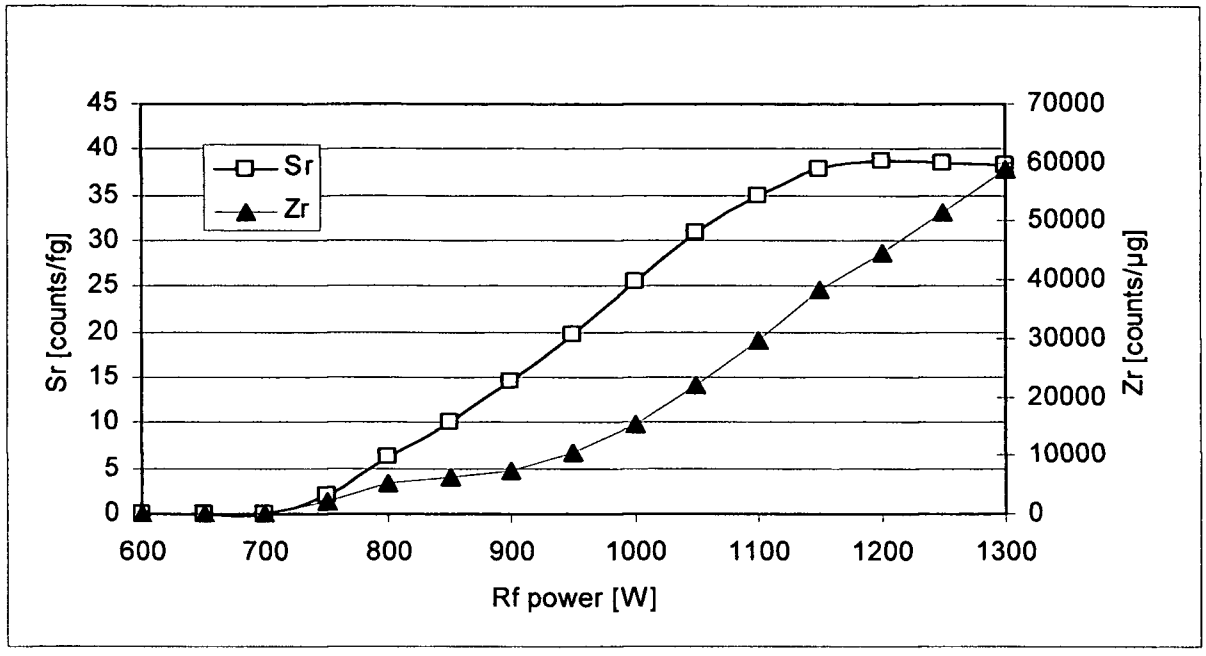


**Fig. A 17** Effect of Rf power and reaction gas on the absolute sensitivity of Sr and Zr. Ultrasonic nebuliser is used, cell gas flow is 2.5 mL $min^{-1}$ and nebuliser gas flow rate is 1.08 mL $min^{-1}$. Concentration of Sr is 2 ng $g^{-1}$ and concentration of Zr is 7 µg $g^{-1}$.

## 6.1.5 DRC – Cell rod offset

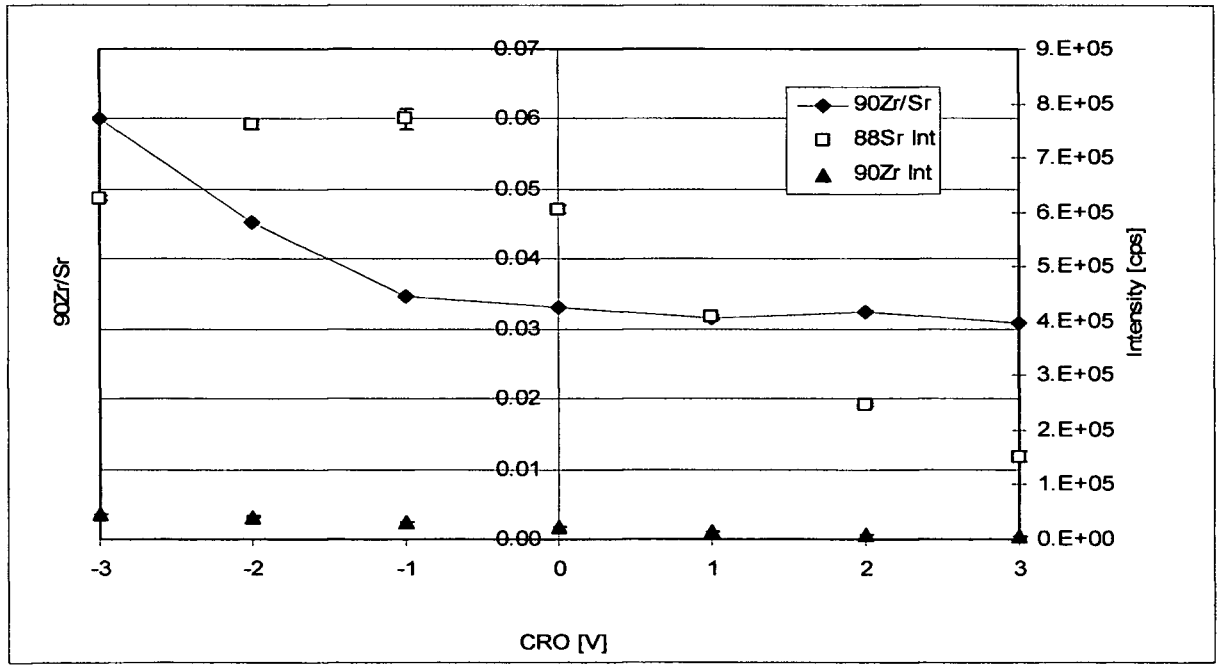


**Fig. A 18** Effect of cell rod offset on the intensity of Sr and Zr. Sr, Rb, Y and Zr concentration is 10 ng $g^{-1}$. Cell gas flow is 0.2 mL $min^{-1}$.

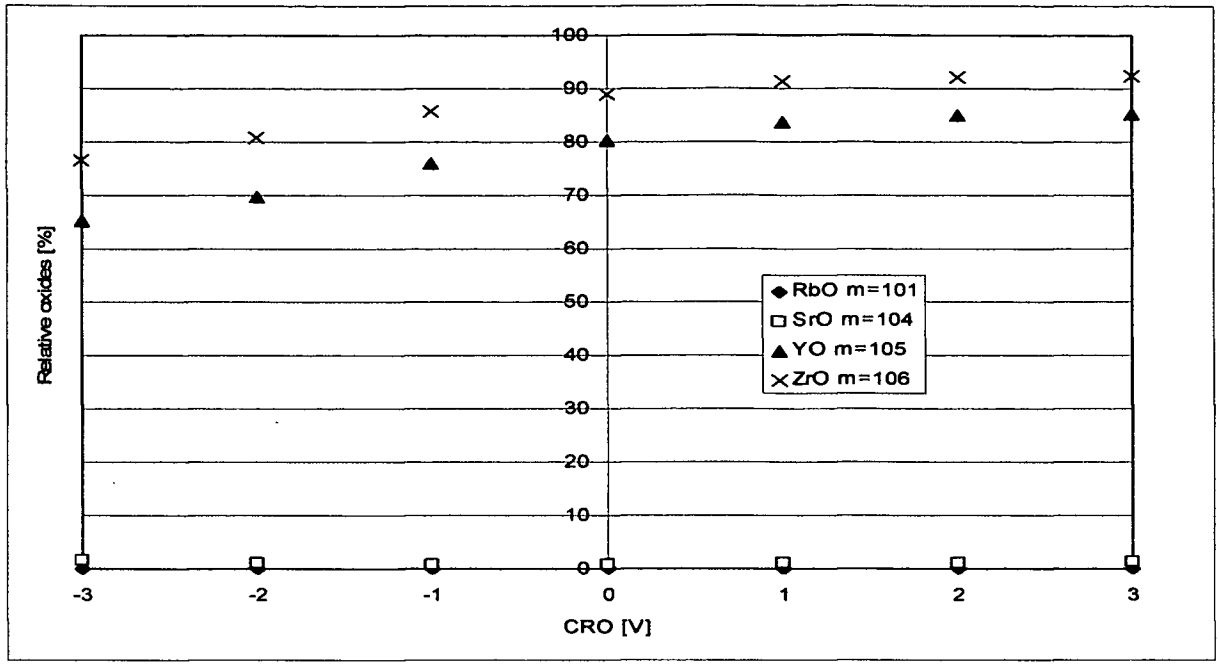


**Fig. A 19** Effect of cell rod offset on the oxide formation. Sr, Rb, Y and Zr concentration is 10 ng $g^{-1}$. Cell gas flow is 0.2 mL $min^{-1}$.

## 6.2 List of Tables

## 6.3 List of Figures

## 6.4 List of Equations

## 6.5 List of Abbreviations

| | |
|---|---|
| A | activity |
| ALI | annual limit on intake |
| AMS | accelerator mass spectrometry |
| AS | abundance sensitivity |
| BEC | background equivalent concentration |
| [Bq] | becquerel |
| [°C] | degree Celsius |
| CID | collision induced dissociation |
| CC | collision cell |
| cps | counts per second |
| CRO | cell rod offset |
| DC | direct current |
| DRC | dynamic reaction cell |
| ETV | electrothermal vaporisation |
| ETV-ICP-MS | electrothermal vaporisation inductively coupled plasma mass spectrometry |
| [g] | gram |
| HCl | hydrochloric acid |
| $HClO_4$ | perchloric acid |
| HF | hydrofluoric acid |
| $HNO_3$ | salpetric acid |
| IAEA | International Atomic Energy Agency |
| ID | isotope dilution |
| IDMS | isotope dilution mass spectrometry |
| ICP-MS | inductively coupled plasma mass spectrometry |
| Int | Intensity |
| KED | kinetic energy discrimination |
| [kg] | kilogram |
| [L] | litre |
| LC | liquid chromatography |
| *m/z* | mass to charge ratio |
| [µL] | microlitre |
| [mg] | milligram |
| [mL] | millilitre |
| M | molar |
| [min] | minute |
| ng | nano gram |
| µg | micro gram |
| pg | pico gram |
| PFA | polyfluoroalkoxy |
| QRO | quadrupol rod offset |
| RF | radio frequency |
| RIMS | resonance ionisation mass spectrometry |
| Rb | rubidium |
| [s] | second |
| SF-ICP-MS | sector field inductively coupled mass spectrometry |
| SRM | standard reference material |
| Sr | strontium |
| $T_{1/2}$ | half-life time |
| TIMS | thermal ionisation mass spectrometry |
| USN | ultrasonic nebuliser |
| [V] | volt |
| [W] | watt |
| Y | yttrium |
| Zr | zirconium |

## 6.6 GUM – workbench uncertainty budgets

# Reverse IDMS - Sr quantification spike

## Model Equation:

$$C_{y1}=C_{z2}*m_z/m_y*(R_{z1}-R_{rb})/(R_{rb}-R_{y1})*(R_{y1}+R_{y2}+R_{y3}+R_{y4})/(R_{z1}+R_{z2}+R_{z3}+R_{z4});$$

$$C_{z2}=C_{z1}*EW/AW/cf;$$

## List of Quantities:

| Quantity | Unit | Definition |
|---|---|---|
| $C_{y1}$ | mg/kg | Sr concentration in sample (86Sr spike) |
| $C_{z2}$ | mg/kg | Sr concentration in reverse spike (Merck Sr) |
| $m_z$ | g | weighted sample reverse spike (Merck Sr) |
| $m_y$ | g | weighted sample (86 Sr spike) |
| $R_{z1}$ | | 88/86 Merck Sr |
| $R_{rb}$ | | 88/86Sr blendratio |
| $R_{y1}$ | | 88/86 sample (86Sr spike) |
| $R_{y2}$ | | 87/86 sample (86Sr spike) |
| $R_{y3}$ | | 86/86 sample (86Sr spike) |
| $R_{y4}$ | | 84/86 sample (86Sr spike) |
| $R_{z2}$ | | 87/86 Merck Sr |
| $R_{z3}$ | | 86/86 Merck Sr |
| $R_{z4}$ | | 84/86 Merck Sr |
| $C_{z1}$ | mg/l | Sr original concentration reverse spike (Merck Sr) |
| EW | g | weighted sample reverse spike (Merck Sr) |
| AW | g | dilution reverse spike (Merck Sr) |
| cf | kg/l | conversion factor litre to kilogram (specific weight, certificate Merck Sr) |

**$m_z$:** Type B rectangular distribution
Value: 0.2686 g
Halfwidth of Limits: 0.0002 g

**$m_y$:** Type B rectangular distribution
Value: 0.2045 g
Halfwidth of Limits: 0.0002 g

**$R_{z4}$:** Type A
Method of observation: Direct
Number of observations: 6

| No. | Observation |
|---|---|
| 1 | 0.05549 |
| 2 | 0.05579 |
| 3 | 0.05596 |
| 4 | 0.05613 |
| 5 | 0.05621 |
| 6 | 0.05622 |

Arithmetic Mean: 0.055967
Standard Deviation: $290 \cdot 10^{-6}$
Standard Uncertainty: $117 \cdot 10^{-6}$
Degrees of Freedom: 5

**$C_{z1}$:** Type B rectangular distribution
Value: 1004 mg/l
Halfwidth of Limits: 5 mg/l

**EW:** Type B rectangular distribution
Value: 1.0241 g
Halfwidth of Limits: 0.0002 g

**AW:** Type B rectangular distribution
Value: 10.3252 g
Halfwidth of Limits: 0.0002 g

**cf:** Constant
Value: 1.014 kg/l

## Interim Results:

| Quantity | Value | Standard Uncertainty |
|---|---|---|
| $C_{z2}$ | 98.206 mg/kg | 0.283 mg/kg |

## Uncertainty Budgets:

**$C_{y1}$: Sr concentration in sample (86Sr spike)**

| Quantity | Value | Standard Uncertainty | Distribution | Sensitivity Coefficient | Uncertainty Contribution | Index |
|---|---|---|---|---|---|---|
| $m_z$ | 0.268600 g | $115 \cdot 10^{-6}$ g | rectangular | 400 | 0.046 mg/kg | 2.1 % |
| $m_y$ | 0.204500 g | $115 \cdot 10^{-6}$ g | rectangular | -520 | -0.060 mg/kg | 3.6 % |
| $R_{rb}$ | 0.965167 | $305 \cdot 10^{-6}$ | normal | -130 | -0.039 mg/kg | 1.5 % |
| $C_{z1}$ | 1004.00 mg/l | 2.89 mg/l | rectangular | 0.11 | 0.31 mg/kg | 92.7 % |
| EW | 1.024100 g | $115 \cdot 10^{-6}$ g | rectangular | -100 | 0.012 mg/kg | 0.1 % |
| $C_{y1}$ | 106.954 mg/kg | 0.319 mg/kg | | | | |

## Results:

| Quantity | Value | Expanded Uncertainty | Coverage factor | Coverage |
|---|---|---|---|---|
| $C_{y1}$ | 106.95 mg/kg | 0.64 mg/kg | 2.00 | 95% (normal) |

# IDMS - Sr quantification IAEA-375

## Model Equation:

$$C_x=C_y*m_y/m_x*(R_{y1}-R_b)/(R_b-R_{x1})*(R_{x1}+R_{x2}+R_{x3}+R_{x4})/(R_{y1}+R_{y2}+R_{y3}+R_{y4})$$

## List of Quantities:

| Quantity | Unit | Definition |
|---|---|---|
| $C_x$ | mg/kg | Sr concentration in soil |
| $C_y$ | mg/kg | Sr concentration in 86Sr spike |
| $m_y$ | g | weighted sample 86Sr spike |
| $m_x$ | g | weighted sample |
| $R_{y1}$ | | 88/86Sr spike |
| $R_b$ | | 88/86Sr spike-sample blend |
| $R_{x1}$ | | 88/86Sr sample |
| $R_{x2}$ | | 87/86Sr sample |
| $R_{x3}$ | | 86/86Sr sample |
| $R_{x4}$ | | 84/86Sr sample |
| $R_{y2}$ | | 87/86Sr 86Sr spike |
| $R_{y3}$ | | 86/86Sr 86Sr spike |
| $R_{y4}$ | | 84/86Sr 86Sr spike |

**$C_y$:** Type B normal distribution
Value: 106.95 mg/kg
Expanded Uncertainty: 0.64 mg/kg
Coverage Factor: 2

**$m_y$:** Type B rectangular distribution
Value: 0.2002 g
Halfwidth of Limits: 0.0002 g

**$m_x$:** Type B rectangular distribution
Value: 0.2188 g
Halfwidth of Limits: 0.0002 g

$R_{y4}$: Type A
Method of observation: Direct
Number of observations: 6

| No. | Observation |
|---|---|
| 1 | 0.000156 |
| 2 | 0.000125 |
| 3 | 0.000114 |
| 4 | 0.000126 |
| 5 | 0.000137 |
| 6 | 0.000144 |

Arithmetic Mean: $133.67 \cdot 10^{-6}$
Standard Deviation: $15 \cdot 10^{-6}$
Standard Uncertainty: $6.16 \cdot 10^{-6}$
Degrees of Freedom: 5

## Uncertainty Budgets:

$C_x$: **Sr concentration in soil**

| Quantity | Value | Standard Uncertainty | Distribution | Sensitivity Coefficient | Uncertainty Contribution | Index |
|---|---|---|---|---|---|---|
| $C_y$ | 106.950 mg/kg | 0.320 mg/kg | normal | 0.93 | 0.30 mg/kg | 93.6 % |
| $m_y$ | 0.200200 g | $115 \cdot 10^{-6}$ g | rectangular | 490 | 0.057 mg/kg | 3.5 % |
| $m_x$ | 0.218800 g | $115 \cdot 10^{-6}$ g | rectangular | -450 | -0.052 mg/kg | 2.9 % |
| $C_x$ | 99.055 mg/kg | 0.306 mg/kg | | | | |

## Results:

| Quantity | Value | Expanded Uncertainty | Coverage factor | Coverage |
|---|---|---|---|---|
| $C_x$ | 99.05 mg/kg | 0.61 mg/kg | 2.00 | 95% (normal) |

# IDMS - Sr quantification KRA

## Model Equation:

$$C_x=C_y*m_y/m_x*(R_{y1}-R_b)/(R_b-R_{x1})*(R_{x1}+R_{x2}+R_{x3}+R_{x4})/(R_{y1}+R_{y2}+R_{y3}+R_{y4});$$

$$C_y=C_{y1}*EW/AW;$$

## List of Quantities:

| Quantity | Unit | Definition |
|---|---|---|
| $C_x$ | mg/kg | Sr concentration in soil |
| $C_y$ | mg/kg | Sr concentration in 86Sr spike |
| $m_y$ | g | weighted sample 86Sr spike |
| $m_x$ | g | weighted sample |
| $R_{y1}$ | | 88/86Sr spike |
| $R_b$ | | 88/86Sr spike-sample blend |
| $R_{x1}$ | | 88/86Sr sample |
| $R_{x2}$ | | 87/86Sr sample |
| $R_{x3}$ | | 86/86Sr sample |
| $R_{x4}$ | | 84/86Sr sample |
| $R_{y2}$ | | 87/86Sr 86Sr spike |
| $R_{y3}$ | | 86/86Sr 86Sr spike |
| $R_{y4}$ | | 84/86Sr 86Sr spike |
| $C_{y1}$ | mg/kg | Sr concentration 86Sr spike undiluted |
| EW | g | 86Sr spike |
| AW | g | 1:10 dilution of 86Sr spike |

**$m_y$:** Type B rectangular distribution
Value: 0.2007 g
Halfwidth of Limits: 0.0002 g

**$m_x$:** Type B rectangular distribution
Value: 0.2033 g
Halfwidth of Limits: 0.0002 g

*Educational version, for training usage only!*

## Uncertainty Budgets:

**$C_x$: Sr concentration in soil**

| Quantity | Value | Standard Uncertainty | Distribution | Sensitivity Coefficient | Uncertainty Contribution | Index |
|---|---|---|---|---|---|---|
| $m_y$ | 0.200700 g | $115 \cdot 10^{-6}$ g | rectangular | 82 | $9.4 \cdot 10^{-3}$ mg/kg | 3.4 % |
| $m_x$ | 0.203300 g | $115 \cdot 10^{-6}$ g | rectangular | -80 | $-9.3 \cdot 10^{-3}$ mg/kg | 3.4 % |
| $C_{y1}$ | 106.950 mg/kg | 0.320 mg/kg | normal | 0.15 | 0.049 mg/kg | 93.0 % |
| EW | 1.024100 g | $115 \cdot 10^{-6}$ g | rectangular | 16 | $1.8 \cdot 10^{-3}$ mg/kg | 0.1 % |
| $C_x$ | 16.3592 mg/kg | 0.0507 mg/kg | | | | |

## Results:

| Quantity | Value | Expanded Uncertainty | Coverage factor | Coverage |
|---|---|---|---|---|
| $C_x$ | 16.36 mg/kg | 0.10 mg/kg | 2.00 | 95% (normal) |

# IDMS - Sr quantification RAD

## Model Equation:

$$C_x=C_y*m_y/m_x*(R_{y1}-R_b)/(R_b-R_{x1})*(R_{x1}+R_{x2}+R_{x3}+R_{x4})/(R_{y1}+R_{y2}+R_{y3}+R_{y4})$$

## List of Quantities:

| Quantity | Unit | Definition |
|---|---|---|
| $C_x$ | mg/kg | Sr concentration in soil |
| $C_y$ | mg/kg | Sr concentration in 86Sr spike |
| $m_y$ | g | weighted sample 86Sr spike |
| $m_x$ | g | weighted sample |
| $R_{y1}$ | | 88/86Sr spike |
| $R_b$ | | 88/86Sr spike-sample blend |
| $R_{x1}$ | | 88/86Sr sample |
| $R_{x2}$ | | 87/86Sr sample |
| $R_{x3}$ | | 86/86Sr sample |
| $R_{x4}$ | | 84/86Sr sample |
| $R_{y2}$ | | 87/86Sr 86Sr spike |
| $R_{y3}$ | | 86/86Sr 86Sr spike |
| $R_{y4}$ | | 84/86Sr 86Sr spike |

**$C_y$:** Type B normal distribution
Value: 106.95 mg/kg
Expanded Uncertainty: 0.64 mg/kg
Coverage Factor: 2

**$m_y$:** Type B rectangular distribution
Value: 0.2047 g
Halfwidth of Limits: 0.0002 g

**$m_x$:** Type B rectangular distribution
Value: 0.2222 g
Halfwidth of Limits: 0.0002 g

**$R_{y4}$:** Type A
Method of observation: Direct
Number of observations: 6

| No. | Observation |
|---|---|
| 1 | 0.000156 |
| 2 | 0.000125 |
| 3 | 0.000114 |
| 4 | 0.000126 |
| 5 | 0.000137 |
| 6 | 0.000144 |

Arithmetic Mean: $133.67 \cdot 10^{-6}$
Standard Deviation: $15 \cdot 10^{-6}$
Standard Uncertainty: $6.16 \cdot 10^{-6}$
Degrees of Freedom: 5

## Uncertainty Budgets:

**$C_x$:** **Sr concentration in soil**

| Quantity | Value | Standard Uncertainty | Distribution | Sensitivity Coefficient | Uncertainty Contribution | Index |
|---|---|---|---|---|---|---|
| $C_y$ | 106.950 mg/kg | 0.320 mg/kg | normal | 0.60 | 0.19 mg/kg | 93.6 % |
| $m_y$ | 0.204700 g | $115 \cdot 10^{-6}$ g | rectangular | 310 | 0.036 mg/kg | 3.3 % |
| $m_x$ | 0.222200 g | $115 \cdot 10^{-6}$ g | rectangular | -290 | -0.033 mg/kg | 2.8 % |
| $R_b$ | 0.5603467 | $74.4 \cdot 10^{-6}$ | normal | 130 | $9.6 \cdot 10^{-3}$ mg/kg | 0.2 % |
| $C_x$ | 63.926 mg/kg | 0.198 mg/kg | | | | |

## Results:

| Quantity | Value | Expanded Uncertainty | Coverage factor | Coverage |
|---|---|---|---|---|
| $C_x$ | 63.93 mg/kg | 0.40 mg/kg | 2.00 | 95% (normal) |

# IDMS - Sr quantification MAS

## Model Equation:

$$C_x=C_y*m_y/m_x*(R_{y1}-R_b)/(R_b-R_{x1})*(R_{x1}+R_{x2}+R_{x3}+R_{x4})/(R_{y1}+R_{y2}+R_{y3}+R_{y4});$$

$$C_y=C_{y1}*EW/AW;$$

## List of Quantities:

| Quantity | Unit | Definition |
|---|---|---|
| $C_x$ | mg/kg | Sr concentration in soil |
| $C_y$ | mg/kg | Sr concentration in 86Sr Spike |
| $m_y$ | g | weighted sample 86Sr Spike |
| $m_x$ | g | weighted sample |
| $R_{y1}$ | | 88/86Sr spike |
| $R_b$ | | 88/86Sr spike-sample blend |
| $R_{x1}$ | | 88/86Sr sample |
| $R_{x2}$ | | 87/86Sr sample |
| $R_{x3}$ | | 86/86Sr sample |
| $R_{x4}$ | | 84/86Sr sample |
| $R_{y2}$ | | 87/86Sr 86Sr spike |
| $R_{y3}$ | | 86/86Sr 86Sr spike |
| $R_{y4}$ | | 84/86Sr 86Sr spike |
| $C_{y1}$ | mg/kg | Sr concentration 86Sr spike undiluted |
| EW | g | 86Sr spike |
| AW | g | 1:10 dilution of 86Sr spike |

**$m_y$:** Type B rectangular distribution
Value: 0.2000 g
Halfwidth of Limits: 0.0002 g

**$m_x$:** Type B rectangular distribution
Value: 0.2099 g
Halfwidth of Limits: 0.0002 g

## Uncertainty Budgets:

**$C_x$: Sr concentration in soil**

| Quantity | Value | Standard Uncertainty | Distribution | Sensitivity Coefficient | Uncertainty Contribution | Index |
|---|---|---|---|---|---|---|
| $m_y$ | 0.200000 g | $115 \cdot 10^{-6}$ g | rectangular | 96 | 0.011 mg/kg | 3.4 % |
| $m_x$ | 0.209900 g | $115 \cdot 10^{-6}$ g | rectangular | -91 | -0.011 mg/kg | 3.1 % |
| $R_b$ | 1.397620 | $630 \cdot 10^{-6}$ | normal | 17 | 0.010 mg/kg | 3.0 % |
| $C_{y1}$ | 106.950 mg/kg | 0.320 mg/kg | normal | 0.18 | 0.057 mg/kg | 90.4 % |
| EW | 1.024100 g | $115 \cdot 10^{-6}$ g | rectangular | 19 | $2.2 \cdot 10^{-3}$ mg/kg | 0.1 % |
| $C_x$ | 19.1785 mg/kg | 0.0603 mg/kg | | | | |

## Results:

| Quantity | Value | Expanded Uncertainty | Coverage factor | Coverage |
|---|---|---|---|---|
| $C_x$ | 19.18 mg/kg | 0.12 mg/kg | 2.00 | 95% (normal) |

*Educational version, for training usage only!*

# 90Sr concentration IAEA-375

## Model Equation:

$C_x=C_y*0.8258/y*C_z*1000000;$

$C_z=a-b-c-(y*9.99*10^{-9});$

$c=(d-f)/0.1715*0.5145;$

## List of Quantities:

| Quantity | Unit | Definition |
|---|---|---|
| $C_x$ | ppt | 90Sr concentration in soil |
| $C_y$ | mg/kg | Sr concentration in soil |
| y | | 88 Sr peak tailing |
| $C_z$ | | 90 Sr |
| a | | mass 90 |
| b | | blank 90 |
| c | | 90 Zr |
| d | | 92 Zr |
| f | | blank 92 |

**$C_y$:** Type B normal distribution
Value: 99.05 mg/kg
Expanded Uncertainty: 0.64 mg/kg
Coverage Factor: 2

**y:** Constant
Value: 246839558

**a:** Constant
Value: 1661.283

**b:**

Type A
Method of observation: Direct
Number of observations: 3

| No. | Observation |
|---|---|
| 1 | 8.867 |
| 2 | 8.75 |
| 3 | 8.9 |

Arithmetic Mean: 8.8390
Standard Deviation: 0.079
Standard Uncertainty: 0.0455
Degrees of Freedom: 2

**d:**

Constant
Value: 212.269

**f:**

Type A
Method of observation: Direct
Number of observations: 3

| No. | Observation |
|---|---|
| 1 | 4.75 |
| 2 | 5 |
| 3 | 4.95 |

Arithmetic Mean: 4.9000
Standard Deviation: 0.13
Standard Uncertainty: 0.0764
Degrees of Freedom: 2

## Interim Results:

| Quantity | Value | Standard Uncertainty |
|---|---|---|
| $C_z$ | 1027.871 | 0.234 |
| c | 622.107 | 0.229 |

## Uncertainty Budgets:

**$C_x$: 90Sr concentration in soil**

| Quantity | Value | Standard Uncertainty | Distribution | Sensitivity Coefficient | Uncertainty Contribution | Index |
|---|---|---|---|---|---|---|
| $C_y$ | 99.050 mg/kg | 0.320 mg/kg | normal | 3.4 | 1.1 ppt | 99.5 % |
| f | 4.9000 | 0.0764 | normal | 0.99 | 0.076 ppt | 0.5 % |
| $C_x$ | 340.61 ppt | 1.10 ppt | | | | |

## Results:

| Quantity | Value | Expanded Uncertainty | Coverage factor | Coverage |
|---|---|---|---|---|
| $C_x$ | 340.6 ppt | 2.2 ppt | 2.00 | 95% (normal) |

# 90Sr concentration KRA

## Model Equation:

$C_x=C_y*0.8258/y*C_z*1000000;$

$C_z=a-b-c-(y*9.99*10^{-9});$

$c=(d-f)/0.1715*0.5145;$

## List of Quantities:

| Quantity | Unit | Definition |
|---|---|---|
| $C_x$ | ppt | 90Sr concentration in soil |
| $C_y$ | mg/kg | Sr concentration in soil |
| y | | 88 Sr peak tailing |
| $C_z$ | | 90 Sr |
| a | | mass 90 |
| b | | blank 90 |
| c | | 90 Zr |
| d | | 92 Zr |
| f | | blank 92 |

**$C_y$:** Type B normal distribution
Value: 16.36 mg/kg
Expanded Uncertainty: 0.10 mg/kg
Coverage Factor: 2

## Uncertainty Budgets:

**$C_x$: 90Sr concentration in soil**

| Quantity | Value | Standard Uncertainty | Distribution | Sensitivity Coefficient | Uncertainty Contribution | Index |
|---|---|---|---|---|---|---|
| $C_y$ | 16.3600 mg/kg | 0.0500 mg/kg | normal | 0.28 | 0.014 ppt | 1.2 % |
| y | $83.92 \cdot 10^6$ | $1.63 \cdot 10^6$ | normal | $-57 \cdot 10^{-9}$ | -0.093 ppt | 49.5 % |
| a | 46.522 | 0.480 | normal | 0.16 | 0.077 ppt | 34.0 % |
| b | 9.172 | 0.216 | normal | -0.16 | -0.035 ppt | 6.9 % |
| d | 4.6057 | 0.0669 | normal | -0.48 | -0.032 ppt | 5.9 % |
| f | 2.0777 | 0.0434 | normal | 0.48 | 0.021 ppt | 2.5 % |
| $C_x$ | 4.657 ppt | 0.133 ppt | | | | |

## Results:

| Quantity | Value | Expanded Uncertainty | Coverage factor | Coverage |
|---|---|---|---|---|
| $C_x$ | 4.66 ppt | 0.27 ppt | 2.00 | 95% (normal) |

*Educational version, for training usage only!*

# 90Sr concentration RAD

## Model Equation:

$C_x$=$C_y$*0.8258/y*$C_z$*1000000;

$C_z$=a-b-c-(y*9.99*10^-9);

c=(d-f)/0.1715*0.5145;

## List of Quantities:

| Quantity | Unit | Definition |
|---|---|---|
| $C_x$ | ppt | 90Sr concentration in soil |
| $C_y$ | mg/kg | Sr concentration in soil |
| y | | 88 Sr peak tailing |
| $C_z$ | | 90 Sr |
| a | | mass 90 |
| b | | blank 90 |
| c | | 90 Zr |
| d | | 92 Zr |
| f | | blank 92 |

**$C_y$:**

Type B normal distribution
Value: 63.93 mg/kg
Expanded Uncertainty: 0.40 mg/kg
Coverage Factor: 2

## Uncertainty Budgets:

**$C_x$: 90Sr concentration in soil**

| Quantity | Value | Standard Uncertainty | Distribution | Sensitivity Coefficient | Uncertainty Contribution | Index |
|---|---|---|---|---|---|---|
| $C_y$ | 63.930 mg/kg | 0.200 mg/kg | normal | 0.21 | 0.042 ppt | 1.5 % |
| y | $364.23 \cdot 10^6$ | $1.06 \cdot 10^6$ | normal | $-38 \cdot 10^{-9}$ | -0.041 ppt | 1.4 % |
| a | 159.82 | 1.40 | normal | 0.14 | 0.20 ppt | 35.5 % |
| d | 20.958 | 0.614 | normal | -0.43 | -0.27 ppt | 61.3 % |
| f | 1.6610 | 0.0388 | normal | 0.43 | 0.017 ppt | 0.2 % |
| $C_x$ | 13.479 ppt | 0.341 ppt | | | | |

## Results:

| Quantity | Value | Expanded Uncertainty | Coverage factor | Coverage |
|---|---|---|---|---|
| $C_x$ | 13.48 ppt | 0.68 ppt | 2.00 | 95% (normal) |

# 90Sr concentration MAS

## Model Equation:

$C_x=C_y*0.8258/y*C_z*1000000;$

$C_z=a-b-c-(y*9.99*10^{-9});$

$c=(d-f)/0.1715*0.5145;$

## List of Quantities:

| Quantity | Unit | Definition |
|---|---|---|
| $C_x$ | ppt | 90Sr concentration in soil |
| $C_y$ | mg/kg | Sr concentration in soil |
| y | | 88 Sr peak tailing |
| $C_z$ | | 90 Sr |
| a | | mass 90 |
| b | | blank 90 |
| c | | 90 Zr |
| d | | 92 Zr |
| f | | blank 92 |

**$C_y$:**

Type B normal distribution
Value: 19.18 mg/kg
Expanded Uncertainty: 0.12 mg/kg
Coverage Factor: 2

## Uncertainty Budgets:

**$C_x$: 90Sr concentration in soil**

| Quantity | Value | Standard Uncertainty | Distribution | Sensitivity Coefficient | Uncertainty Contribution | Index |
|---|---|---|---|---|---|---|
| $C_y$ | 19.1800 mg/kg | 0.0600 mg/kg | normal | 0.67 | 0.040 ppt | 0.3 % |
| y | $71.03 \cdot 10^6$ | $4.04 \cdot 10^6$ | normal | not valid! | -0.74 ppt | 93.3 % |
| a | 76.298 | 0.648 | normal | 0.22 | 0.14 ppt | 3.5 % |
| b | 5.900 | 0.126 | normal | -0.22 | -0.028 ppt | 0.1 % |
| d | 7.228 | 0.128 | normal | -0.67 | -0.086 ppt | 1.2 % |
| f | 3.267 | 0.144 | normal | 0.67 | 0.097 ppt | 1.6 % |
| $C_x$ | 12.889 ppt | 0.770 ppt | | | | |

## Results:

| Quantity | Value | Expanded Uncertainty | Coverage factor | Coverage |
|---|---|---|---|---|
| $C_x$ | 12.9 ppt | 1.5 ppt | 2.00 | 95% (normal) |

*Educational version, for training usage only!*

# 90Sr activity IAEA-375

## Model Equation:

$C_x$=ln(2)/912014640*($C_y$*0.8258/y*$C_z$*1000000*10^-12/(89.907738*1.66053886*10^-27*1000));

$C_z$=a-b-c-(y*9.99*10^-9);

c=(d-f)/0.1715*0.5145;

## List of Quantities:

| Quantity | Unit | Definition |
|---|---|---|
| $C_x$ | Bq/g | 90Sr activity in soil |
| $C_y$ | mg/kg | Sr concentration in soil |
| y | | 88 Sr |
| $C_z$ | | 90 Sr |
| a | | mass 90 |
| b | | blank 90 |
| c | | 90 Zr |
| d | | 92 Zr |
| f | | blank 92 |

**$C_y$:** Type B normal distribution
Value: 99.05 mg/kg
Expanded Uncertainty: 0.61 mg/kg
Coverage Factor: 2

**y:** Constant
Value: 246839558

**a:** Constant
Value: 1661.283

**b:**

Type A
Method of observation: Direct
Number of observations: 3

| No. | Observation |
|---|---|
| 1 | 8.867 |
| 2 | 8.75 |
| 3 | 8.9 |

Arithmetic Mean: 8.8390
Standard Deviation: 0.079
Standard Uncertainty: 0.0455
Degrees of Freedom: 2

**d:**

Constant
Value: 212.269

**f:**

Type A
Method of observation: Direct
Number of observations: 3

| No. | Observation |
|---|---|
| 1 | 4.75 |
| 2 | 5 |
| 3 | 4.95 |

Arithmetic Mean: 4.9000
Standard Deviation: 0.13
Standard Uncertainty: 0.0764
Degrees of Freedom: 2

## Interim Results:

| Quantity | Value | Standard Uncertainty |
|---|---|---|
| $C_z$ | 1027.871 | 0.234 |
| c | 622.107 | 0.229 |

## Uncertainty Budgets:

**$C_x$: 90Sr activity in soil**

| Quantity | Value | Standard Uncertainty | Distribution | Sensitivity Coefficient | Uncertainty Contribution | Index |
|---|---|---|---|---|---|---|
| $C_y$ | 99.050 mg/kg | 0.305 mg/kg | normal | 18 | 5.3 Bq/g | 99.5 % |
| f | 4.9000 | 0.0764 | normal | 5.1 | 0.39 Bq/g | 0.5 % |
| $C_x$ | 1733.93 Bq/g | 5.35 Bq/g | | | | |

## Results:

| Quantity | Value | Expanded Uncertainty | Coverage factor | Coverage |
|---|---|---|---|---|
| $C_x$ | 1734 Bq/g | 11 Bq/g | 2.00 | 95% (normal) |

# 90Sr activity KRA

## Model Equation:

$C_x$=ln(2)/912014640*($C_y$*0.8258/y*$C_z$*1000000*10^-12/(89.907738*1.66053886*10^-27*1000));

$C_z$=a-b-c-(y*9.99*10^-9);

c=(d-f)/0.1715*0.5145;

## List of Quantities:

| Quantity | Unit | Definition |
|---|---|---|
| $C_x$ | Bq/g | 90Sr activity in soil |
| $C_y$ | mg/kg | Sr concentration in soil |
| y | | 88 Sr |
| $C_z$ | | 90 Sr |
| a | | mass 90 |
| b | | blank 90 |
| c | | 90 Zr |
| d | | 92 Zr |
| f | | blank 92 |

**$C_y$:**

Type B normal distribution
Value: 16.36 mg/kg
Expanded Uncertainty: 0.10 mg/kg
Coverage Factor: 2

## Uncertainty Budgets:

**$C_x$: 90Sr activity in soil**

| Quantity | Value | Standard Uncertainty | Distribution | Sensitivity Coefficient | Uncertainty Contribution | Index |
|---|---|---|---|---|---|---|
| $C_y$ | 16.3600 mg/kg | 0.0500 mg/kg | normal | 1.4 | 0.072 Bq/g | 1.2 % |
| y | $83.92 \cdot 10^6$ | $1.63 \cdot 10^6$ | normal | $-290 \cdot 10^{-9}$ | -0.47 Bq/g | 49.5 % |
| a | 46.522 | 0.480 | normal | 0.82 | 0.39 Bq/g | 34.0 % |
| b | 9.172 | 0.216 | normal | -0.82 | -0.18 Bq/g | 6.9 % |
| d | 4.6057 | 0.0669 | normal | -2.5 | -0.16 Bq/g | 5.9 % |
| f | 2.0777 | 0.0434 | normal | 2.5 | 0.11 Bq/g | 2.5 % |
| $C_x$ | 23.707 Bq/g | 0.675 Bq/g | | | | |

## Results:

| Quantity | Value | Expanded Uncertainty | Coverage factor | Coverage |
|---|---|---|---|---|
| $C_x$ | 23.7 Bq/g | 1.3 Bq/g | 2.00 | 95% (normal) |

*Educational version, for training usage only!*

# 90Sr activity RAD

## Model Equation:

$C_x$=ln(2)/912014640*($C_y$*0.8258/y*$C_z$*1000000*10^-12/(89.907738*1.66053886*10^-27*1000));

$C_z$=a-b-c-(y*9.99*10^-9);

c=(d-f)/0.1715*0.5145;

## List of Quantities:

| Quantity | Unit | Definition |
|---|---|---|
| $C_x$ | Bq/g | 90Sr activity in soil |
| $C_y$ | mg/kg | Sr concentration in soil |
| y | | 88 Sr |
| $C_z$ | | 90 Sr |
| a | | mass 90 |
| b | | blank 90 |
| c | | 90 Zr |
| d | | 92 Zr |
| f | | blank 92 |

**$C_y$:** Type B normal distribution
Value: 63.93 mg/kg
Expanded Uncertainty: 0.40 mg/kg
Coverage Factor: 2

## Uncertainty Budgets:

**$C_x$: 90Sr activity in soil**

| Quantity | Value | Standard Uncertainty | Distribution | Sensitivity Coefficient | Uncertainty Contribution | Index |
|---|---|---|---|---|---|---|
| $C_y$ | 63.930 mg/kg | 0.200 mg/kg | normal | 1.1 | 0.21 Bq/g | 1.5 % |
| y | $364.23 \cdot 10^6$ | $1.06 \cdot 10^6$ | normal | $-200 \cdot 10^{-9}$ | -0.21 Bq/g | 1.4 % |
| a | 159.82 | 1.40 | normal | 0.74 | 1.0 Bq/g | 35.5 % |
| d | 20.958 | 0.614 | normal | -2.2 | -1.4 Bq/g | 61.3 % |
| f | 1.6610 | 0.0388 | normal | 2.2 | 0.086 Bq/g | 0.2 % |
| $C_x$ | 68.62 Bq/g | 1.74 Bq/g | | | | |

## Results:

| Quantity | Value | Expanded Uncertainty | Coverage factor | Coverage |
|---|---|---|---|---|
| $C_x$ | 68.6 Bq/g | 3.5 Bq/g | 2.00 | 95% (normal) |

# 90Sr activity MAS



## Model Equation:

$C_x$=ln(2)/912014640*($C_y$*0.8258/y*$C_z$*1000000*10^-12/(89.907738*1.66053886*10^-27*1000));

$C_z$=a-b-c-(y*9.99*10^-9);

c=(d-f)/0.1715*0.5145;



## List of Quantities:

| Quantity | Unit | Definition |
|---|---|---|
| $C_x$ | Bq/g | 90Sr activity in soil |
| $C_y$ | mg/kg | Sr concentration in soil |
| y | | 88 Sr |
| $C_z$ | | 90 Sr |
| a | | mass 90 |
| b | | blank 90 |
| c | | 90 Zr |
| d | | 92 Zr |
| f | | blank 92 |



**$C_y$:**

Type B normal distribution
Value: 19.18 mg/kg
Expanded Uncertainty: 0.12 mg/kg
Coverage Factor: 2

## Uncertainty Budgets:

**$C_x$: 90Sr activity in soil**

| Quantity | Value | Standard Uncertainty | Distribution | Sensitivity Coefficient | Uncertainty Contribution | Index |
|---|---|---|---|---|---|---|
| $C_y$ | 19.1800 mg/kg | 0.0600 mg/kg | normal | 3.4 | 0.21 Bq/g | 0.3 % |
| y | $71.03 \cdot 10^6$ | $4.04 \cdot 10^6$ | normal | not valid! | -3.8 Bq/g | 93.3 % |
| a | 76.298 | 0.648 | normal | 1.1 | 0.74 Bq/g | 3.5 % |
| b | 5.900 | 0.126 | normal | -1.1 | -0.14 Bq/g | 0.1 % |
| d | 7.228 | 0.128 | normal | -3.4 | -0.44 Bq/g | 1.2 % |
| f | 3.267 | 0.144 | normal | 3.4 | 0.49 Bq/g | 1.6 % |
| $C_x$ | 65.62 Bq/g | 3.92 Bq/g | | | | |

## Results:

| Quantity | Value | Expanded Uncertainty | Coverage factor | Coverage |
|---|---|---|---|---|
| $C_x$ | 65.6 Bq/g | 7.8 Bq/g | 2.00 | 95% (normal) |